LT-XFD_PDR_SRX-00124

NSLS-II Project

PRELIMINARY DESIGN REPORT for the

SUBMICRON RESOLUTION X-RAY SPECTROSCOPY (SRX) BEAMLINE AT NSLS-II

Issued September 2010

Intentionally blank.

Approvals and Reviewers

Compiled by	**Signature**	**Date**
Juergen Thieme, Beamline Scientist		
Approved		
Qun Shen, XFD Director, NSLS-II		
Reviewers		
Antonio Lanzirotti, BAT Spokesperson, signing on behalf of the BAT		
Andy Broadbent, Beamlines Manager		
Nicholas Gmür, ESH Coordinator, NSLS-II		
P. K. Job, Radiation Physicist, NSLS-II		
Sushil Sharma, Mechanical Engineering Group Leader, NSLS-II		

Document Updates

The Preliminary Design Report for the Submicron Resolution X-ray Spectroscopy (SRX) beamline at NSLS-II is a controlled document, revised under change control.

Version No.	Date	Changes made
0	9/26/2010	Initial draft
1	9/30/2010	Uploaded to Sharepoint for comments from BAT and directors
Final		First official release

Intentionally blank.

Contents

Introduction **7**
Scientific scope 7
Team of SRX Beamline 9
Beamline Advisory Team 9

Insertion Device **9**
KB Branch 10
ZP Branch 13
IVU 21 Scanning Requirements for the KB Branch 14

Front End **16**
Description of components 17
Preliminary ray-tracing 18

Beamline Design **18**
Optical layout 18
Raytracing calculations KB branch 24
High Heat Load Optics 25
Optimization of the location of the optical elements 32
Raytracing calculations ZP branch 41
Alignment of Beam Defining Optics 43
Description of major components for KB branch 46
White Beam Slits *46*
Horizontal Focusing Mirror *46*
Double crystal monochromator *47*
Secondary source aperture slits *47*

KB End Station **48**
Description of KB optics 49
Description of sample stage 51
Constraints linked to the high flux 51
Constraints linked to the high spatial resolution 51
Stage Assembly *51*
Working distance *53*
Spatial stability of the sample *53*
Sample considerations 56

Infrastructure **58**
Surveying of Beamline Components at NSLS-II using a laser tracker. *58*
Utilities requirements 58
Special beamline requirements 59
Research with nanomaterials and nanoparticles *59*
Research with actinides *59*

Summary of Day 1 performance **59**

Future upgrade options **60**
Zone plate branch 60
Experiments with cryo-cooled samples *60*
Coherent diffraction imaging *60*

Appendix A: Schedule **61**

Appendix B: Reference Drawings **62**
Personal Protection System 62
Controls diagrams 63
Front end ray tracing (preliminary) 68

Raytracing KB branch 72

Appendix C: Feasibility of Design and Procurement Plan 77

First optical enclosure 77

End station 78

Introduction

Scientific scope

Scientific communities (such as earth and environmental sciences, medical and life sciences, hard and soft condensed matter and materials sciences, chemical and energy sciences) have identified the need to develop analytical resources to advance the understanding of complex natural and engineered systems that are heterogeneous on the micron to nanometer scale. These communities specified a need for high intensity x-ray nanoprobes and made it clear in the Letter of Interest they submitted to the NSLS-II Project for the Sub-Micron Resolution X-Ray (SRX) Spectroscopy Beamline, that NSLS-II would provide one of the best sources in the world for such instruments. The research topics these scientific communities hoped to better address using such an instrument require characterization of elemental abundances and speciation in samples that are heterogeneous at the sub-micrometer scale.

The targeted scientific issues show a wide range of environmental and health issues of high societal impact. Interactions between micro-organisms and minerals control the speciation, migration and toxicity of contaminated materials produced by human activity. Micro-organisms and particulates are likely major players in the cycling of nutrients and metals in the Earth's oceans, processes that can have a significant impact on conditions at the planetary scale, such as global climate change. The properties of airborne particulates can have a profound effect on the toxicity of atmospheric dust introduced to the human body by inhalation. The study of how genetic variations in organisms affect their interactions with contaminant and nutrient metal species in the environment is in its infancy but likely to be greatly advanced with this new technology because of the ability to observe in detail the chemical modifications in organisms caused by genetic modification.

Equally significant will be studies of the varied sources, pathways and functions of metals in organisms, in particular their role in human health. Some metals are required for normal metabolic function, with optimal amounts for maximum benefit. Others are only known to cause toxic effects. Metal ions are also used both as treatments for disease and as image contrast agents within the body. Yet, in order to understand at the molecular level how metal ions function in life, disease, and therapy, a multi-dimensional approach is necessary.

Such an instrument will allow studies of catalysis and chemical processes at the scale of a single particle using coupled μXAS/μXRD of catalytic particles and interfaces to follow processes such as oxidation. In the materials sciences scientists will be able to research the elemental partitioning in microelectronics and elemental diffusion into microcrystalline domains that occur due to aging of plastics and alloys and tracking redox changes of single particle contaminants in batteries and silicon solar cells.

The SRX beamline with its unique combination of high spectral resolution over a very broad energy range and very high beam intensity in a sub-micrometer spot will be a tool very well suited for the study of the scientific issues mentioned above.

The design shows a canted undulator beamline that consists of two branches, each optimized to reach very high spatial resolution for a specific energy range. The first branch is optimized to access higher energy and is included in the initial scope of NSLS-II for the SRX beamline. It will access an energy range of E = 4.65 keV to E = 25 keV. Mirror optics in Kirkpatrick-Baez (KB) geometry will focus the beam and create a sub-micrometer sized focal spot. The second branch, optimized for lower energies, accessing spectroscopic edges from E = 2 keV to E = 15 keV, will require additional funding to be completed. Zone plates (ZP) will be used as focusing optics for this branch. The high energy cut-off of E = 25 keV of the first branch is determined by the energy at which the brightness of the NSLS-II undulators has dropped by approximately two orders of magnitude from that of the third harmonic at closed gap. Also, the K-absorption edge of rhodium, the best suited coating for mirrors at these high X-ray energies, lies at about E = 23 keV. Consequently, reflectivity drops significant above that energy. The low energy cut-off of E = 4.65 keV is the energy at which the undulator third harmonic begins. This is the energy of the K-absorption edge of titanium, thus giving access to this element. The low energy cut-off of E = 2 keV of the second branch is set by the limits of the Si (111) monochromator. The K-absorption edge of phosphorus, an important element to study in life and environmental sciences, is however still in reach. The high-energy cut-off of E = 15 keV is determined by the need to access the L_3-absorption edge of lead at E = 13 keV.

The wide energy range covered by both branches will allow the scientific community to address a wide range of research topics, as absorption edges of a large number of elements can be reached with the SRX beamline, allowing elemental mapping as well as spectroscopy studies (see Figure 1). The two branches are required to cover this large energy range without compromising the aim of combining X-ray spectroscopy and sub-micron spatial resolution in an optimal way.

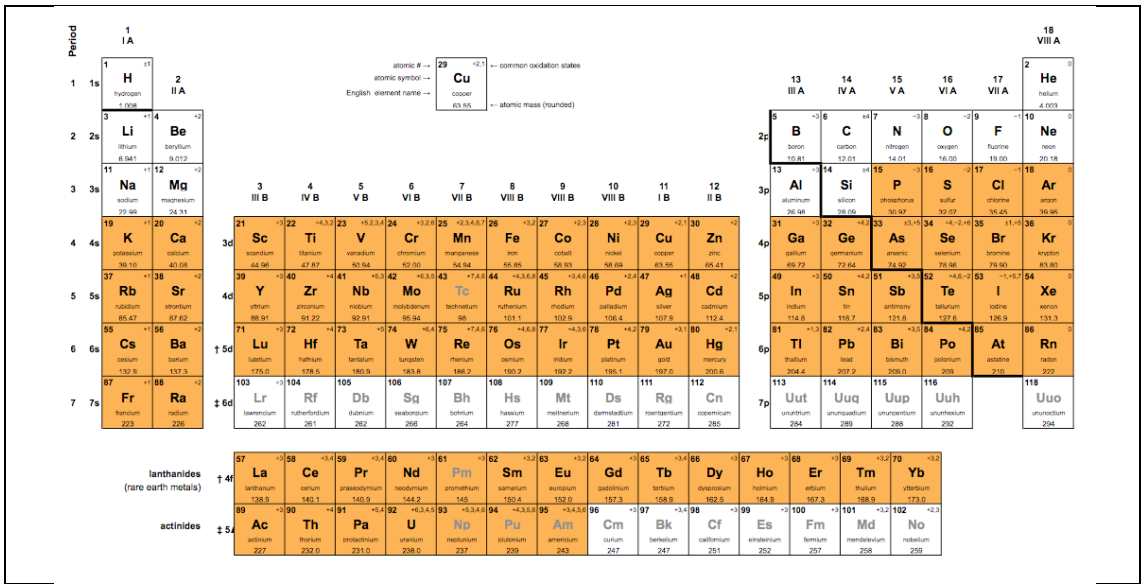

Figure 1. Periodic table of elements showing highlighted the elements with absorption edges at X-ray energies in reach by the SRX beamline.

Team of SRX Beamline

Juergen Thieme, Group Leader
Vincent de Andrade, Beamline Scientist
Paul Northrup, Contractor
Yuan Yao, Mechanical Engineer
Niaja Farve, Summer student (June-August 2010)

Beamline Advisory Team

Peter Eng: Senior Research Associate, University of Chicago
Jeffrey Fitts: Assistant Geochemist, Brookhaven National Laboratory
Chris Jacobsen: Professor, Stony Brook University
Keith Jones: Senior Physicist, Brookhaven National Laboratory
Antonio Lanzirotti (BAT Spokesperson): Senior Research Associate, University of Chicago
Lisa Miller: Biophysical Chemist, Brookhaven National Laboratory
Matt Newville: Senior Research Associate, University of Chicago
Paul Northrup: Associate Environmental Scientist, Brookhaven National Laboratory
Richard Reeder: Professor, Stony Brook University
Mark Rivers: Senior Scientist, University of Chicago
Stephen Sutton: Senior Scientist, University of Chicago
Stefan Vogt: Beamline Scientist, Advanced Photon Source, Argonne National Laboratory
Gayle Woloschak: Professor, Northwestern University

Insertion Device

Table 1. Source Parameters of NSLS-II.

Electron Energy	E = 3 GeV
Stored Current	I = 500 mA
Electron Beam Emittance:	
Horizontal	$\varepsilon_x = 0.55 \times 10^{-9}$ m rad
Vertical (1.5% Coupling)	$\varepsilon_y = 8.25 \times 10^{-12}$ m rad
Betatron Function:§	
Horizontal	$\beta_x = 1.5$ m
Vertical	$\beta_y = 0.8$ m
Electron Beam Size:§	
Horizontal	$\sigma_x = 28.7$ μm
Vertical	$\sigma_y = 2.57$ μm
Electron Beam Divergence:§	
Horizontal	$\sigma'_{yx} = 19.2$ μrad
Vertical	$\sigma'_{yy} = 3.21$ μrad

Intrinsic Photon Size*	σ_r = 1.95 μm	
Intrinsic Photon Divergence*	σ'_y = 4.08 μrad	§ Low b straight. *Quantities evaluated for 12.4keV x-rays and a 3m-long undulator.
Total Photon Source Size:§*		
Horizontal	Σ_x = 28.8 μm	
Vertical	Σ_y = 3.2 μm	
Total Photon Source Divergence:§*		
Horizontal	$\Sigma'_{y\,x}$ = 28.8 μrad	
Vertical	Σ'_y = 5.19 μrad	

The two branches of the SRX beamline are designed for different energy ranges, making the undulator design unusual amongst the initial suite of project beamlines at NSLS-II. However, it is expected that in the long run more sectors will be equipped with this design. Two undulators in canted geometry on this short (low beta) straight section will serve the two instruments as light sources. As there is the need to do spectroscopy at the titanium K-absorption edge, the specified lowest energy the undulator for the KB branch should reach is E = 4.65 keV. There are a couple of restrictions applied to the choice of the insertion device as a light source for the SRX beamline. The length of the device and the minimum gap have to be adjusted to the limitations stemming from the beta function of the short straight section (stay-clear condition). A length of 0.5 m minimum has to be removed from the total length of the straight section available for the two undulators to give room for the canting magnets as well as room has to be given to transition pieces and a full canting magnet at the end of the straight, which is also assumed to be 0.5 m long. From the Accelerator Science Division, a stay-clear minimum gap of 5 mm at a length of 1.5 m for the two undulators has been set.

KB Branch

Focusing on the KB-branch, the optimized period of the undulator will depend on the gap (itself related to the length of the device through the beta-function restrictions) and the minimum photon energy (E = 4.65 keV). Oleg Tchoubar from NSLS-II has performed the calculations presented below, which are the basis for the decision on the actual undulator for the KB branch.

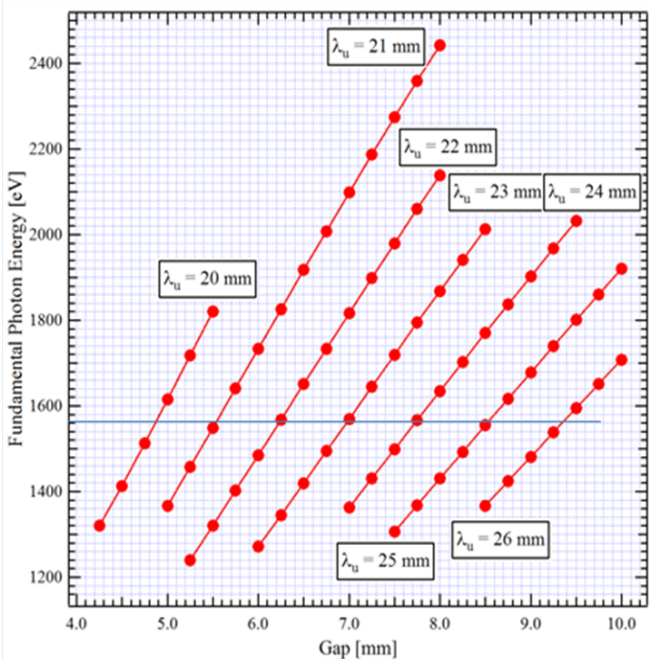

Figure 2. Fundamental photon energy as a function of the gap for IVU periods from 20 – 26 mm. The blue line indicates a fundamental energy of E = 1560 eV.

In Figure 2 the fundamental photon energy as a function of the gap for in-vacuum undulator (IVU) periods from 20 – 26 mm are plotted. The blue line in figure 2 indicates the energy E = 1560 eV, of the first undulator harmonic. With this, the 3rd harmonic would start around the desired X-ray energy of E = 4.65 keV. From the graphs in Figure 2 it becomes visible that for a minimum gap of 4.9 mm a period of 20 mm would be allowable, a minimum gap of 5.5 mm would relate to a period of 21 mm and for a gap of 6.2 mm the period would be 22 mm.

The maximum device length for a given minimum gap is determined by the beta function for the straight. Toshi Tanabe from NSLS-II calculated the possible lengths, assuming a canted device placed into a half-straight, as listed in Table 2.

Table 2. Maximum canted device lengths for given gaps in a canted device setup.

Gap	Maximum canted device length.
5.0mm	1.25m
5.5mm	1.5m
6.0mm	1.75m
6.26mm	1.85m
6.6mm	2.0m
7.2mm	2.25m

As a result of these consideration three options have been calculated, an undulator with 20 mm period and 1.25 m length at a gap of 4.9 mm, an undulator with 21 mm period and 5.5 mm gap and 1.5 m length, and an undulator with 22 mm period and 6.2 mm gap and 1.8 m length. For these calculations the center of the device is located approximately 1 m from the center of the low-beta straight, resulting from the design described above.

Figure 3 shows the spectral flux in phot/sec/0.1%BW for these three configurations at odd harmonics as a function of photon energy. Figure 4 shows for the same configurations the calculated spectral flux through an aperture of 0.1 x 0.1 mrad^2 at minimal gap. As a result and taking the stay-clear minimum gap of 5.5 mm into account, an IVU21 is the undulator of choice. Table 3 summarizes the parameters. Figure 5 shows the flux coming from this undulator in Watts/eV/mm^2 as a function of X-ray energy for odd and even harmonics, calculated using the SRW program package of Oleg Tchoubar.

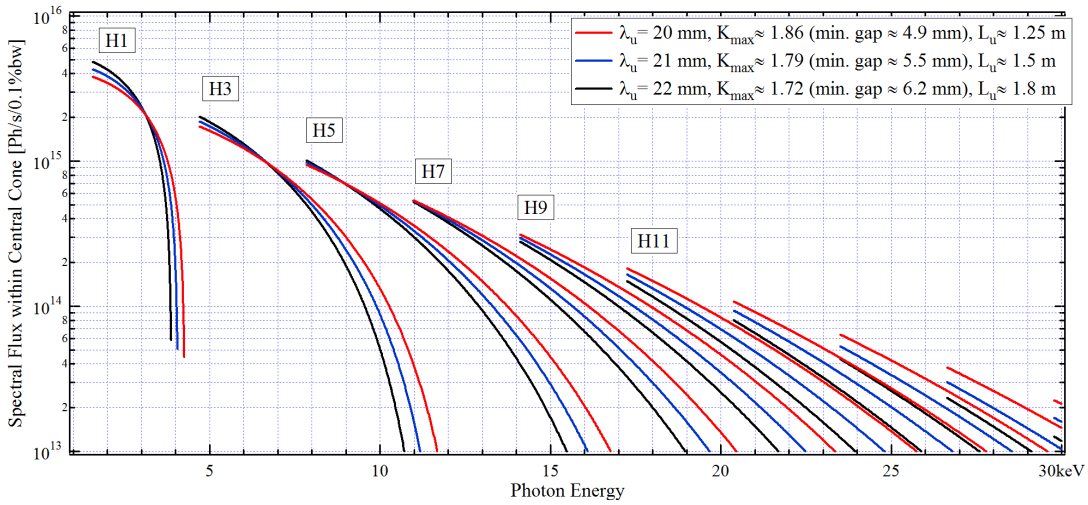

Figure 3. Spectral flux at odd harmonics for undulator setups as seen in the legend.

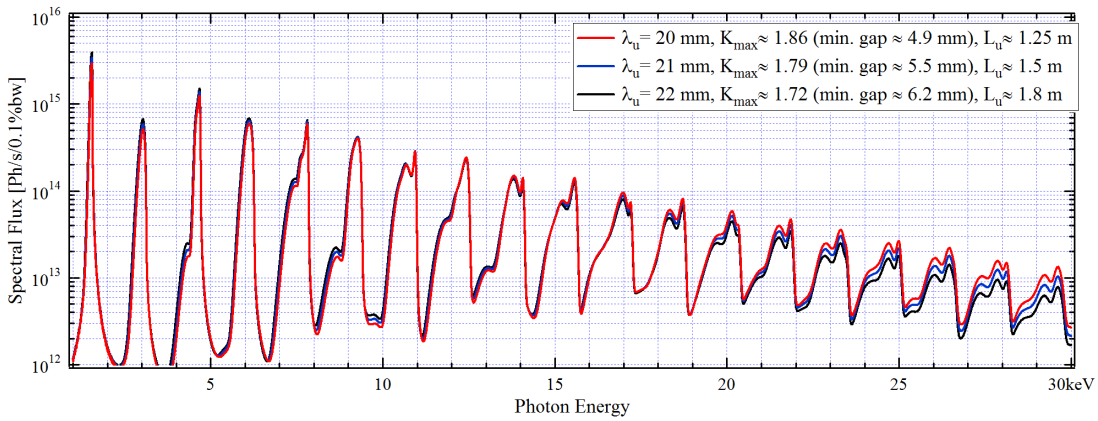

Figure 4. Spectral flux through an aperture with 0.1 x 0.1 mrad^2 size at minimal gap for undulator setups as seen in the legend.

Table 3: Parameters in-vacuum undulator U21.

Undulator length	1.5 m
Period length	21 mm
Minimum gap	5.5 mm
Lowest energy in 3rd harmonic (E=3GeV)	4.65 keV
Maximum energy	28 keV
K-Value	1.79

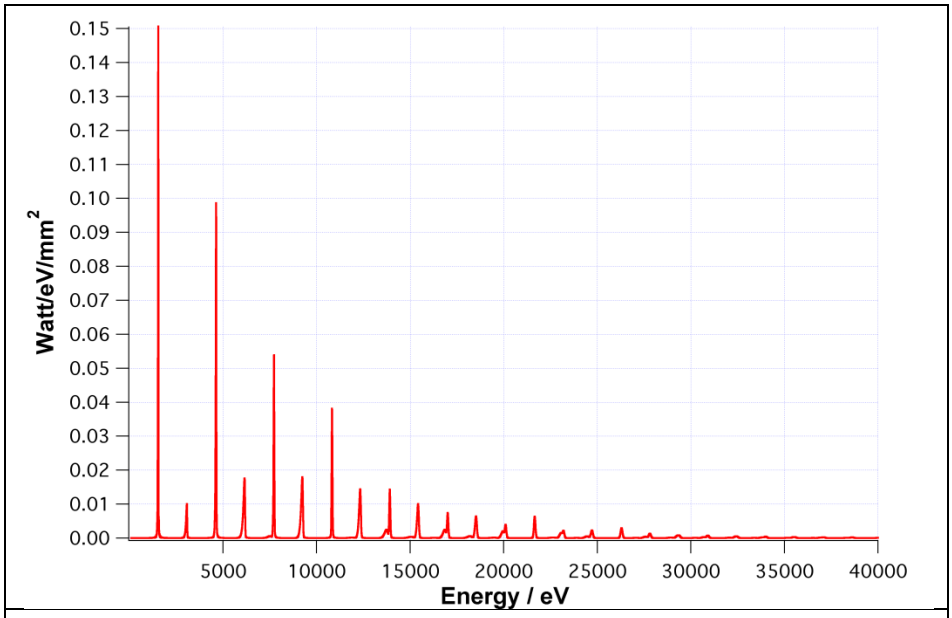

Figure 5. Spectrum of the undulator IVU21

ZP Branch

The ZP branch is dedicated to an energy range from E = 2 keV up to E = 15 keV. From figure 3 it becomes clear for undulator types IVU 20, IVU 21, or IVU 22, again considering the allowable minimum gap, that due to these limitations there will be an energy range between E = 4 keV and E = 5 keV, where no radiation can be used for experiments. From the viewpoint of scientific applications this cannot be accepted, therefore a solution has to be found to close this energy gap. Several ways to solve this problem are possible. One solution would be to shorten the length of an undulator IVU 22 to 1.2 m. This would allow the minimum gap to be reduced without deteriorating the electron beam. Due to the resulting higher magnetic field strength the full desired energy range would be covered. However, due to the shorter length, the overall performance in terms of photon flux will be poorer. Another solution would be to use a cryo-cooled undulator. Due to cryo-cooling a higher K-value would be achievable resulting in a full coverage of the desired energy range without hampering the electron beam. A super-conducting undulator could be another solution for filling the energy gap. A decision has not been made yet, as the ZP branch is not in the baseline scope of the NSLS-II project. Figure 6 shows the spectral brightness as a function of X-ray energy for bend magnet, wiggler and undulators as sources of X-radiation. This plot will be the starting point for discussions about the right choice of insertion device. As the CPMU17 shown in figure 6 still has a gap at medium X-ray energies, probably a higher K-value above 2 and a longer period length will be a solution.

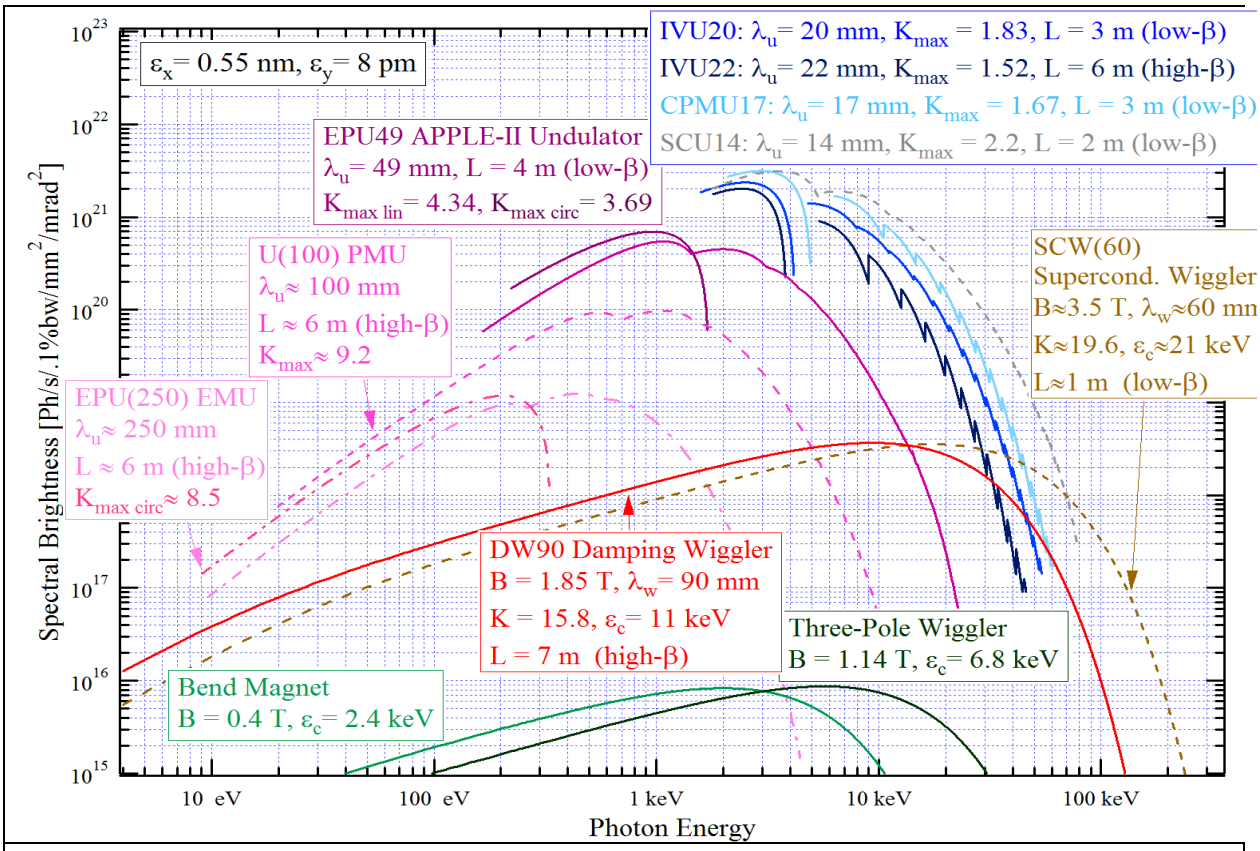

Figure 6: Spectral Brightness of different NSLS-II sources for X-radiation.

IVU 21 Scanning Requirements for the KB Branch

The SRX beamline is dedicated to X-ray spectroscopy with high spatial but as well high spectral resolution. To achieve the task of measuring spectra with stable high beam intensity, with very precise energy tuning and with reliable reproducibility, the undulator control has to be very accurate. The undulator gap needs to be changed during the experiment to obtain a usable spectrum of a sample. The following calculations have been made to determine, what requirements are needed to perform reasonable XANES- and EXAFS-spectroscopy. Significant contributions to these calculations came from Roger Dejus, Matt Newville and Mark Rivers, all from the Advanced Photon Source at Argonne National Laboratory, and Antonio Lanzirotti, Univ. of Chicago/NSLS.

Figure 2 shows the fundamental photon energy as a function of the gap G for different IVU periods. Looking at the curve for λ = 21 mm, the two end points of the line are:

$$G = 5.0\ \text{mm} \quad \Rightarrow \quad E = 1370\ \text{eV}$$
$$G = 8.0\ \text{mm} \quad \Rightarrow \quad E = 2440\ \text{eV}$$

For the following calculation it is just to determine the slope, assuming a straight line, which results in

$$\Delta E/\Delta G_{1st\ order} = 0.357\ \text{keV/mm}$$

The slope of the so-defined line for the n-th order is the now calculated using the slope of the 1st order multiplied with n.

The full width half maximum (FWHM) of single harmonics of IVU 21 have been determined using the result of the SRW calculation, which is shown graphically in figure 5. With this and to cover the extremes, the FWHM of the 3rd and the 17th harmonic have been determined to

3rd harmonic at E = 4635 eV ⇒ FWHM = 35 eV corresponds to 0.75%
17th harmonic at E = 26300 eV ⇒ FWHM = 130 eV corresponds to 0.50%

To cover these FWHM's or the σ-values the following gap changes are necessary:

3rd harmonic: ΔG_{FWHM} = 32.45 µm, $\Delta G_{Sigma} = \Delta G_{FWHM} / 2.35$ = 13.81 µm
17th harmonic: ΔG_{FWHM} = 21.65 µm, $\Delta G_{Sigma} = \Delta G_{FWHM} / 2.35$ = 9.21 µm

To achieve useful spectroscopy data, it would be necessary, to allow fluctuations in the intensity of the maximum of an undulator harmonic of only 1%. Assuming a Gaussian shape of the harmonic, this would demand a positioning accuracy of 14% of the σ-value,

3rd harmonic: $\Delta G_{1\%}$ = 1.9 µm
17th harmonic: $\Delta G_{1\%}$ = 1.29 µm

Therefore, to achieve reasonable spectroscopy data across the covered energy range, a minimum stepsize of 1 µm in driving the IVU21 undulator will be necessary.
The minimum gap of IVU21 allowed by the stay-clear constraints of the Accelerator Science Division is G = 5.5 mm, corresponding to an energy in the 1st order of E = 1560 eV, see figure 2. As the X-ray energy of a higher harmonic is obtained by multiplying this fundamental energy with the order n of the harmonic, this gap corresponds to an energy of E = 4680 eV in the 3rd harmonic. The K-absorption edge of rhodium lies at E = 23.2 keV, which is probably the highest X-ray energy useful for experiments, as the reflectivity of the mirrors will drop drastically above that edge. This would be reached at the same gap in 17th harmonic, reducing however significantly the usable beam intensity. At a gap of G = 8.0 mm, the fundamental energy lies at E = 2440 eV, corresponding to the 9th harmonic for energies above E = 21 keV. This assessment clarifies, that practically all spectroscopy experiments will need gap changes in the gap range of G = 5.5 mm up to G = 8.0 mm.

The following list summarizes the above mentioned and further parameters necessary for the undulator IVU21. A homonymic list can be found in the RSI (Requirements, Specifications, and List of Interfaces) document for the SRX beamline.

Gap Adjustment for Energy Positioning

- Range of gap: 5.5 mm to maximum gap.
- Minimum reproducible step: less than 1 micron.
- "Stepping time," time for accomplishment and confirmation of position and parallelism at minimum step: less than 1 sec.
- Position readback precision: smaller than 1 micron.
- Speed: greater than 1mm/min
- Parallelism at each position as required for less than 1% variation in intensity .

Gap Adjustment for Energy Scanning

- Range of gap for energy-scanning: 5.5 to 10.5 mm
- Minimum reproducible step: less than 1 micron
- Position readback precision: less than 1 micron
- Position readback rate: greater than 1 khz
- Continuous smooth scanning speed (min., max.) range: 10 to 1,000 microns/minute
- Parallelism maintained during continuous scanning motion: as required for less than 1% variation in intensity

Motion Control

- Gap under beamline control
- Parallelism maintained by machine and/or feedback loop, but can be checked by beamline
- Elevation under machine control

Duty Cycle

- Periodic stepping at 0.1 sec to ~4 hour frequency
- Repeated continuous-motion energy scans (0.02 to 2.0 mm in length) for >24 hours

Front End

The design of the front end for the SRX beamline is not finished yet, therefore only interim design considerations can be presented here. The preliminary layout of a front end designed by NSLS-II for two undulators in a canted geometry can be seen in Figure 7. All elements shown there will accommodate both beams from the two undulators. It is taken into account, that the control of the two beams for the two branches needs to be independent, meaning that a change in parameters of components for the KB branch should not cross-talk to the ZP branch and vice versa. The layout incorporating these constraints and special demands is work in progress. A list of the components can be found in the next chapter, a first ray tracing is attached in Appendix A.

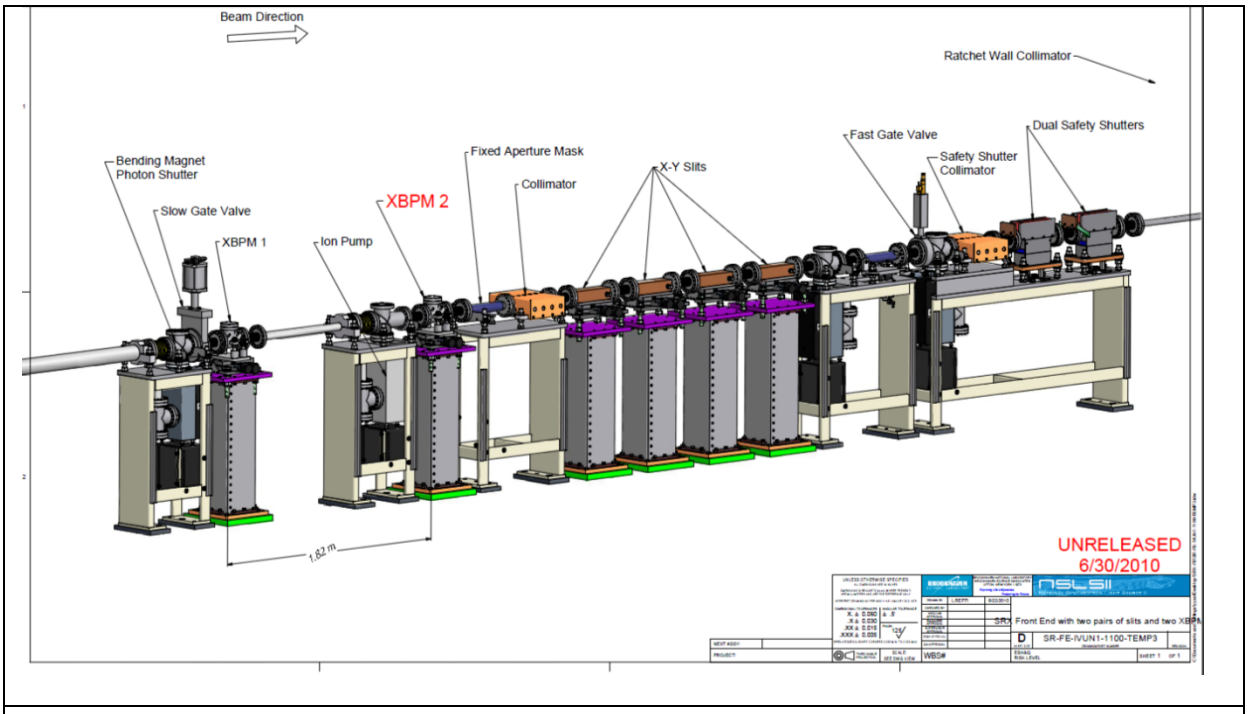

Figure 7: Model of components of front end for the SRX beamline, having two undulators in canted geometry as independent X-radiation sources.

Description of components

Bending Magnet Photon Shutter (BMPS)
The BMPS is designed to protect the slow gate valve (SGV) from bending magnet radiation before the upstream straight is fitted with an insertion device and a complete front end.

Slow Gate Valve (SGV)
The SGV is included to isolate the machine and front end, but will not withstand white beam from insertion device or bending magnet radiation. The SGV is controlled and monitored by storage ring vacuum PLC using a voting scheme with inputs from vacuum sensors at both sides of the valves and position of BMPS.

Beam Position Monitor 1 (XBPM1)
The XBPMs shall be designed to work with the insertion devices. It will consist of tungsten blades and water cooled mountings and it will be motorized to allow centering of the device around the beam. The XBPMs shall be mounted on X/Y stages with the very high position stability in the 1 μm-range and a position resolution well below 1 μm.

The X/Y stage for the XBPM and the X/Y slits are expected to be the same design, including the stand, where possible.

Beam Position Monitor 2 (XBPM2)
This device and X/Y stages shall be identical to XBPM1, however the blades shall be relocated to avoid masking effects.

Fixed Aperture Mask (FAPM)

The fixed aperture mask shall provide radiation fans to the first optical enclosure (FOE). No tolerance shall be added to the mask for mis-positioning, however a manufacturing tolerance of +/-0.2mm for the aperture (at the downstream end of the mask) shall be included in the downstream fan definition. For IVU beamlines, it is permissible for the mask aperture to have corner radii equivalent to half the aperture height.

Bremsstrahlung Collimator (BC1)
BC1 restricts the bremsstrahlung radiation fan exiting the shield wall. This should be as tight to the beam as is reasonable without undue mechanical tolerances or alignment difficulty.

X-Y Slits
The X-Y slits shall be of the SPring8 dual "L" type design, connected with bellows to allow full adjustment of all four "blades" via two X-Y stages. General specifications are: The material will be water-cooled Glidcop with Tungsten blocks. A pre-mask may be included for power protection. The maximum opening angle shall be sufficient to allow full FAPM fan to continue to the FOE without clipping. The slits will be motorized to allow selection of any part of the FAPM fan. As mentioned, the same X/Y stage shall be used for the XBPMs. The aperture stability shall be in the 1 µm range. This aperture stability specification is governed by the differential movement between the two X/Y slit units. For the high stability stages some form of additional coupling between stands may be required to constrain any differential movement.

Two sets of slits will be needed to operate independently both, the KB-branch and the ZP-branch. It has to be ensured that manipulating the beam of one branch does not influence the other branch.

Fast Gate Valve (FV)
The fast gate valve is to shut within a few milliseconds once triggered by FV sensors located in the front end and beamline whenever there is a sudden increase of pressure of a few decades. The stored beam has to be dumped prior to FV closing, and the cause then investigated and mitigated.

Safety Shutter
The safety shutter is actually a pair of shutters, required for redundancy, air actuated with independent redundant and diverse position sensing.

Preliminary ray-tracing

The design of the front end is not yet finalized, therefore a concluding ray-tracing cannot be presented at this time. However, in Appendix B the results of a ray-tracing calculation using a standard arrangement of the front end components is presented.

Beamline Design

Optical layout

The general concept of the SRX beamline is to offer two end stations where x-ray spectromicroscopy experiments can be performed with a spatial resolution in the sub-micrometer range. The energy range from E = 2 keV up to E = 25 keV will be covered. This concept will be realized by dividing the beamline into two branches, each served by an optimized, in-vacuum undulator with the two insertion devices arranged in a canted geometry. One branch will be equipped with focusing mirrors in a Kirkpatrick-Baez (KB) setup. As described later in this document, two sets of KB's will offer sub-µm focal spot sizes, where one set gives high flux at moderate resolution and the second set aims for a spatial resolution in the range of 100 x 100 nm^2. Using a slit system as a secondary horizontal source, the user of the SRX beamline will be able to choose between high flux or very high spatial resolution, depending on the application. By changing the slit settings, it will be possible to a certain extend to tune the focal spot size, as to better accommodate certain samples. The KB branch will operate with X-ray energies ranging from E = 4.65 keV up to E = 28 keV. The maximum of flux that can be delivered to the focal spot will be around 1.5 x 10^{13} phot/sec, and even with the highest possible spatial resolution 3.6 x 10^{11} phot/sec will be possible, according to the calculations. The second branch will use a Fresnel zone plate to reach a spatial resolution in the range of 30 nm or smaller in the energy range of E = 2 keV up to E = 15 keV, where the expected flux will be up to 10^{10} phot/sec. Photon flux and spatial resolution in that energy range will be unprecedented when comparing these key parameters to similar beamlines worldwide, which is due to the excellent performance of NSLS-II. The KB branch is a project beamline of the NSLS-II project; the ZP branch is not in the original scope. To ensure that a reasonable design and layout for the latter will be available when an approving decision will be due as well as to avoid mistakes when placing critical optical components of the KB branch, the design of the KB branch has to take basic design results for the ZP branch into account, as will be described in this report. A schematic layout of both branches starting with the two canted undulators and showing major optical components of the two branch lines is seen in figure 8. Note, that the angle between the two branches is exaggerated for illustration purposes.

For stability and performance reasons the double crystal monochromator for the KB branch will be horizontally deflecting. A positive side effect is an increase in distance between the two branches. The horizontal focusing mirror creates at the position of the secondary horizontal source aperture an image of the source. The image of the HFM is the source point for the horizontally deflecting KB mirror located downstream, whereas the vertically deflecting KB mirror is still looking at the original source. The KB mirrors will create a demagnified image of these both source points as a focal spot through which the sample will be scanned. A variety of detectors will be available for fluorescence, transmission and diffraction measurements. In the ZP branch two horizontally outward deflecting mirrors will create a secondary source spot as well, which is then again the source point for a zone plate creating a very small focus at the position of the sample. The two deflecting mirrors advantageously increase the distance between the branches even more, creating a manageable distance of about 57 cm to the KB branch at the downstream end of the ZP branch.

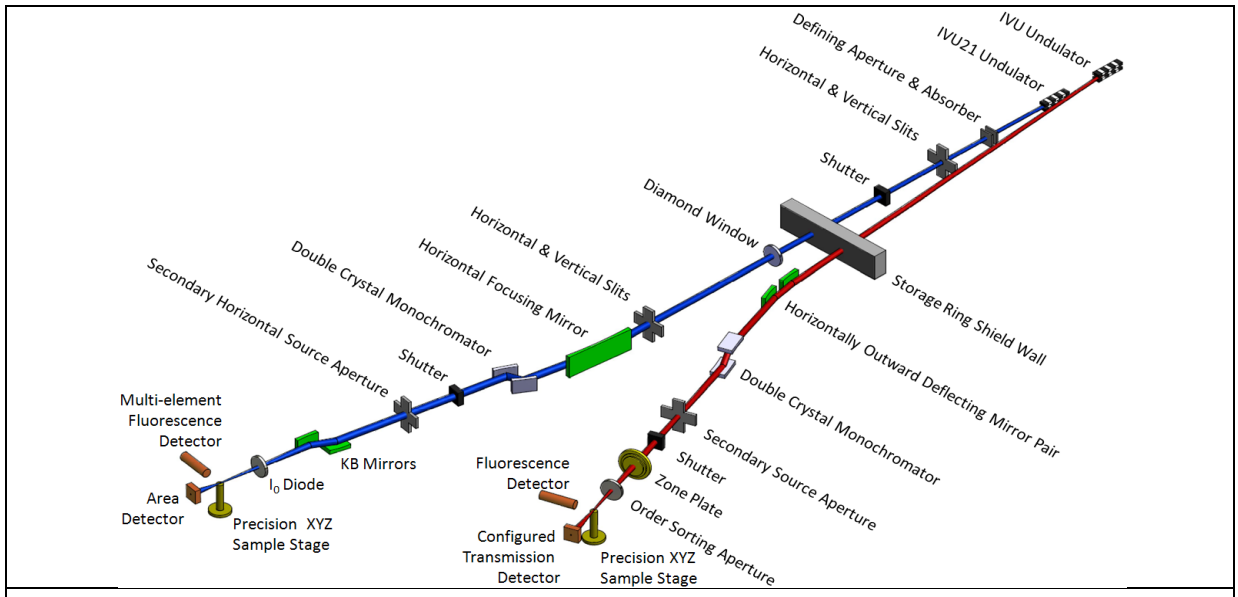

Figure 8: Sketch of optical layout of both branches of the SRX beamline. The branch hosting the ZP ist not in the baseline scope of the NSLS-II project.

Figures 9, 10 and 11 show the layout of the optical components of the KB and the ZP branch of the SRX beamline itself including the surrounding hutches and the beam pipes. The first hutch, starting at the ratchet wall, will be the First Optical Enclosure (FOE). Here, the horizontally focusing mirror and the double crystal monochromator of the KB-branch, and the mirror pair and the double-crystal monochromator of the ZP-branch will be installed. Due to the canted design of the undulators the x-ray beams for the two branches are very close. Therefore, the optical components for the KB branch have to be constructed in a way that room is available for the x-ray beam feeding the ZP-branch, which may be implemented at a later time. The hutch in the middle will host the end station of the ZP branch, the hutch farthermost downstream will be the place for the end station of the KB branch, including the KB mirror, the sample holder and the detectors. The secondary horizontal source aperture of the KB branch will be at the upstream end of the ZP branch hutch. Positions and dimensions are given in figure 9 and will be explained in later chapters of this document.

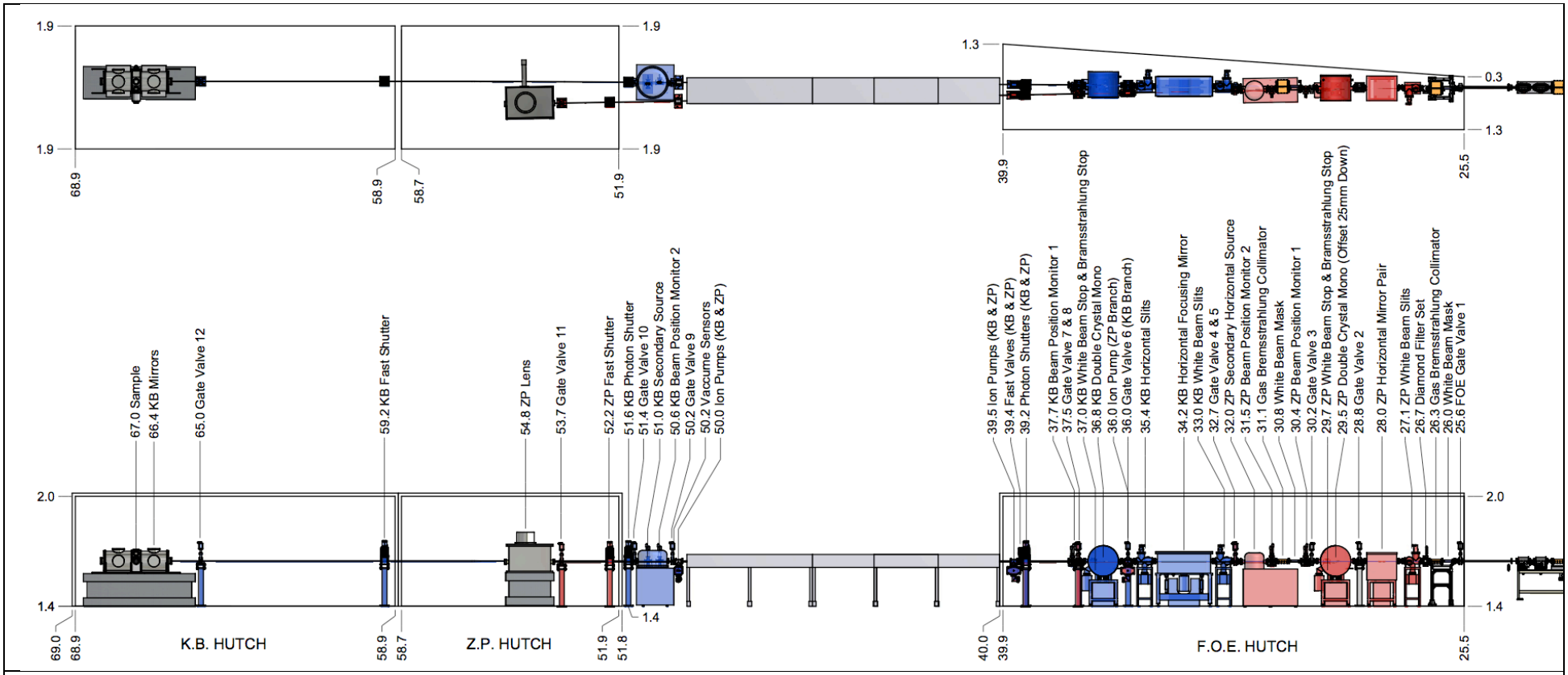

Figure 9: Sketch of optical layout of both branches of the SRX beamline. The branch hosting the ZP ist not in the baseline scope of the NSLS-II project.

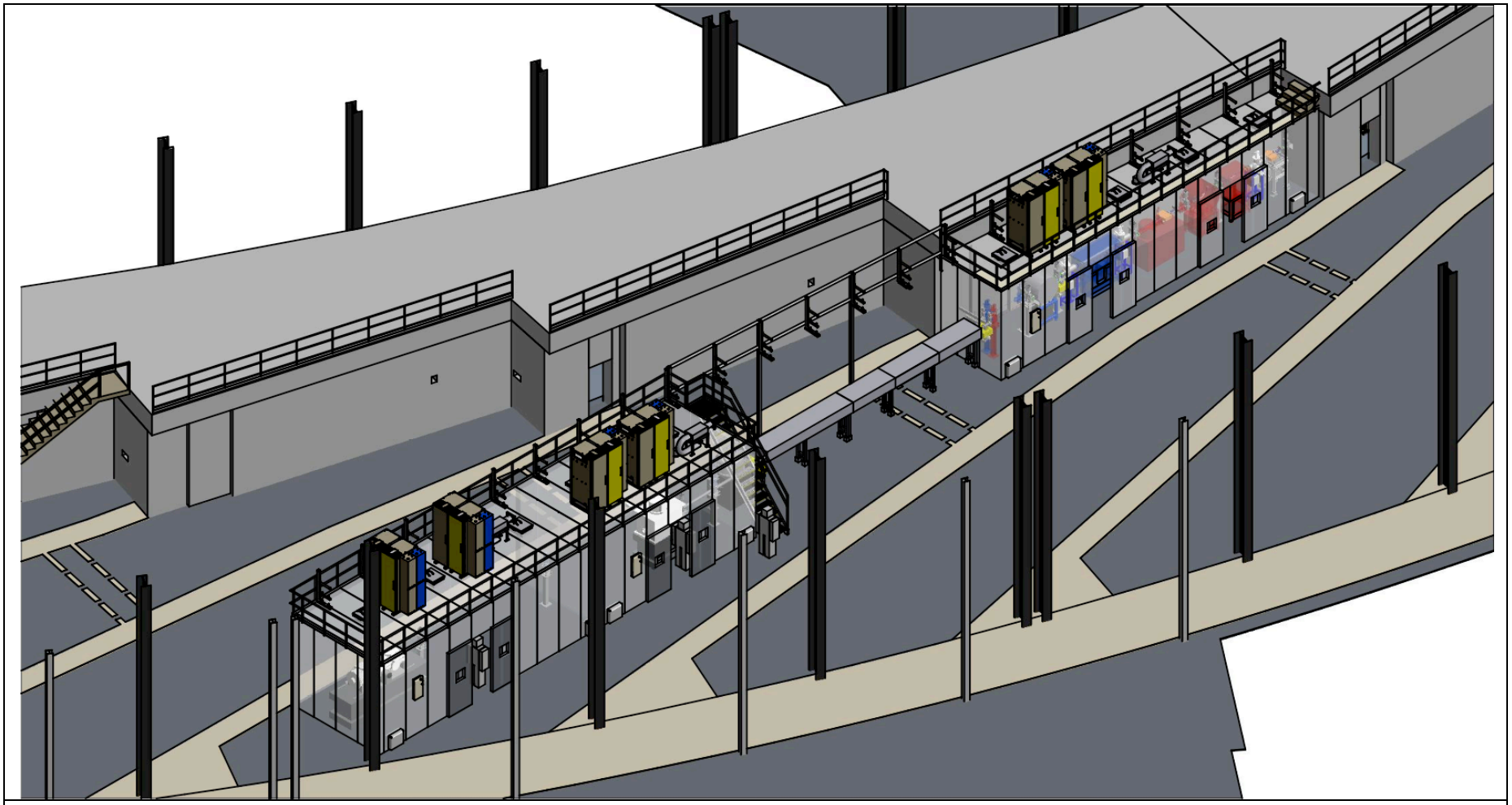

Figure 10: Model of the layout of both branches of the SRX beamline. The hutches are presented semi-transparent to show the optical components within.

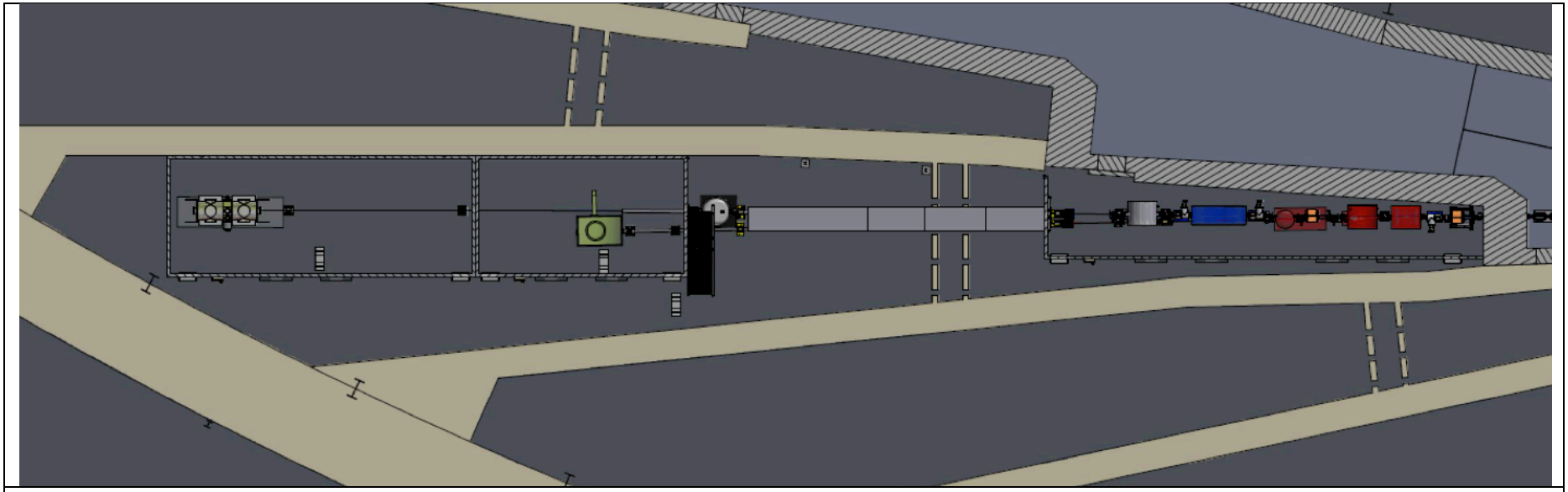

Figure 11: Model of the layout of both branches of the SRX beamline as in figure 14, but top view. The roofs and the components on top have been removed to show the interior.

Raytracing calculations KB branch

Ray tracing calculations have been performed to optimize the beamline layout proposed in the Conceptual Design Report. The location and the shape of main optical beamline components have been scanned, taking into account effects like the optics characteristics as well as the thermal load on crystal and optics. Attention was particularly paid to finding a way to improve the size and the spatial stability of the focal spot of the KB mirrors and the flux within.
The beamline has been parameterized for calculations with the ray-tracing program SHADOW VUI (by M.S. Del Rio) as follows:

- IVU21 undulator.
- Elliptical horizontally focusing mirror (HFM): useful length of 1.2 m, 2.5 mrad incident angle, 0.3 µrad average tangential slope errors.
- Double crystal monochromator (DCM): The two crystals are 8 and 18 cm long. Si (111) and Si (311) crystals are considered.
- Slits pair around the secondary source.
- 1 set of wide field KB mirrors: 40 cm / 40 cm long, 85 cm / 45 cm focal distance, 0.2 µrad / 0.2 µrad slope errors (horizontally / vertically focusing).
- 1 set of high resolution KB mirrors: 10 cm / 8 cm long, 18 cm / 8 cm focal distance, 0.1 µrad / 0.1 µrad slope error (horizontally / vertically focusing).

Reflectivity curves are applied to calculate the performance of the mirrors. The reflectivity of stripes of rhodium or silicon has been chosen according to the undulator energy. The reflectivity is graphically displayed in figure 12. Slopes errors of optical surfaces (deviation to perfect elliptical shapes) are taken into account by incorporating a 3D model of a ZEISS mirror surface, measured in an optical laboratory, into SHADOW. The measurements resulted in an average longitudinal slope error of 0.2 µrad (see figure 13). The surface elevation was linearly rescaled to reach slope errors of 0.1 µrad for the short KB mirrors and 0.3 µrad for the long HFM.

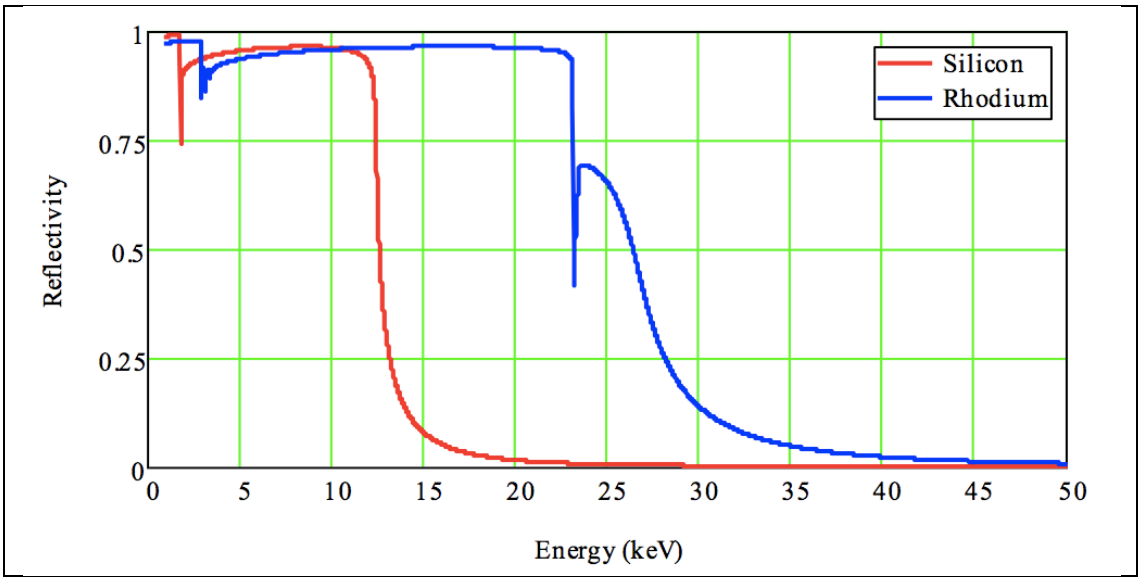

Figure 12. Reflectivity of silicon- or rhodium-coated mirror surfaces as a function of incident x-ray energy.

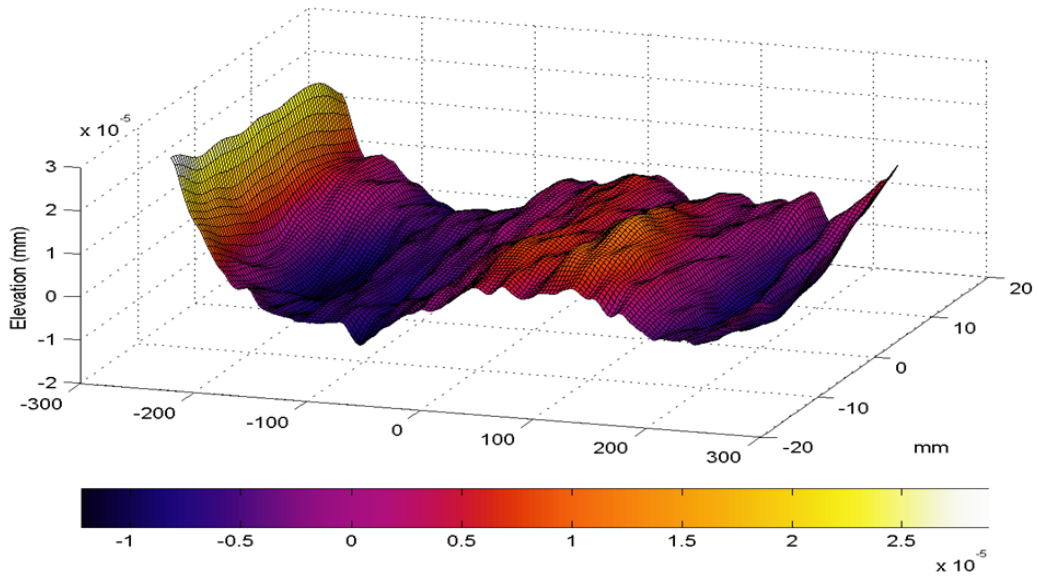

Figure 13: Topographic surface measured on a 50 cm long ZEISS mirror. The average tangential slope error is 0.2 µrad. This has been used with a rescaling factor for the SHADOW ray tracing calculations in this document.

High Heat Load Optics

In the layout proposed in the frame of the Conceptual Design Report, the first optical element has been the monochromator, thus being exposed to the white beam. The effects of the thermal load on the first crystal surface, in term of energy resolution changes, had been investigated. It was calculated by finite element analysis that the crystalline lattice deformation does not affect the monochromator's energy resolution, because the slopes generated on the expanded crystal by the white beam stay within the limit of the crystals rocking curve (see table 4). However, no attention was paid to the crystal distortion effects on the size of the beam at the secondary source aperture and at the position of the focal spot of the KB's. This point has been considered in detail, because residual slopes are significant in extreme cases, i.e. at the lowest energy, where the Bragg law requires obtuse incident angles. For instance, sagittal and tangential slope errors reach 35.1 µrad and 26.9 µrad respectively on a Si (311) crystal at E = 6.5 keV. The results are given below.

Table 4: Slope errors on the 1st DCM crystal exposed to white beam

Crystal Face	Energy	Rocking Curve Width	Tangential Slope Error	Sagittal Slope Error
Si(111)	4.65 keV	65.8 µrad	11.6 µrad	20.9 µrad
Si(111)	28 keV	9.9 µrad	2.5 µrad	1.0 µrad
Si(311)	6.5 keV	20.1 µrad	26.9 µrad	35.1 µrad
Si(311)	28 keV	3.8 µrad	2.6 µrad	0.8 µrad

The calculation of the effect of the slope error on the beamline performance has been performed with the program SHADOW. When a topographic surface as seen in figure 13 is applied to a crystal, the Bragg reflections are modified in the same way as for the total reflection. This means, in the program SHADOW the surface geometry is seen as a change in orientation of the crystalline lattice. The implication of this effect on the propagation of X-rays reflected from thermally deformed surfaces (derived from finite element analysis FEA calculations) was then calculated for several beamline configurations (see figures 14 to 17). FEA used the footprint on the crystal of the beam power density generated by the software SRW (developed by Oleg Tchoubar, NSLS-II). The total power of the beam of synchrotron radiation through a 94.6 x 100 μrad^2 aperture, which is slightly larger than the numerical aperture of the horizontally focusing mirror, is determined to 286 W. The calculations have been performed using just one set of KB's to focus the beam, as described in the conceptual design report. The slope errors for the KB mirrors were set to 0.1 μrad. With perfectly flat DCM crystals, the obtained focal spot size is 1290 x 100 nm^2 (H x V). However, the calculations using real numbers clearly show that placing a monochromator in the white beam will prevent us from getting a sub-micron resolution at low energy, where the power density on the crystals is very high due to large angles necessary for Bragg reflection. In the worst case, using Si (311) at E = 6.5 keV, local changes in the Si thermal expansion coefficient generate a narrow and relatively high bump in the middle of the crystal. In this case, the achieved spot size worsens dramatically to 1.6 x 7.2 μm^2. This would be unacceptable as a performance figure of the SRX beamline.

To enlarge upon these findings, more FEA and SHADOW calculations were performed, the FEA by V. Ravindranath, NSLS-II. First additional results showed that adding a diamond window upstream of the DCM is not sufficient to make the heat load effects negligible. As a result, the position of the DCM in the white beam, as it was initially proposed in the CDR, is not a useful option anymore. It has to be swapped with the HFM. The mirror is submitted to a much smaller power density due to its low incident angle with the beam. To understand the impact on the focal spot sizes, the thermal deformation of the HFM in the white beam and the DCM in the pink beam were calculated. Calculating the undulator spectra in two dimensions (here, 45 x 45 spectra through the 100 x 94.6 μrad^2 window at 33 m distance) using the SRW software, it is possible to model the power absorption due to the reflectivity of materials or through filters. FEA results show that the absorption of the high energy harmonics by the silicon of the HFM drastically decreases the slope errors of the 1st DCM crystal. Even in the most unfavorable cases, the vertical spot size is not anymore affected (see figure 19 and its associated table). Additional tests, consisting in adding diamond filters upstream of the HFM in the white beam, are very convincing, as the power is reduced even more. The spot size increase with the two, DCM and HFM, thermally deformed is smaller than with a perfectly flat DCM and a HFM showing slope errors of 0.3 μrad as a result of the polishing procedure. This confirms the location of the HFM as the first optical element and the use of diamond filters in the perspective of achieving a sub-100 nanometer resolution.

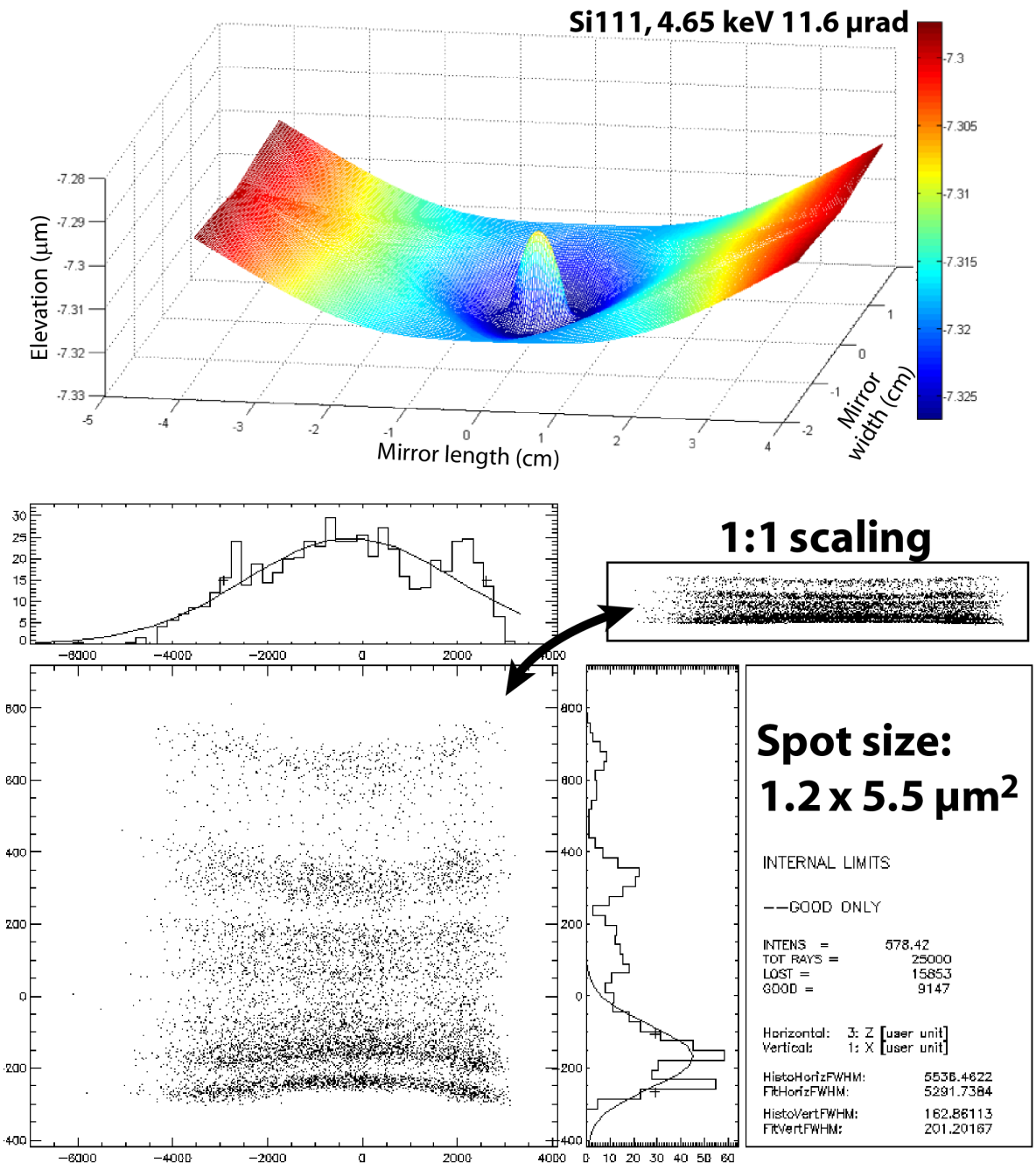

Figure 14: Top: Topographic surface calculated by Finite Element Analysis of the first DCM crystal in a white beam, the surface is Si (111), the X-ray energy is E = 4.65 keV. **Bottom:** SHADOW ray tracing calculation of the spot size on the sample, taking into account the deformed surface of the first DCM crystal due to the thermal load. The vertical spot size increases here of a factor 10 compared to an ideal surface.

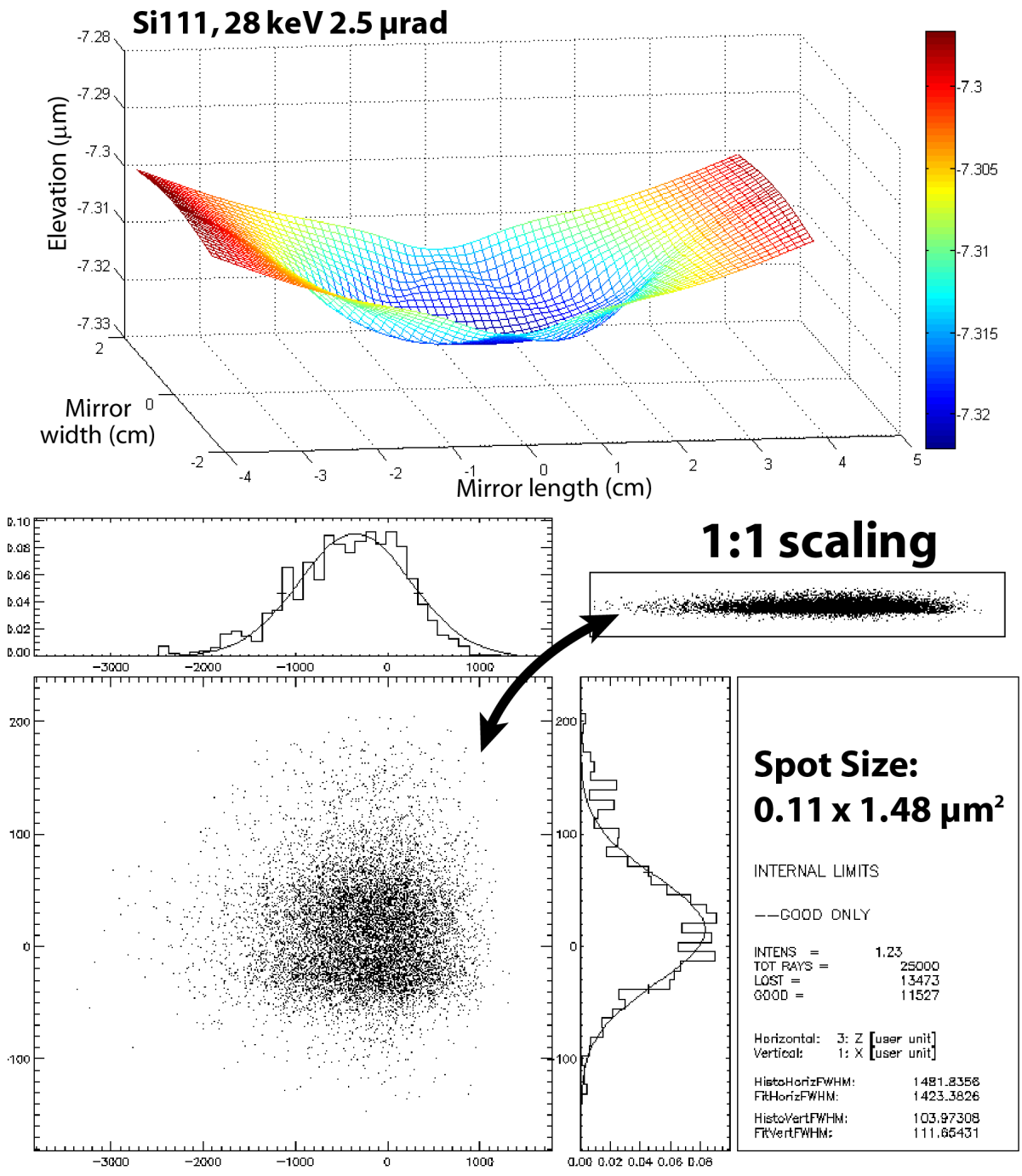

Figure 15: Top: Topographic surface calculated by Finite Element Analysis of the first DCM crystal in a white beam, the surface is Si (111), the X-ray energy is E = 28 keV. **Bottom:** SHADOW ray tracing calculations of the spot size on the sample, taking into account the deformed surface of the first DCM crystal due to the thermal load. The vertical spot size increases here only 10 nm.

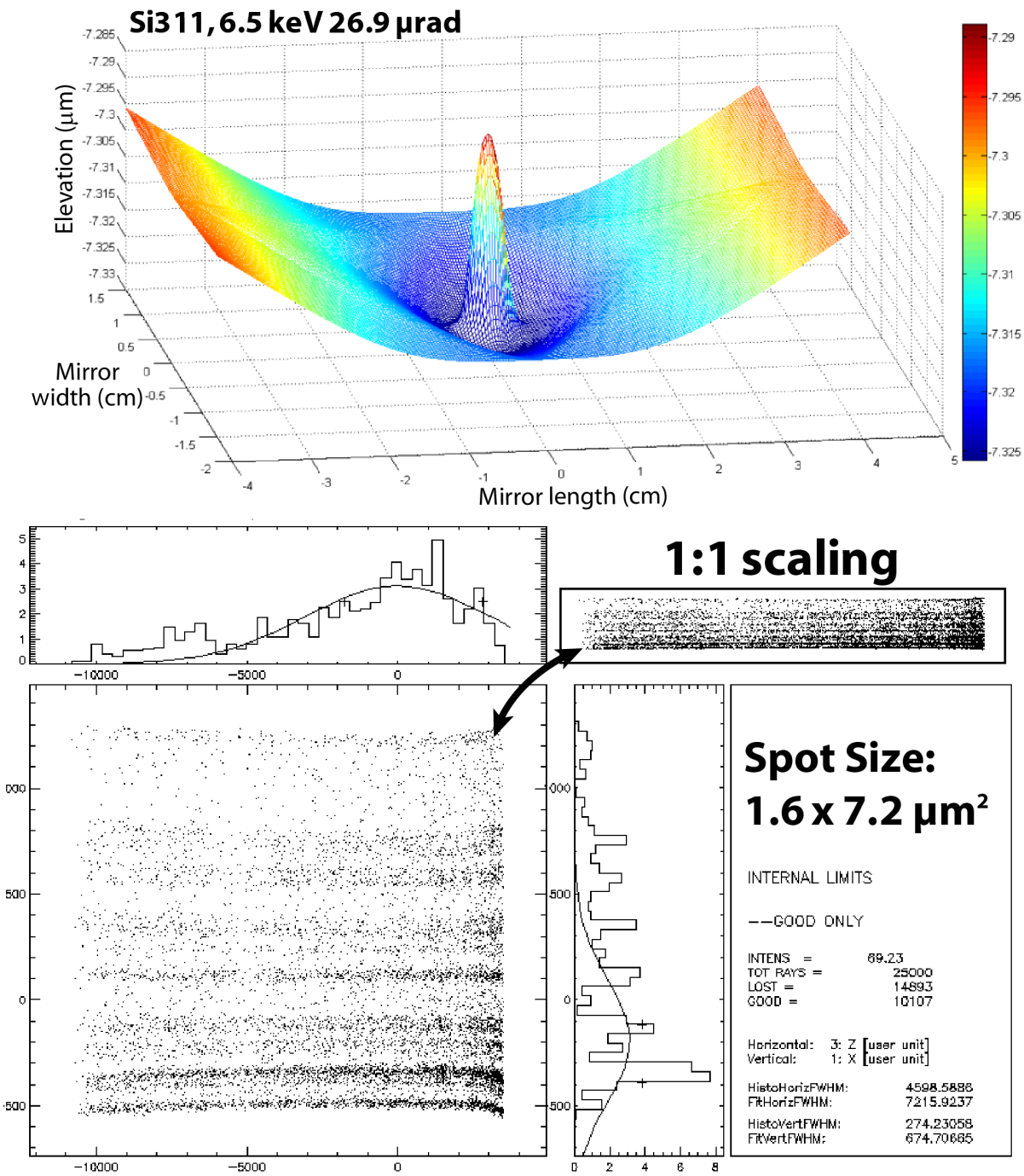

Figure 16: Top: Topographic surface calculated by Finite Element Analysis of the first DCM crystal in a white beam, the surface is Si (311), the X-ray energy is E = 6.9 keV. **Bottom:** SHADOW ray tracing calculations of the spot size on the sample, taking into account the deformed surface of the first DCM crystal due to the thermal load. In this worst case in terms of power density, the horizontal spot size exceeds 7 µm.

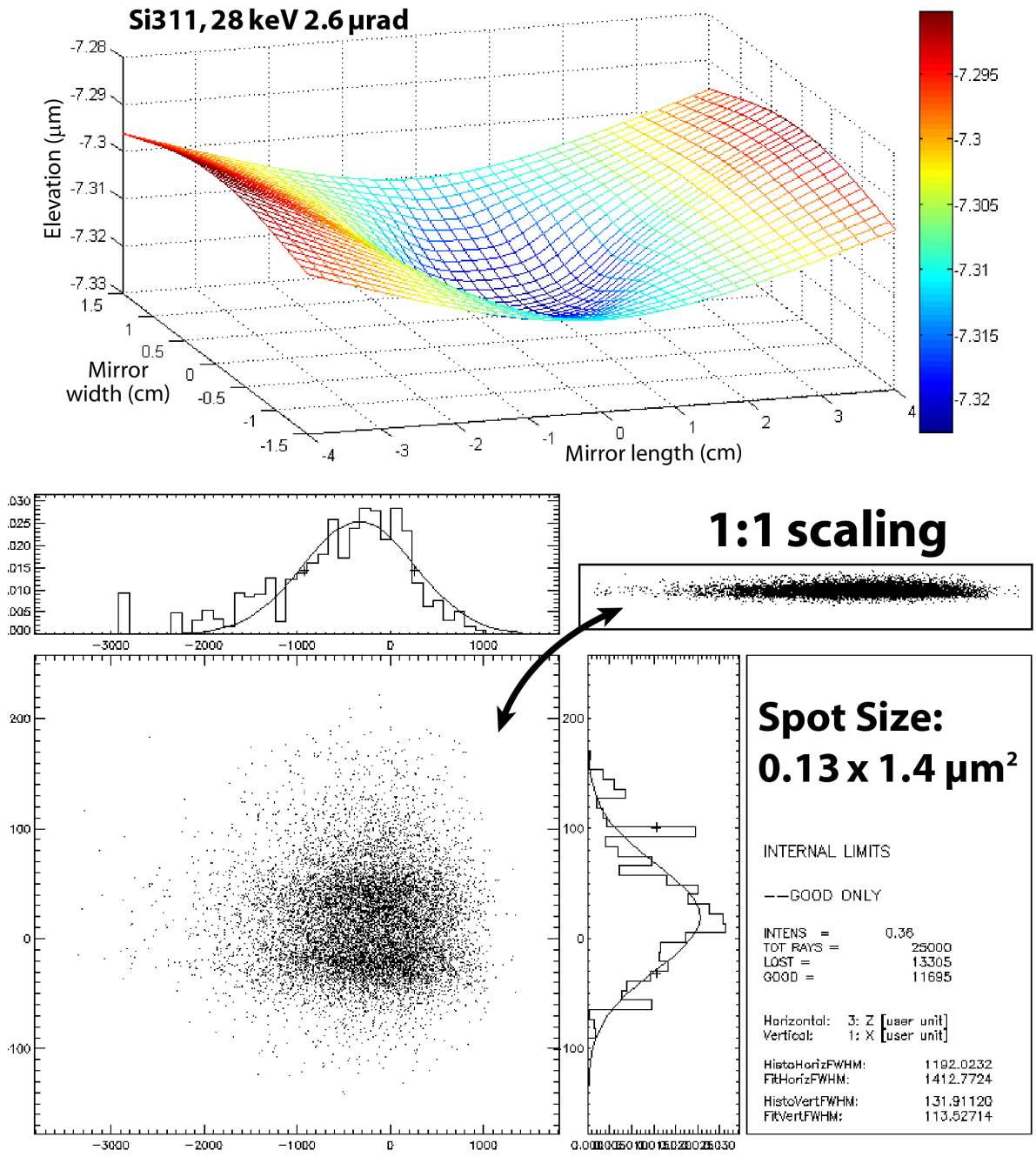

Figure 17: Top: Topographic surface calculated by Finite Element Analysis of the first DCM crystal in a white beam, the surface is Si (311), the X-ray energy is E = 28 keV. **Bottom:** SHADOW ray tracing calculation of the spot size on the sample, taking into account the deformed surface of the first DCM crystal due to the thermal load.

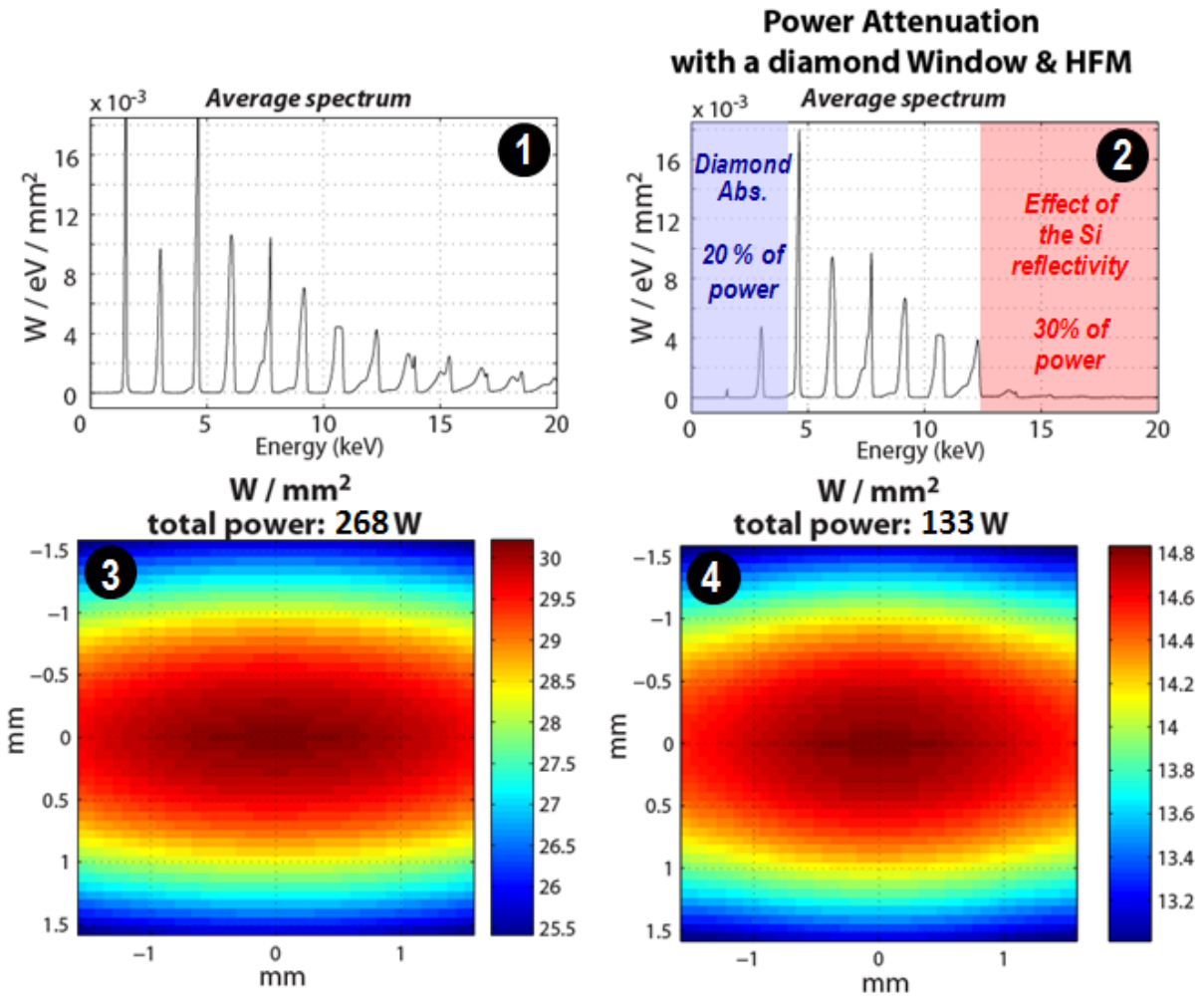

Figure 18: Calculation of the power density deriving from an IVU21 undulator at 33 m through a 94.6 x 100 µrad² aperture, using the SRW software developed by Oleg Tchubar, NSLS-II. (1) Average spectrum of the undulator. (2) Average spectrum after the absorption of power by a 20 µm thick diamond window and after the reflection from the silicon surface of the HFM. In total, 50 % of the white beam power is removed. (3) Cross section of the beam power transmitted through the aperture. (4) Cross section of the beam power transmitted after the transmission through the diamond window and the reflection from the silicon surface. Note the different values of the color scheme.

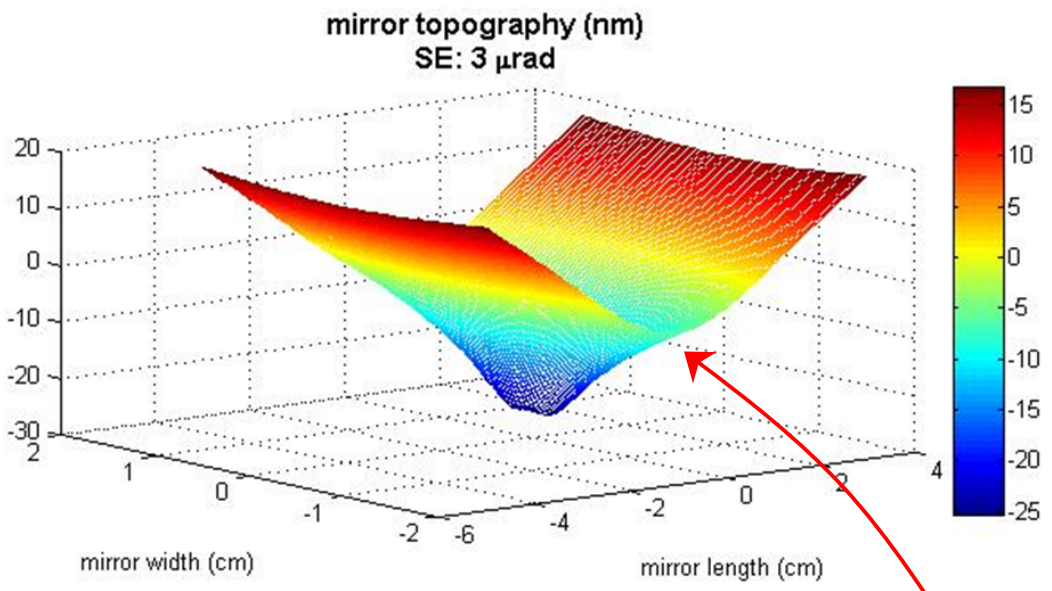

Crystal Face	Energy	Rocking Curve Width	White Beam DCM Slope Error	Pink Beam DCM Slope Error
Si(111)	4.65 keV	65.8 µrad	11.6 µrad	3.0 µrad
Si(111)	28 keV	9.9 µrad	2.5 µrad	2.9 µrad
Si(311)	6.5 keV	20.1 µrad	26.9 µrad	0.3 µrad
Si(311)	28 keV	3.8 µrad	2.6 µrad	4.1 µrad

Figure 19: Summary of slope errors on the 1st DCM crystal located in pink beam downstream the HFM (without a diamond filter). Top: Visualization of the surface for the Si (111) / Pink Beam case with 3.0 µrad slope error. The 3D surface data were derived from FEA for each case displayed in the table and were used for the ray-tracing calculation. In the case of the Si (111) crystal at E = 4.56 keV, the thermal deformation of the surface magnifies the focal spot from 1268 x 103 nm^2 to 1422 x 104 nm^2(H x V), with a loss in intensity of about 25 %.

Optimization of the location of the optical elements

The impact of the locations of the HFM, the secondary source, the KB's and the sample stage on the beamline performance has been calculated using Shadow VUI. IN comparison to the originally planned place on the experimental floor, the new position 29-ID for the SRX beamline allows a beamline length 6 m longer than what was initially foreseen. This makes it possible to get a higher demagnification of the source, at least in the vertical plane. It has been evaluated how the locations of the HFM, the secondary source and the sample stage influence spot size and flux when placed within the intervals [33.8 m to 40 m], [45 m to 65 m], and [55.5 m to 70 m], respectively. These lengths state the distances of the components from the source point, the center of the

undulator. The strong correlation between flux and the focal spot size of the KB's with these lengths were calculated with SHADOW VUI using the macro editor added to the used version of the program. Our code, written in IDL, has permitted to record the flux, the horizontal, and the vertical spot size of the beam at the sample location in three 3D matrices. The dimensions of these matrices are the HFM location, the secondary source location and the sample location, as can be seen in figure 20. A couple of constraint had to be considered throughout the calculations. After first calculations it became clear, that the slope error induced by the white beam on the 1st crystal of the DCM results in a much worse focal spot size than with the HFM put into the white beam. Therefore, the HFM has swapped places with the DCM within the FOE, exposing the HFM now to a white beam. Secondly, it is clear that the larger the distance of secondary source from the KB's is, the better the demagnification is, and the smaller the expected focal spot size can be expected. The constraint is to avoid placing it into the zone plate hutch in order to keep the ZP and the KB hutches as much independent as possible. There is, however, no issue in placing it outside of a hutch, proper shielding provided. This results in a much larger distance to the KB's as in the CDR anticipated. The optical layout of the CDR had foreseen the use of just set of KB mirrors. In combination with an adjustable size of the secondary source aperture, it was possible with that design to tune continuously between a spot-size showing just sub-micron dimension in the horizontal direction and a high-resolution sub-100 nm spot. The vertical spot size stays throughout these adjustments unchanged at about 100 nm in size. An alternative solution, comprising of two KB mirror sets will be discussed in this report. One set allows for a very high spatial resolution, whereas using the other set results in moderate resolution at high flux. Each set is optimized for its specific task. The design will make it possible to have each of the 2 KB sets tuned and ready to use in half a minute by translating very accurately the high flux KB into or out of the beam. The possibility to install the DCM inside the KB hutch was also studied.

In summary, the following three layouts are discussed.

- **Layout 1:** hybrid KB set of the CDR (fig. x & x)
- **Layout 2:** displacement of the secondary source, use of 2 KB sets
- **Layout 3:** Horizontal collimating mirror, no secondary source, DCM in the KB hutch

The first result of these calculations is that the HFM location has little impact on the characteristics of the focal spot. In **layout 1** the secondary source must stay close to the sample (1-2 m distance), if we want to maintain a high flux. This results from the increase of the beam divergence by the HFM, as it is de-magnifying the source. Thus, the numerical aperture of the KB horizontally focusing mirror doesn't match anymore to the beam size if the secondary source moves upstream. Moreover, moving sample position and horizontal secondary source 10 m downstream, because of the extended beamline length in the new position on the experimental floor, leads to a longer focal distance of the HFM, and so, to the drop of the demagnification of the source. This results in a dramatic increase of the horizontal focal spot size of the KB. Also, keeping the positions of secondary source and sample close implies a small demagnification of the secondary source by the KB. In order to reach a small "square" spot (high resolution mode) with a horizontal spot size around 100 nm the slits of the secondary source have to be closed below 4 μm width. Keeping such a small aperture perfectly stable in the course of time is very challenging. It would however be imperative because a 0.1 μm aperture variation results in a modification of the spot size of several tens of nanometers. Another issue to

consider is, that reaching a spot size close to 100 nm with just one set of KB's is at present not realistic because for the demagnification factors it requires, an optical quality of the surface is needed which nowadays is not achieved (see below).

In **layout 2**, the high flux KB's allow to achieve a higher beam intensity in the focal spot than in layout 1, showing as well a less ellipsoidal spot shape (1018 x 827 nm^2 in comparison to 1300 x 103 nm^2, H x V), having the secondary source slits wide open. If an experiment requires an energy resolution better than standard, the slits of the secondary source have to be closed. This will, however, not result simultaneously in a much better spatial resolution, in contrast to layout 1. However, the spot can be adjusted to a more spherical shape. For this, the slits have to be closed to a width of 14 µm, a size that can be much better handled than the very small size needed for layout 1. The high resolution KB's focus to beam down to a spot size of 183 x 63 nm^2 (H x V) even with open slits. The flux obtained with the setup is coming close to the flux delivered with layout 1 having the slits closed. Closing the slits again only to more reasonable values, very high resolution can be achieved with a focal spot size around 60 x 60 nm^2. These excellent results for a vertical spot size of about 60 nm has been achieved with a mirror showing an average slope error (SE) of 0.1 µrad but also a peak to valley (PV) around 10 nm. At present, measurements on mirrors from the company JTEC show a much smaller PV of 0.5 nm. Therefore, an even smaller spot size could be expected. Of course, it has to be secured that vibrations and thermal instabilities are not hampering this excellent optical performance.

In **layout 3** the white beam is just collimated with the HFM. As the mirror surface is adjusted by a bending mechanism, tuning the curvature of the mirror body to the needed value could set up the collimating mode. A horizontally parallel beam, giving very high spectral resolution, will be the result. This allows placing the DCM at whatever position downstream of the HFM, e.g. even in the hutch of the KB end station. The clear advantage of such a layout would be that it provides excellent stability. The DCM could be placed very close to the KB's in order to decrease the lever arm of any beam motion. Moreover, the heat load on the DCM would be also minimized, as instead of a focused beam only a horizontally collimated and vertically divergent beam illuminates the 1st crystal. Finally, because the beam is horizontally parallel due to collimation, the as well horizontally deflecting DCM would work with the best energy resolution possible for a set of crystals. A disadvantage would be that a pink beam has to be transported through the hutch of the ZP branch and would reach the hutch of the KB, causing considerable additional problems with radiation safety. The secondary source aperture would have to be open, showing no influence on the beam anyway. With this setup it is not possible to achieve a very high spatial resolution and to mask the source instabilities in the horizontal plane. Nevertheless, it is worth to keep the possibility to work in a collimated beam mode in order to perform spectroscopy with the maximum energy resolution possible for all sets of crystals.

We strongly give priority to layout 2, for the following reasons. The fact of using just one set KB's prevents the beamline from being fully optimized. For the case of very high resolution as well as for very high flux, there will be trade-offs with one set of KB's. A 10 cm long vertical focusing KB mirror (VFM) as one of the high resolution KB's is much more adapted than a 28 cm long KB VFM of layout 1 for producing very a small spot size as the mass reduction improves the stability of mobile parts a lot, e.g. the pitch mechanism of the mirror. Using a first small mirror in a KB set also permits to reduce its

focal length, and so, to increase demagnification factor. Moreover, it will be extremely difficult to get the same polishing quality for a long mirror as for a short one. Assuming the same mirror quality (slope error: 0.1 µrad), we expect a vertical spot size of 50 nm with layout 2 in comparison to 100 nm obtained with layout 1. If we consider an average slope error of 0.2 µrad on the 28 cm long KB VFM, the vertical focal spot size jumps to more than 200 nm. At present, a slope error of 0.1 µrad can only be achieved on mirror shorter than 10 cm in length. When working in a large beam mode, i.e. the slits of the secondary source open, the spot shape achieved with layout 1 is very asymmetric (1200 x 100 nm^2, H x V). One advantage of layout 2 is that the slits of the secondary source have to be closed to no more than to 15 µm. Instabilities in the position of the slits will lead to much smaller spot size modifications than in layout 1.

Considering the demagnification of the X-ray source on a 66 m long beamline necessary to achieve a sub-100 nanometer resolution, the use of cutting edge optics like mirrors from the company JTEC with an average longitudinal slope error of 0.1 µrad is required. A price estimation for a 10 cm long JTEC mirror lies around $ 80,000. If the price only increases linearly with the length of the mirror, a 28 cm long KB VFM as in layout 1 would cost around $ 225,000. However, it is clear from experience, that this is too low an estimate. Again, the question stays unanswered, whether such a mirror can be fabricated at all.

The simplicity for a user to tune between high and lower spatial resolution is in favor of layout 1, as only the slits of the secondary source have to be moved. However, this switching should be simple and easily manageable for layout 2. The reason is, that high resolution and low resolution KB's are lined up behind each other. This means, the high resolution KB's, which are at the downstream end, have to be adjusted only once. After that, these mirrors will be left statically in place. Only the high flux KB's will go in and out of the beam. When these KB's are moved into the beam, they will deviate the beam from hitting the high resolution KB's and focus the radiation directly onto the sample. This can be done by a simple and reproducible translation. The focused beam will be sufficiently deviated to not touch the high resolution KBs. Therefore, even for an inexperienced user of the beamline, it will be possible to switch easily between the two resolution modes. The company Bruker-ASC has performed repeatability tests vertical KB positioner (data recorded in opened loop, without feedback of the encoders), showing that the mechanics of such a KB set should be precise enough to keep the high flux KB's still tuned after many in/out cycles. An even better test for this would have been to perform a knife edge measurement after each movement, however, this is still a pending experiment.

If it is inescapable for an experiment to work with very voluminous samples or complex extended environments, requiring a significant working distance, the setup can be designed in such a way, that it will be possible to remove the high resolution KB's including the mechanics as one module and to adapt the focal length of the high flux KB's mirror with dynamic bending according to the needs of the experiments. This characteristic is particularly important for tomography.

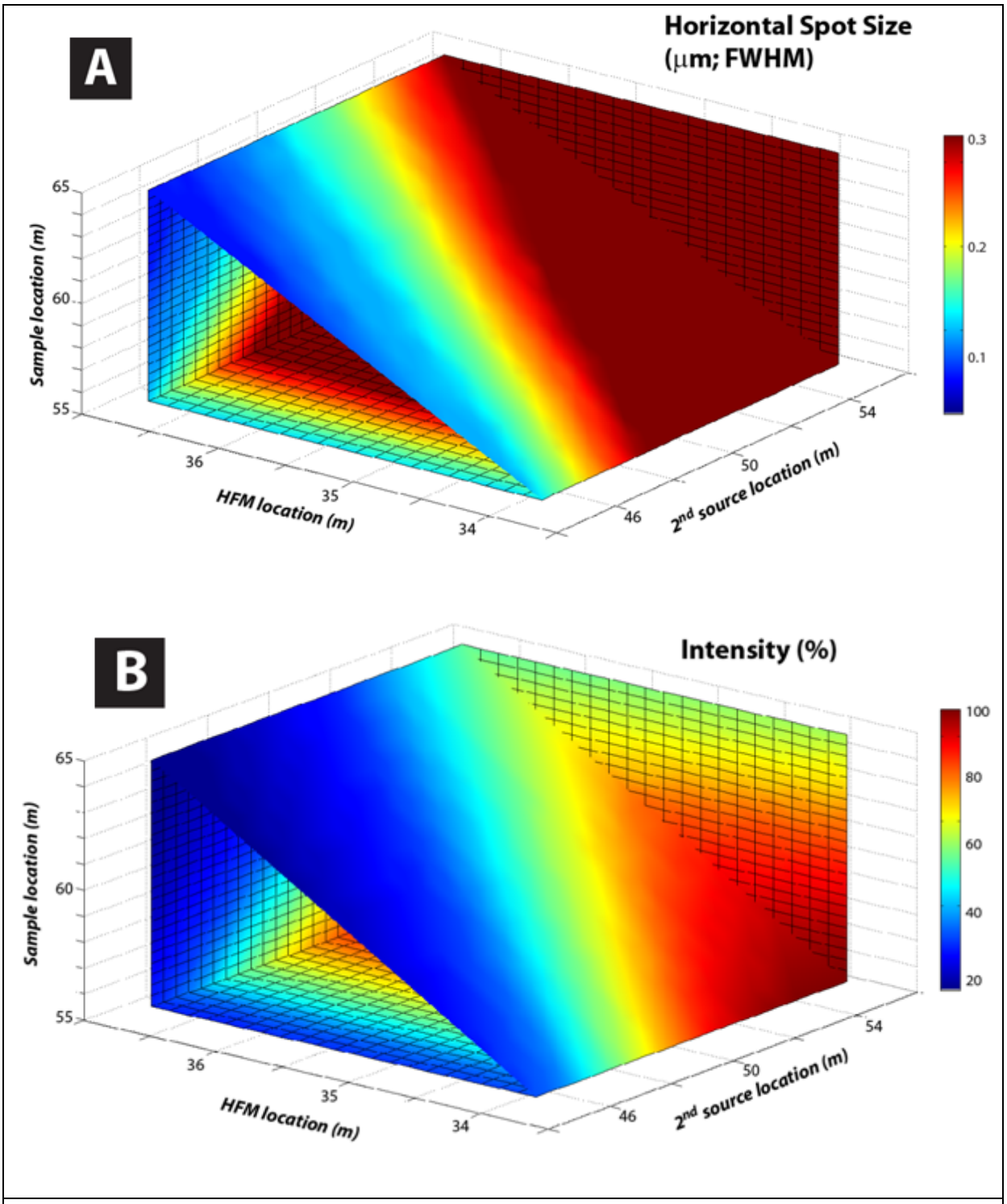

Figure 20: 3D matrices of the flux (A) and the horizontal spot size at the sample location (B) as functions of the HFM location, the secondary source location and the sample location. These 3D matrices were calculated for the layout 1 and 2. The scale of flux is arbitrarily normalized between 0 and 100%, 100% being attributed to the voxel having the highest flux.

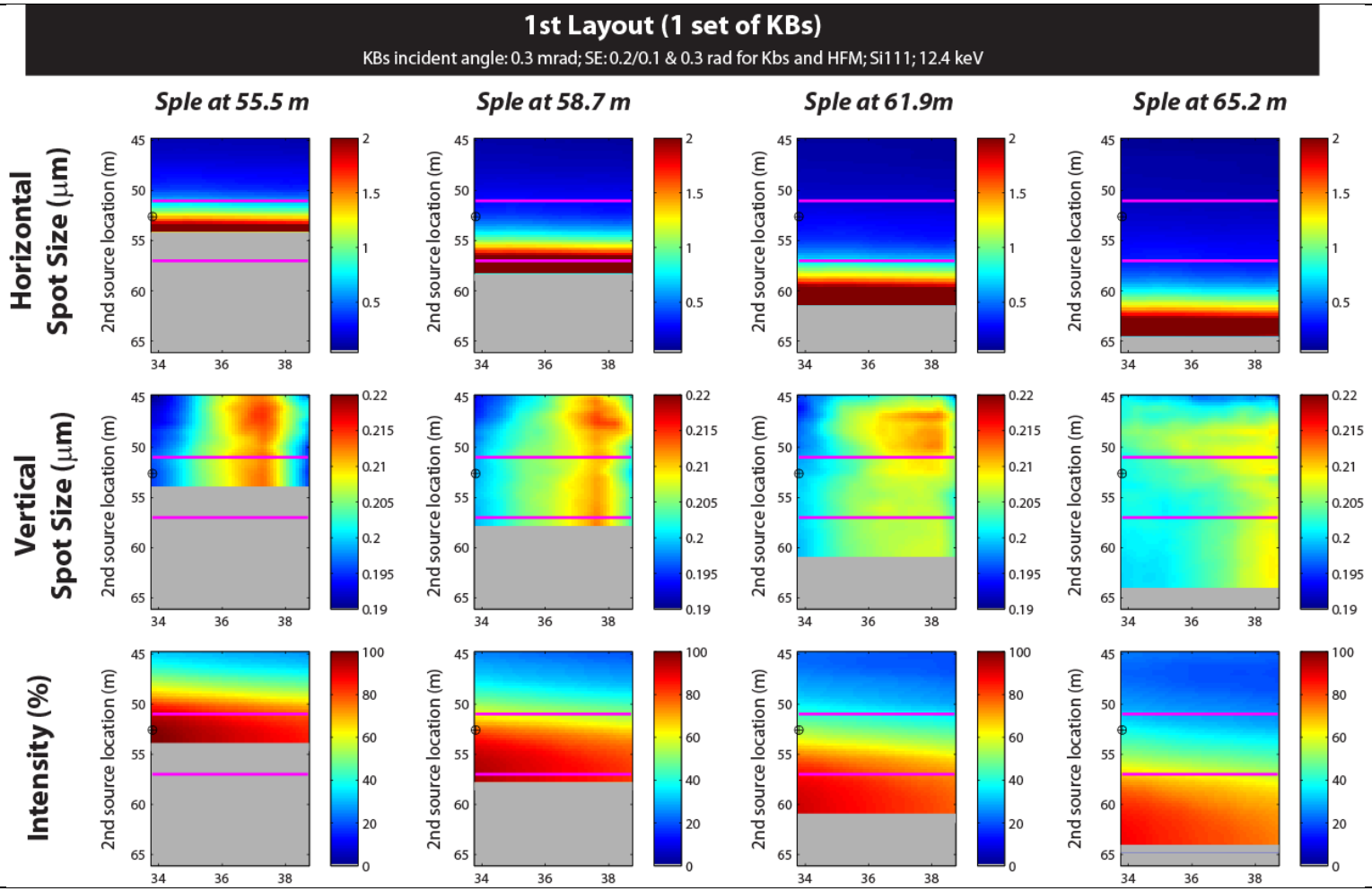

Figure 21: SHADOW ray tracing results for layout 1, the layout presented in the CDR. These 2D maps represent slices of the 3D matrices shown in figure 20, cut along the "sample location" axis. Columns correspond to different "sample locations whereas rows correspond to the horizontal spot size, the vertical spot size and the intensity (100% of intensity is attributed to the flux obtained in the CDR configuration: marker ⊕). Purple lines represent the ZP hutch walls.

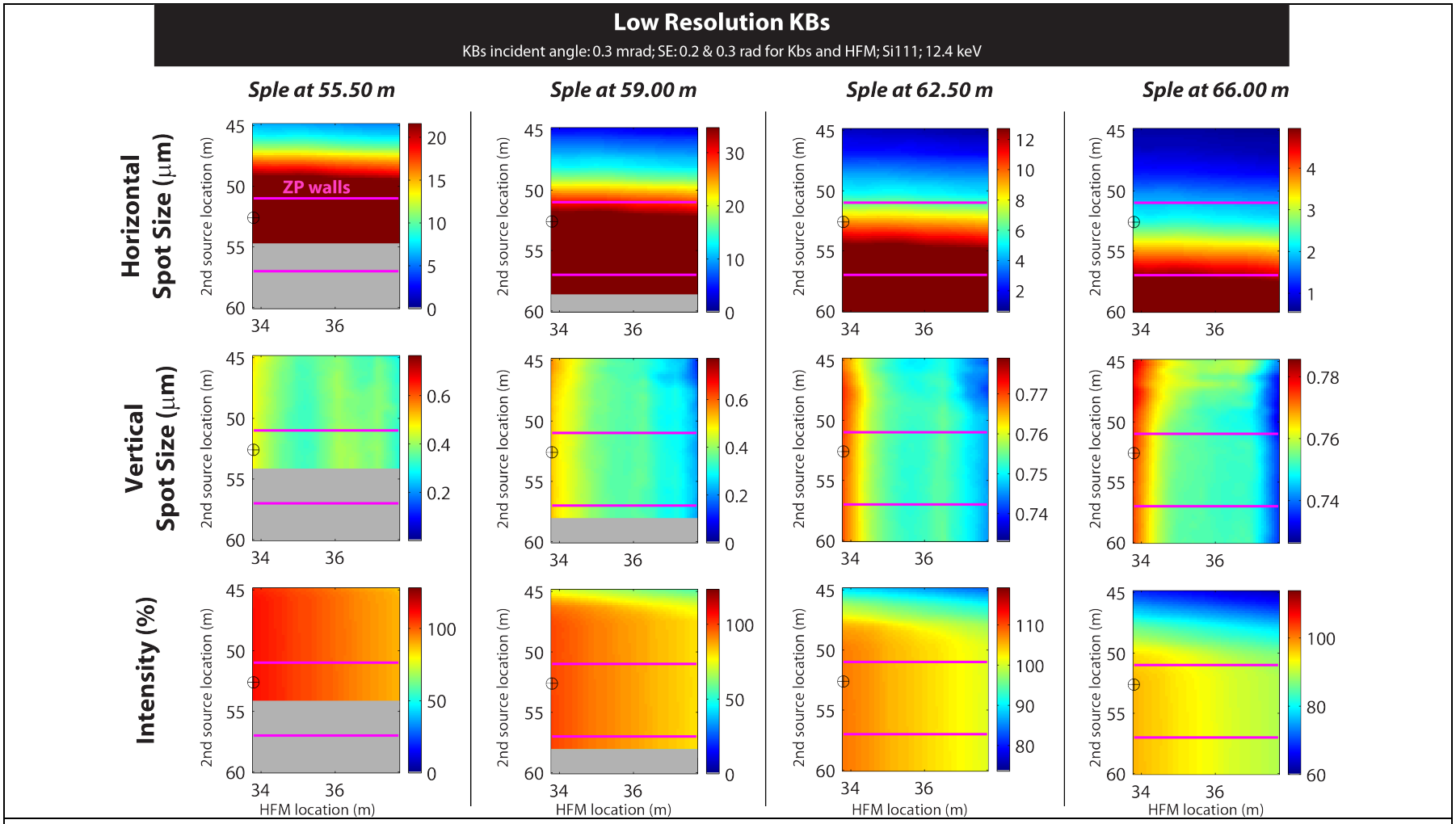

Figure 22: SHADOW ray-tracing results for the high flux KB set. For an explanation of this visualization see figure 21.

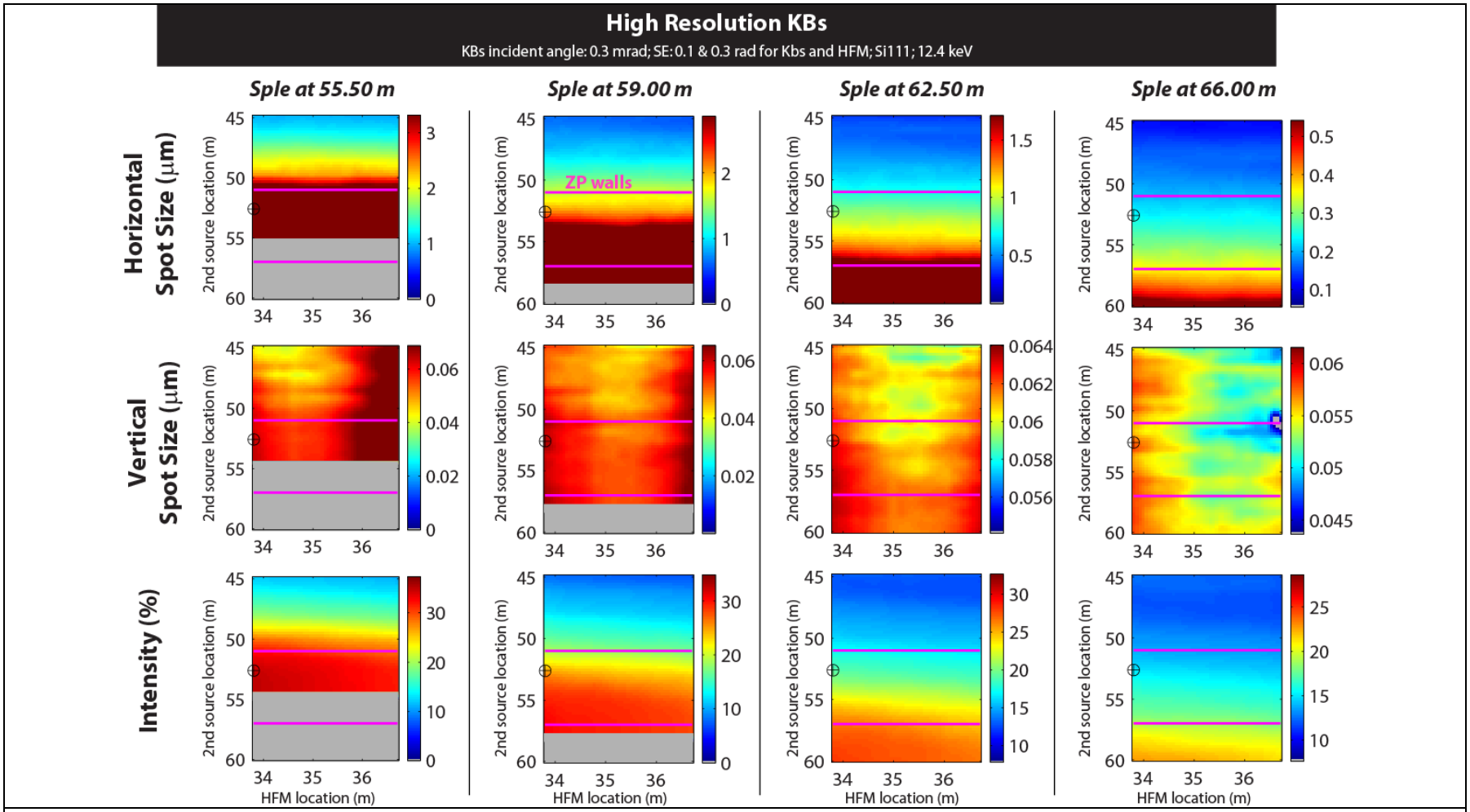

Figure 23: SHADOW ray-tracing results for the high resolution KB set. For an explanation of this visualization see figure 21.

Table 5: Results of the SHADOW ray tracing calculations for layouts 1-3 (see text). The size (FWHM) of the smallest obtainable focal spot along with parameters as photons/sec, secondary source aperture slit size and energy resolution can be seen. The calculations were made for a central energy of E = 12 keV.

Parameters for the flux calculation		
IVU21 ph/s/0.1%bw	Energy range	Central energy
2.2124E+14	10	12000

			12 keV, Si111, KB angle: 4 mrad Slope errors: 0.3 µrad on HFM, variable on KBs												
			Elliptical FHM --> secondary hor. Source												
	Sample distance (m)	SE KBs (µrad) M1/M2	Slits opened						Slits closed						
			Intensity shadow	Intensity %	Intensity ph/s	H FWHM (nm)	V FWHM (nm)	En. Res. (eV)	Intensity shadow	Intensity %	Intensity ph/s	H FWHM (nm)	V FWHM (nm)	Slits aperture	En. Res. (eV)
Original layout (CDR)	*55.5*	*0.2 / 0.1*	*1376*	*100*	*1.01E+13*	*1288*	*198*	*2.12*	*217*	*16*	*1.6E+12*	*193*	*193*	*8 µm*	*2.00*
Original layout	*66*	*0.2 / 0.1*	*1290*	*94*	*9.51E+12*	*1967*	*194*	*2.27*	*128*	*9*	*9.4E+11*	*195*	*193*	*8 µm*	*2.02*
High Res. KBs	*66*	*0.1 / 0.1*	**137**	**10**	**1.01E+12**	**183**	**63**	**1.38**	**49**	**4**	**3.6E+11**	**61**	**62**	**14 µm**	**1.27**
Wide Field KBs	*66*	*0.2 / 0.2*	**2118**	**154**	**1.56E+13**	**1284**	**756**	**2.98**	**1031**	**75**	**7.6E+12**	**782**	**754**	**35 µm**	**2.07**
			Collimating HM --> secondary hor. Source to the infinity												
Original layout (CDR)	*55.5*	*0.2 / 0.1*	*379*	*28*	*2.80E+12*	*176*	*193*	*1.36*							
Original layout	*66*	*0.2 / 0.1*	*340.6*	*25*	*2.51E+12*	*175*	*194*	*1.37*							
High Res. KBs	*66*	*0.1 / 0.1*	**131**	**10**	**9.65E+11**	**176**	**62**	**1.36**							
Wide Field KBs	*66*	*0.2 / 0.2*	**1621**	**118**	**1.20E+13**	**1163**	**748**	**2.28**							

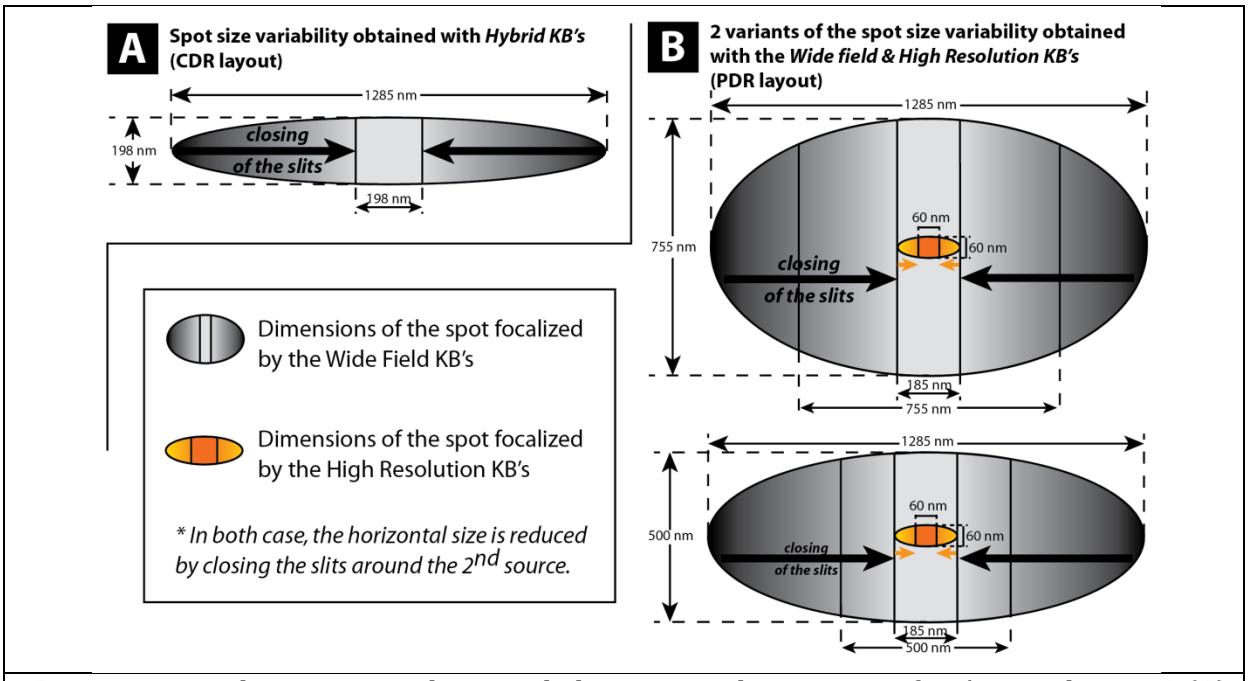

Figure 24: Focal spot size at the sample location with a one set of KB's as in layout 1 (A) and with two sets of KB's as in layout 2 (B). The use of two sets allows to achieve a better spatial resolution (high resolution KB set, orange ellipse) and to get a higher flux (high flux KB set, gray ellipse). The possibility to change the spot size by adjusting the slits of the secondary source aperture exists for each set in both layouts. In (B), two versions of the high flux KB's are shown. The top one delivering a vertical spot size of 755 nm has been used for the calculations of the table 5. The second version, below, uses a shorter vertical focusing mirror allowing a better demagnification but with a shorter numerical aperture (vertical spot size down by 50%, flux decrease of about 15 %).

In summary, all calculations result in that the use of the DCM as the first optical element in the white beam is not suitable for a sub-micron resolution and even more for a sub-100 nanometer focal spot size, which is the objective of the SRX beamline. The addition of diamond filters with an adaptive thickness to remove as much as possible the power of not-used low harmonics of the undulator in relation to the selected X-ray energy, combined with the swap of positions of the DCM and the HFM, allow to reduce dramatically the slope errors generated by heat load on the DCM surface. The increase of the distance between the KB's and the secondary source aperture permits to solve the issue pointed out in the CDR about the slit stability of the secondary source, without affecting the SRX beamline performance. The use of two sets of KB's provides sub-µm resolution with the possibility to additionally obtain sub-100 nm resolution.

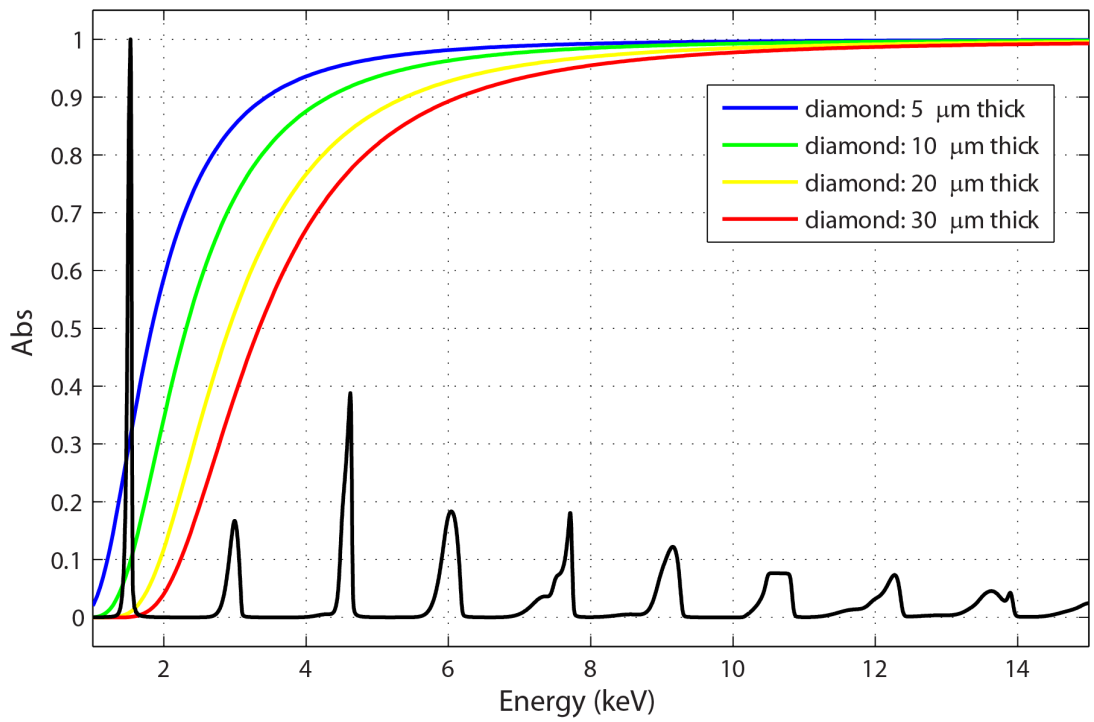

Figure 25: Absorption of diamond as a function of X-ray energy. Four different thicknesses of diamond windows are plotted together with the peaks of the undulator harmonics of IVU 21 (the spectrum is averaged through a 100 x 94.6 µrad^2 numerical aperture and normalized to 1).

Raytracing calculations ZP branch

The layout of the zone plate branch presented in the CDR aims to illuminate coherently a 300 µm wide Fresnel zone plate in order to get diffraction limited resolution with a focal spot size around 30 nm. Looking in more detail into the design, a concern about the layout has been found. The zone plate will image a source of radiation and thus create a focal spot. The source points horizontally and vertically, however, differ significantly. In the original design, the undulator source will be focused horizontally into the position of the secondary source, whereas vertically the zone plate would see the undulator directly

as a light source. The distance between horizontal and vertical source would then be 32 m, having the secondary source 18 m upstream of the zone plate and the undulator in 50 m distance. This difference would cause a large astigmatism. With the image equation

$$1/g + 1/b = 1/f\,,$$

the positions of the horizontal focus and the vertical focus can be calculated. A zone plate with 330 µm diameter, an outermost zone width of 25 nm and a focal length of 82.5 mm at E = 12 keV considered, the difference in image distance would be

$$\Delta b = 0.244 \text{ mm}.$$

This is much more than the depth of focus of

$$\Delta f = +/- 12.5\ \mu\text{m},$$

therefore diffraction limited resolution cannot be achieved. Therefore, the 1st mirror of the horizontal mirror pair (HMP) shall be used to focus the beam vertically as well instead of simply only deflecting the beam outboard. This mirror can be bent elliptically in the sagittal direction. The required radius of curvature being short, the ideal shape of the optic can only be static and assessed by polishing.

First ray-tracing calculations were performed for this new layout. This has been done in the frame of the work of the summer student Niaja Farve in our group. As SHADOW does not provide the possibility to calculate zone plate optics, a macro implementing zone plate equations was written to implement a predefined zone plate with an outer zone width of 25 nm and diameter of 300 µm. Optimizing parameters, a spot size of 3.8 nm FWHM horizontally and 32.07 nm FWHM vertically was obtained. These sizes are diameters of the circle of confusion resulting from ray tracing, the diffraction limit of the zone plate has to be convoluted to it. A spot size of 30 nm would fit very well to current state of the art zone plates. However, it is likely that smaller zone widths and thus better resolutions could be achieved in a near future. First calculations show that the zone plate demagnification can be increased without losing too much flux, translating zone plate and secondary source simultaneously downstream (see figure 26). These calculations have been started as the positions of mirrors and secondary source have limited degrees of freedom due to adjacent components from the KB branch. The first results look promising and are sufficient for defining placeholders for the ZP components but need to be continued in more detail when funding for this branch becomes available.

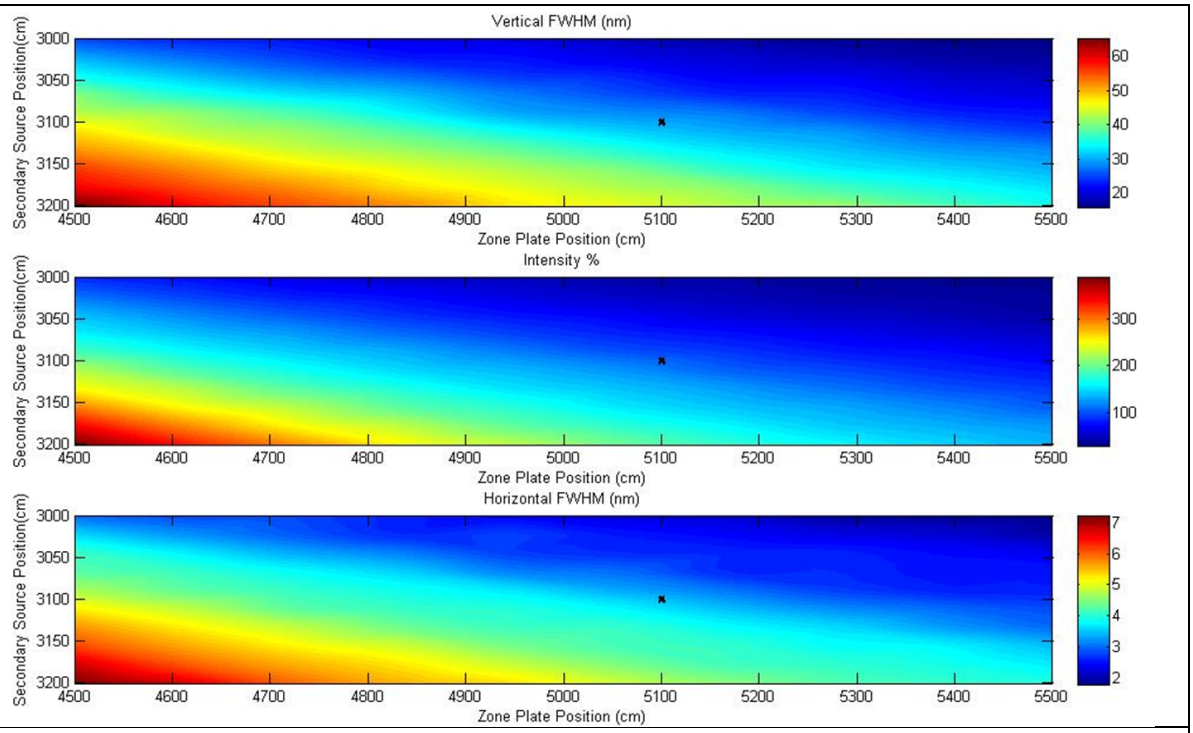

Figure 26: study of the vertical, the horizontal spot size and the flux at the sample location according to zone plate and the secondary source location

Alignment of Beam Defining Optics

The most important optical components defining the beam in the KB branch are the horizontally focusing mirror (HFM) and the horizontally deflecting double crystal monochromator (DCM). The exact positions of these two components are the result of the ray tracing calculations described in the previous chapters. They mark anchor points in the first optical enclosure (FOE) around which minor components as valves and shutters have to be arranged. In addition, radiation safety components as fixed mask, white beam stop and bremsstrahlung stop have to be arranged. The final arrangement of these components is plotted in figure 27, where a side view and a top view of this part of the beamline can be seen. The limitations of the FOE are marked as boxes around the colored components. In the side view each component is marked and annotated with component name and distance to the source origin. The graph in figure 27 shows the components necessary for the KB branch in blue color, the components for the ZP branch in red. Please note, that the graph shows the fully developed FOE, as it would be seen when both branches are operational. In the first stage of construction, instead of these components, the beam will be transported by pipes to the KB components. The ZP components will replace these, when funding is available for the full expansion of the FOE. Due to the small distance between the two beams of the branches, a separation into two different vacuum systems can only happen downstream of the secondary source of the ZP branch. Upstream, both beams will be kept in the same vacuum system.

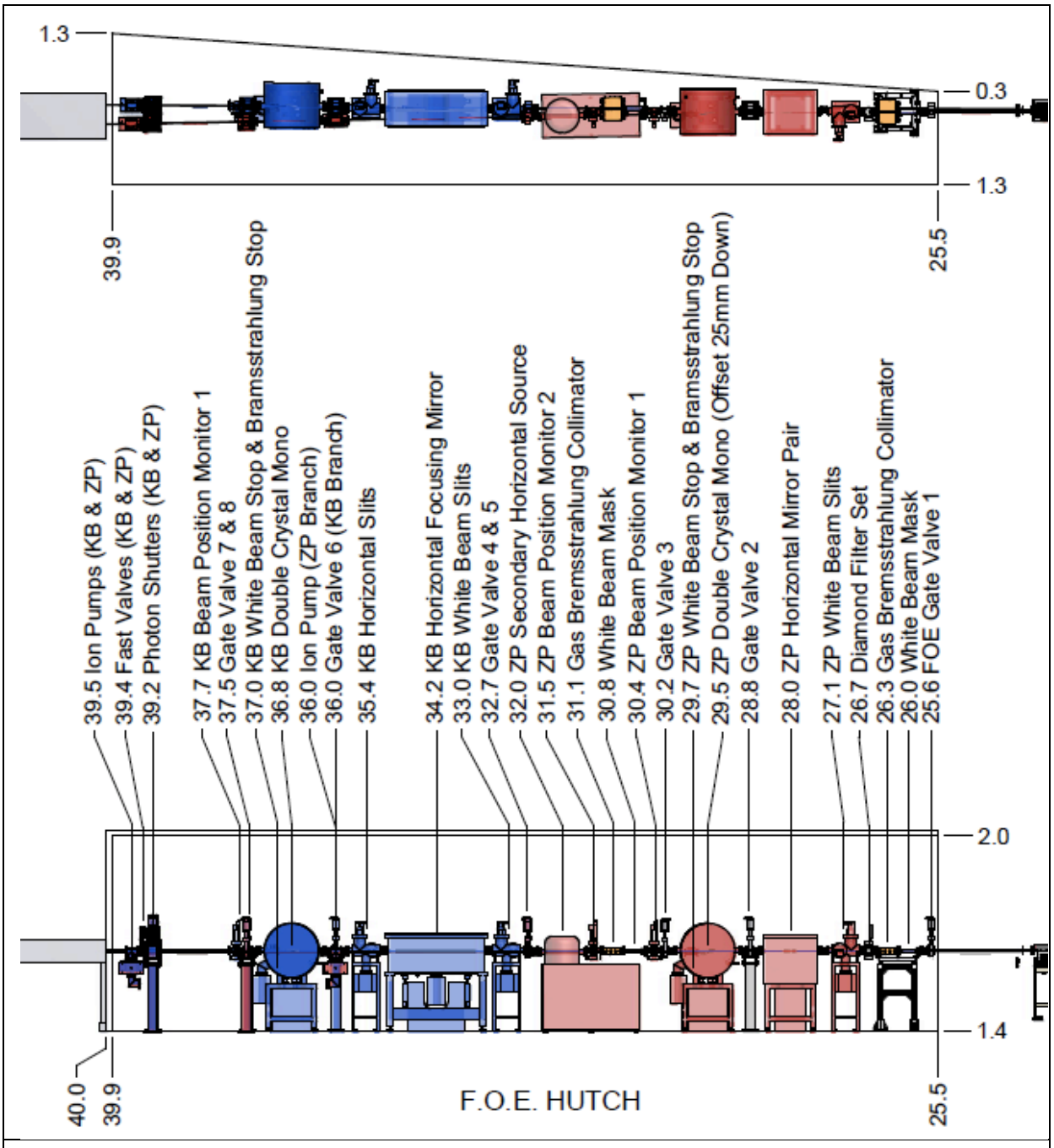

Figure 27: Fully developed FOE with line-up of optical components for the KB branch, marked in blue, and for the ZP branch, marked in red. Top image: top view of components. Bottom: Side view with legend indicating name and position in meter.

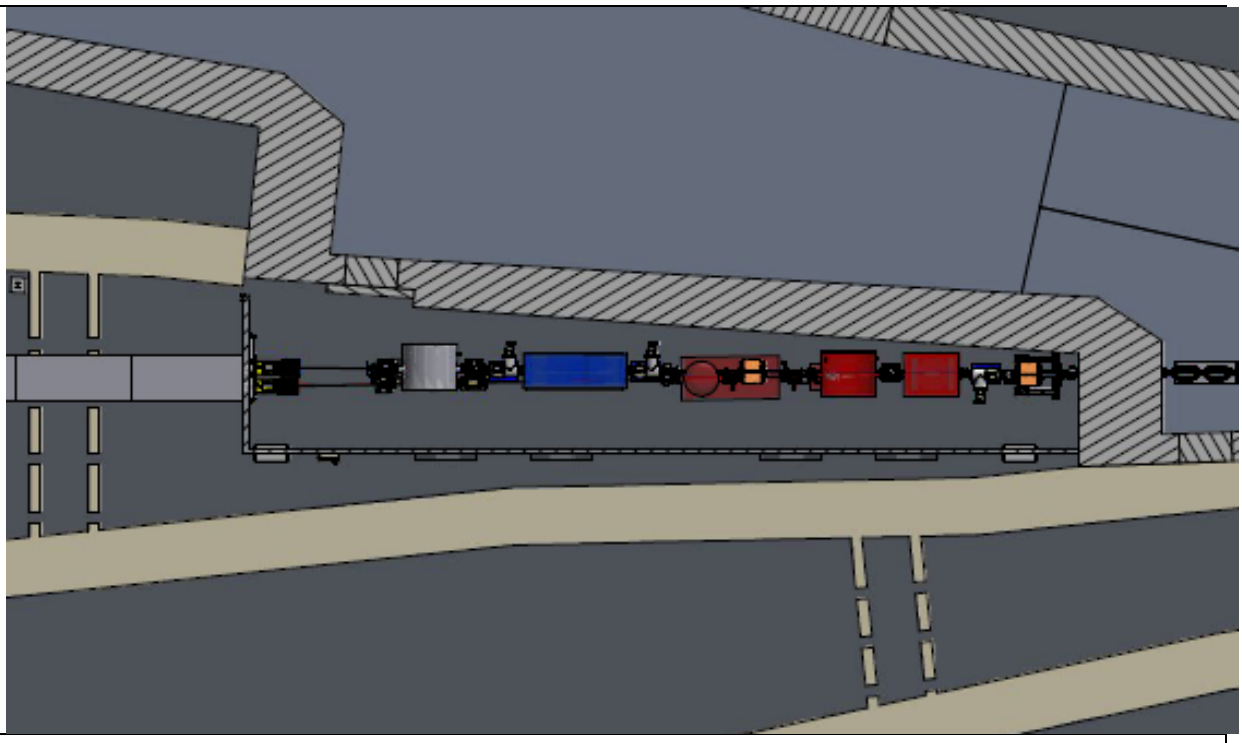

Figure 28: Design model of the first optical enclosure (FOE), top view without roof components to show optical components, compare figure 9 and figure 27.

Figure 29: Design model of the first optical enclosure (FOE), made semi-transparent to uncover the optical components within the hutch.

Description of major components for KB branch

White Beam Slits

The white beam slits must be designed to minimize or even eliminate the influence of the cooling water flow especially if turbulent flow is expected i.e. the drive mechanism must be physically stiff. The blade and support design must minimize drift caused by thermal expansion by the use of low CTE materials, kinematic mounts and thermal isolation. A variation in aperture will in turn cause a variation in heat load on the downstream optics. Suggested performance: A repeatable position equilibrium should be reached in a time below 20 minutes from a no-power situation to full incident power.

Horizontal Focusing Mirror

The specifications of the 1.2 m long mirror are driven by the desire to deliver as much of the horizontal source into the smallest secondary horizontal spot at the secondary source aperture. The presence of a secondary horizontal source slit allows this focal spot to be reduced to a few microns as well as prevents diffuse scattering due to mirror surface roughness from being passed downstream. By keeping the mirror roughness below 0.1 nm RMS the losses due to roughness scattering can be kept to an acceptable level of less than 1% over the operating energy of the mirror. For a perfect mirror figure the secondary source size will be 37 μm FWHM. For this ideal condition and when this full horizontal secondary source is used by a horizontal KB mirror the final focus will be 1 μm FWHM and contain about 95% of the photons available. It can be calculated that for a slope error of 0.73 μrad 50% of the beam is lost. To keep the loss to less than 20% the slope error would need to be less than 0.32 μrad. Due to recent new improvements and results in mirror fabrication it is reasonable to expect that by the time this mirror needs to be procured slope errors of under 0.5 μrad will be routine and values less than 0.3 μrad possible. Therefore, a reasonable mirror specification for this mirror would be an RMS roughness of 0.1 nm and RMS slope error of 0.3 μrad.

For the assembly, similar considerations apply to the mirror as they do to the DCM. The optic cooling and hence possible vibration must be decoupled from the mirror e.g. by cooling via a liquid gallium bath. The pitch piezo stage and support structure must be stiff enough to meet the dynamic requirements of running in closed loop without driving any mechanical resonances. The piezo system and DAC must have sufficient resolution to meet the stability requirements. Although the secondary source aperture is to be overfilled by the upstream optics and hence less sensitive to position; a deviation in position will cause a variation in intensity. The mechanism must also be isolated from external vibration sources from the floor and from the vacuum vessel. Suggested performance: The time to reach thermal equilibrium with reference to beam position should be below 20 minutes from from a no-power situation to full incident power. The vibration amplification factor (ratio) between the mirror support block and the floor in all three directions should approximate 1.0. The instrument should contain no major resonances below 50Hz , best effort 100Hz. The mirror horizontal translation should be stable to < 1μm/24 hours (RMS). The mirror pitch should be stable to <0.05μrad (in closed loop) to maintain spatial stability of below 1 μm stability at the secondary source aperture.

Double crystal monochromator

The double crystal monochromator (DCM) motion stages must operate in a smooth synchronized motion with minimal vibration contamination from the motors, low following errors and low pitch/roll/yaw errors. The optics must be physically isolated from the vibration sources such as the nitrogen and water pipes and yet reach thermal equilibrium quickly between heatload variations. The dynamic performance, stiffness inertia etc. of the 2nd crystal piezo pitch/roll stage is important for closed loop operation. The mechanism must also be isolated from external vibration sources from the floor and vessel. Suggested performance: The energy scale stability should be lower than ΔE = 0.1eV for 24 hours (RMS) at the Cu K-edge. The reproducibility should be better than ΔE = 0.4eV between instrument home sequences. The velocity error for the Bragg axis should be lower than 05%. The time to reach thermal equilibrium with reference to a beam intensity of 99.9% should be lower than 20 minutes from a no-power situation to full incident power. The response and settling time for the 2nd crystal pitch/roll stage for a 5% step move should be below 10ms. The vibration amplification factor (ratio) between the DCM support block and the floor in all three directions should approximate 1.0. The instrument should contain no major resonances below 50Hz , best effort 100Hz The DCM requires DC servo motors for dynamic 'on the fly' measurements.

Secondary source aperture slits

The quad beam position monitor and the precision slits must be supported by a thermally stable base with good vibration damping properties such as natural granite. The mechanism designs must consider the detrimental thermal and vibration effects of their motors and mitigate these influences by minimization of the coefficient of thermal expansion (CTE), CTE matching and thermal isolation. Suggested performance: The size stability of the aperture is wished for as below 0.1µm/24 hours (RMS). The position stability should be below 1µm/24 hours (RMS).

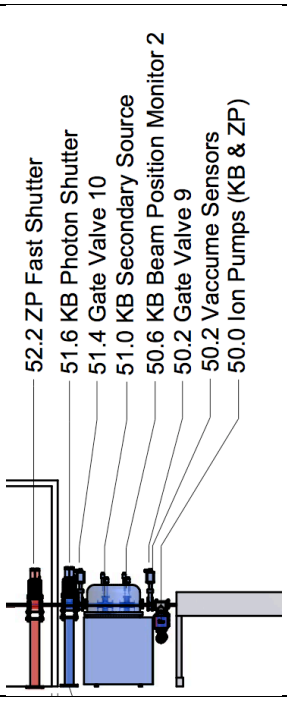

Figure 30: Secondary horizontal source aperture of the KB branch, located just upstream of the hutch for end station of the ZP branch. Due to radiation safety consideration, this arrangement will be shielded with lead. The beampipe leading into the ZP hutch is located in front of the source aperture and shielded as well. This position of the aperture is optimal for the performance of the KB end station, the safety issues have been addressed and can be handled.

KB End Station

The end station design for the KB branch is at present work in progress. We have made significant progress in defining the optical properties necessary for the KB's to deliver sub-micron resolution. As already described above, when presenting the ray tracing results, we have a very clear picture about the size, the shape, the surface roughness, and the slope error of the KB mirrors we would like to implement into the end station. The mechanical design to manipulate the mirrors is, however, not finalized. This has to be done together with the supplier for this mirror setup. Therefore, in figure 31, the sketch of the end station is not a final design. We envision to keep the KB mirrors in vacuum, to ensure maximum protection against damage and contamination. The focused beam will penetrate a vacuum window (beryllium, kapton, or silicon nitride), to allow for experiments with samples under ambient conditions. The end station of the ZP branch should only illustrate a potential place for an end station.

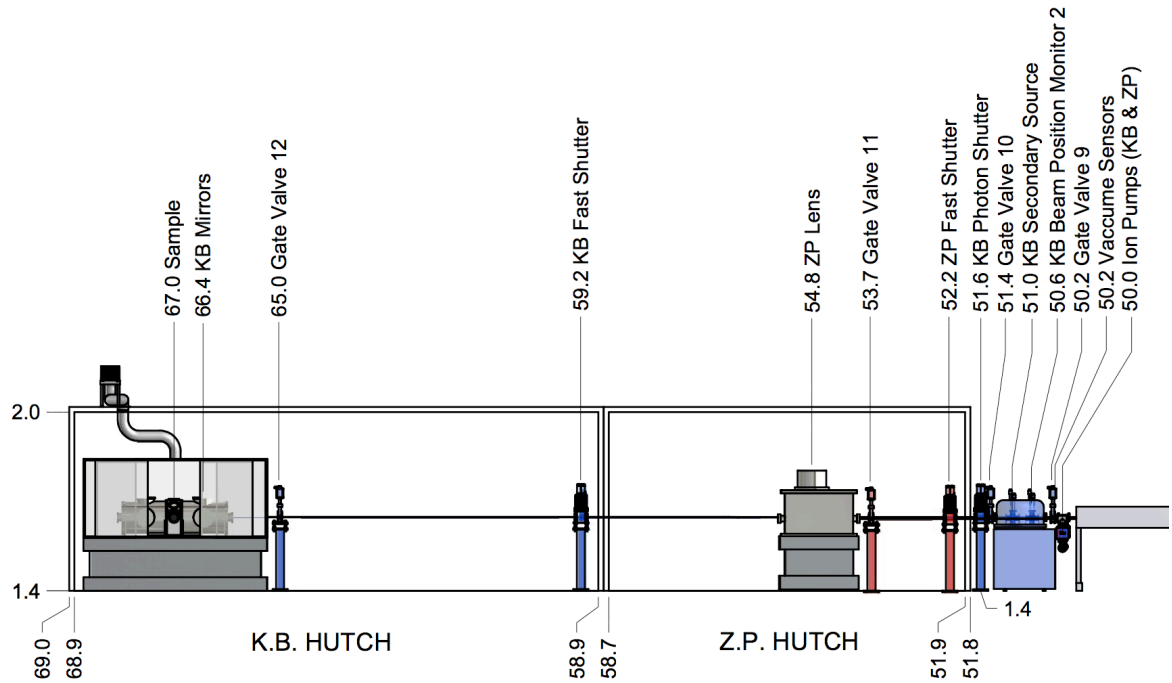

Figure 31: Sketch of the in succession aligned hutches of the KB (left) and the ZP (right) branch. The secondary source aperture for the KB's is installed upstream of both hutches. Please note, that the KB end station is enclosed in an additional cabinet, necessary for experiments with nanoparticles.

Description of KB optics

Several designs, made by several suppliers, have been scrutinized. A final decision, which design would be the most promising has yet to be made. It is however clear, that it will not match the demand of versatility to stay with an optical system for the end station that is capable of either only just sub-micron resolution or the opposite, delivering a very small spot at the expense of flux. Figure 32 shows a design, taken from a leaflet of the company IDT, that is very similar to the design described as layout 1 above. As already mentioned, the weak point of this layout is the demanding specifications for the vertically focusing KB mirror. Figure 33 shows a design and a measured spot size of a very high resolving KB mirror system, taken from an information leaflet of the company JTec. Taking only these mirrors as focusing elements would create a very small focal spot, however on the expense of intensity. Therefore we favor the before explained layout 2 consisting of two mirror sets and shows both, moderate resolution at high flux as well as very high resolution. Figure 34 shows a sketch of a design where a vacuum vessel could host these two mirror sets in a consecutive arrangement. The exact shape and dimensions of the vacuum vessel has still to be determined and depends internally on the space needed for the KB mechanics and externally on the space needed for sample holder and detectors.

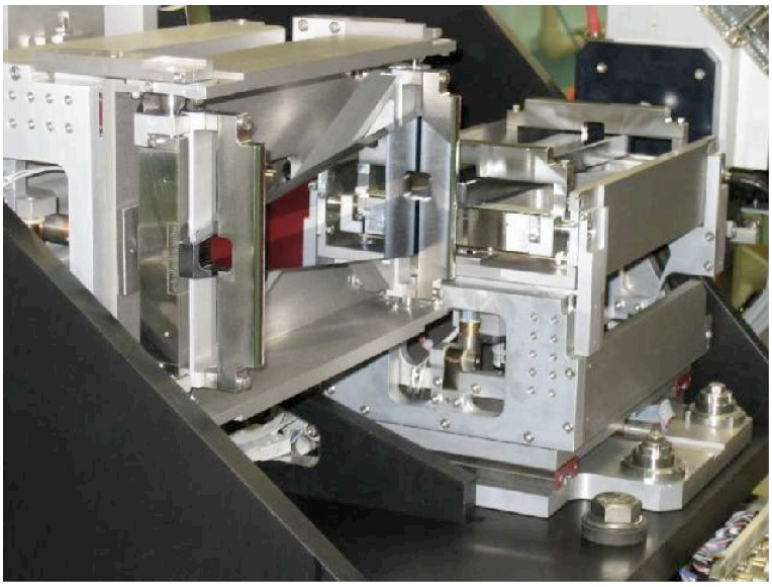

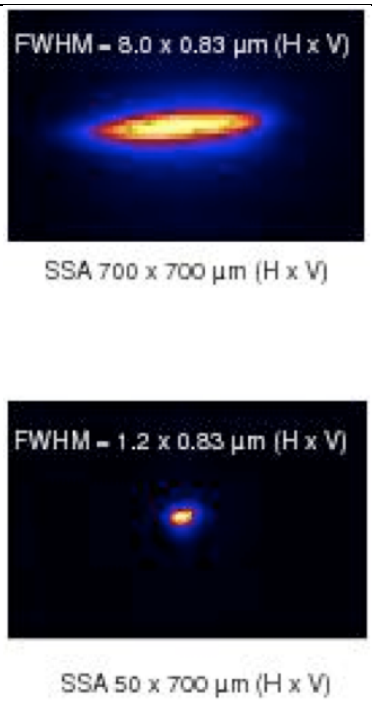

Figure 32: Left: Typical mechanical setup of horizontal and vertical KB mirrors, here in an optical setup very similar to layout 1, described in the chapters above. With a secondary source aperture open, these KB's reach a focal spot size of 8 x 0.83 μm^2 , with slits closed to 50 x 700 μm^2 a focal spot of 1.2 x 0.82 μm^2 (H x V) is reached.

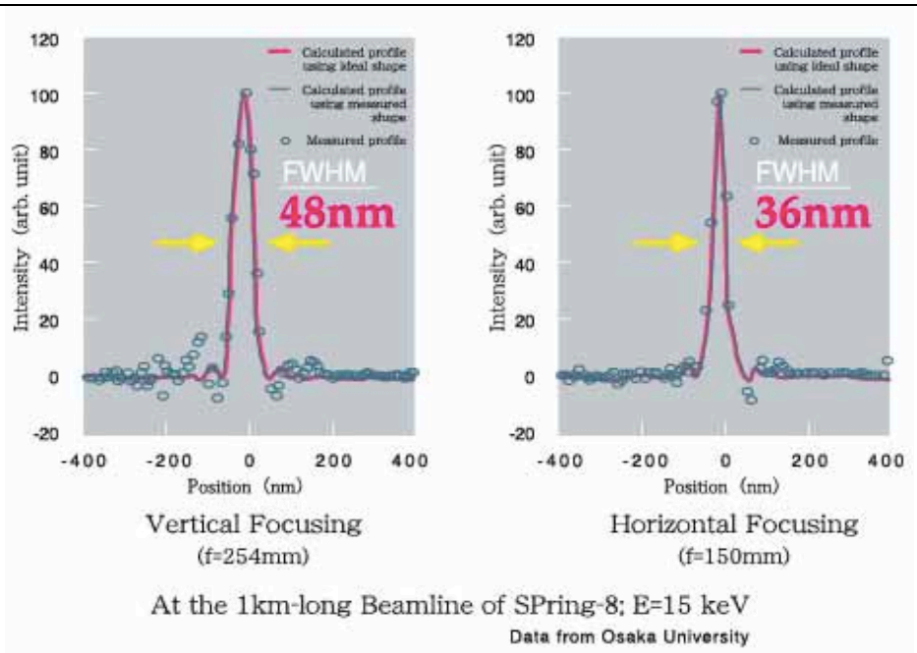

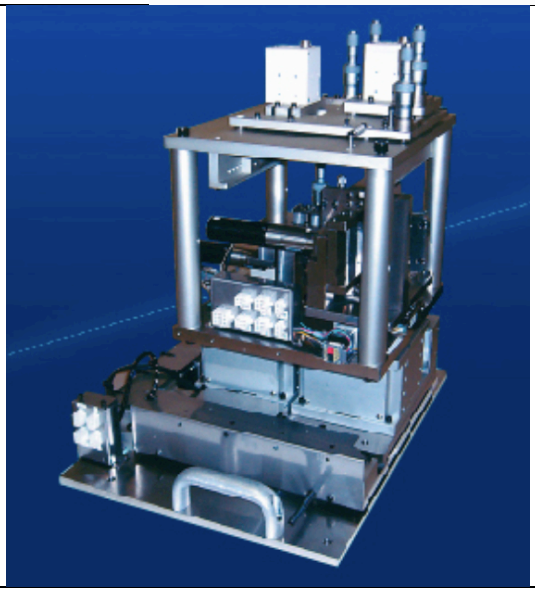

Figure 33: Bottom left: Mechanical setup of horizontal and vertical KB mirrors, taken from a leaflet of the company JTec, hosting KB mirrors delivering very high spatial resolution. Top: Measurement of the focal spot size of 10 cm long mirrors, mounted as seen at the left, and located at the 1 km long beamline of Spring8. A spot size of 48 x 36 nm^2 is achieved with KB mirrors showing a slope error of 0.1 µrad.

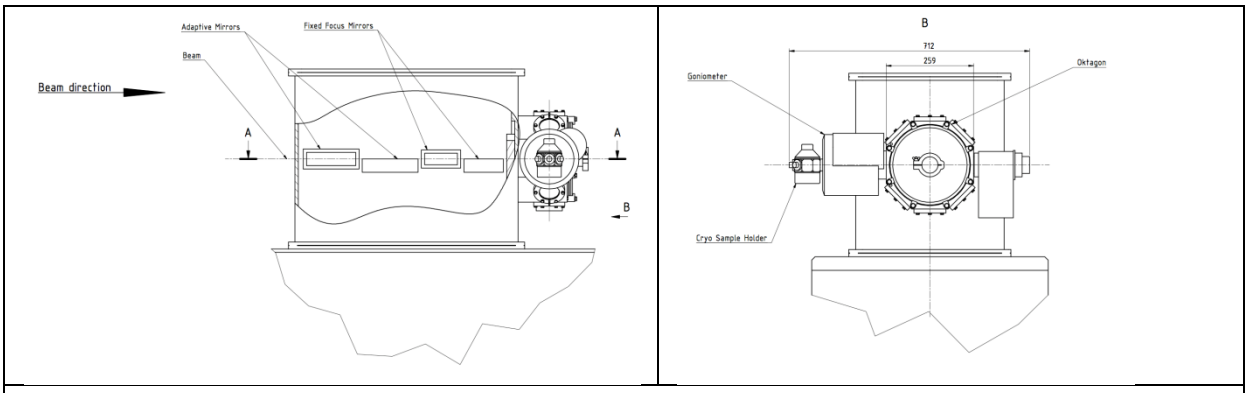

Figure 34: Design of two sets of KB mirrors in a vacuum vessel, a set of larger flexible KB's with long working distance for moderate resolution but high flux and downstream a set of small fixed-curvature KB's for very high spatial resolution (side view and top view). The cryo sample holder flanged to the vacuum vessel is a design by Bruker-ASC which has yet to be tested for feasibility for the SRX beamline. It shows however, where in this design the sample spot will be.

Description of sample stage

The central requirement of a sample stage for the SRX beamline is that it needs to provide the possibility to cover a wide field of analyses and to study heterogeneous samples in terms of shape and composition, with as little compromise as possible. These parameters that have to be integrated into the sample stage are summarized in tables below. Moreover, the main characteristics of SRX, which are the use of a very high flux and a large spatial resolution range spreading from 1 µm to less than 100 nm, impose additional constraints on the sample stage.

Constraints linked to the high flux

In order to take full benefits of the SRX world leading beam intensity in the focal spot, new generation detectors like MAIA will be used. As an example, MAIA has up to now never been saturated on a synchrotron beamline. So, even if at day 1 the operation of SRX will start with more readily available commercial detectors, it is important to adapt the geometry of the sample stage to MAIA, for experiments under ambient conditions as well as for cryo experiments. The rather low energy resolution of the MAIA detector available at present will significantly improve with version 2, where an energy resolution equivalent to current SDD's is expected. The first tests of MAIA-II are foreseen to be performed using the SRX beamline at the beginning of the year 2014.

One consequence of the high flux and new fast detectors which accept radiation from large solid angles is that the acquisition time for fluorescence mapping will be strongly reduced. Given that all considerations presented here become reality, dwell times per pixel low as 5 ms could be routinely used. The cutting edge in speed of currently available stages abilities is still not reached. However, we envision at a later point in time to modify the monochromator to incorporate multi-layer mirrors, in addition to the Si (111) and Si (311) crystals. This would generate a three orders of magnitude higher flux in the focal spot and the dwell time would drop from 5 ms to 5 µs. With a step size of 1 µm, the speed of the stage would reach 250 mm/s. With this the limits of the aspired stages would be reached.

Constraints linked to the high spatial resolution

Stage Assembly

The minimum travel range required is fixed at 2.5 cm, but we are aiming for 5 cm (see figure 35). The accuracy is given by the half of the beam size in order to maximize the resolution power. Taking into account the results of layout 2, an accuracy of 30 nm is asked for. Typical stages with these requirements are composed of a stack of five translations. Three of these translations are driven by stepper motors with a sub-micron resolution and travel ranges in the cm range. The two others are typically piezo motors, showing accuracies of up to 1 nm, however with a very limited travel range. The inconvenience of this kind of assembly is that it brings into play two different coordinates systems, which is a potential source of confusion for the users. Moreover, each time the coarse stages move, regions of interest previously identified with an accuracy above the one of the coarse stages have to be redefined. A semi-automation of experiments, which is necessary for high throughput, will not be possible. On the

contrary, much time will be spend for finding positions back and realigning the sample in the focal spot.

	X	Y	Z	R
Absolute Accuracy (nm)	1000	30	30	
Travel Range (cm)	20	5	5	
Speed (µm.s^{-1})		6-200		
Sample Weight Load	Usually less than 50 g, occasionally up to 200 g			

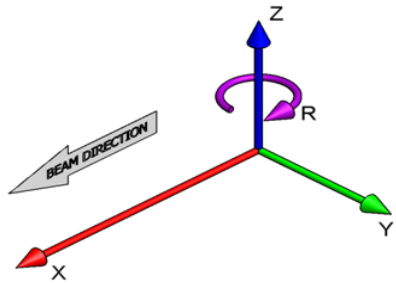

Figure 35: Linear stages requirement in term of accuracy, speed and load.

To overcome these limitations, a technology proposed by companies like *PI* or *Nanomotion*, that offers positioning accuracy in the nanometer range in combination with an unlimited travel range is under consideration. The proposed stages consist of piezoelectric motors that press ceramic finger tips against a ceramic strip inducing elliptical movements, which exert a driving force on a linear stage. The specifications of these motors would fulfill the sample stage demands, however with only one translation per axis (see figure 36). This technology is new, some uncertainties still have to be resolved. One potential issue could be the setting of the motor on the driving ceramic strip. Additional studies by the manufacturer need to be performed before a decision about these resonant drive systems can be made. If this solution needs to be discarded, the fallback solution will be to look into the not so convenient but more secure system of stacking 3 steppers and 2 piezoelectric motors. We foresee to add accurate encoders with length gauges or interferometers (*Heidenhain* or *Renishaw*) in the vicinity of the sample for nano-motion corrections in close loop.

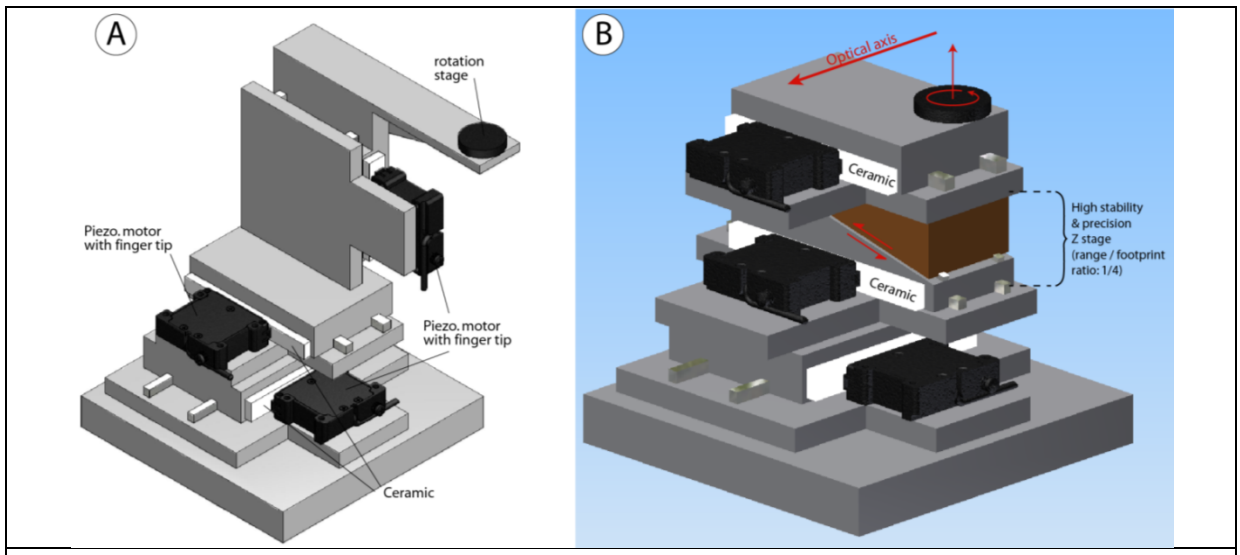

Figure 36: (**A**) XYZ stage drives with 3 piezomotors involving the resonant drive technology (drawing modified from *Nanomotion* catalog). (**B**) Alternative design of the sample stage with a so-called Vertical Mounting Z Wedge that provides a very high stability to the assembly (designed following *Nanomotion* products).

Working distance

Reaching a spot size below 100 nm requires a significant demagnification of the source, causing a short focal distance and thus a short working distance. Therefore, the distance between the downstream wall of the KB vacuum vessel and the sample in its mechanical holder is short. As some flexibility and some degree of freedom in sample handling has to be allowed for and as detectors have to placed close to the focal spot as well, extra attention will be paid to this small but populated area. This work is in process and depends to some extend on the vendor's technical ability. We discussed the possibility to adapt the KB mirror clamping system to these constraints by removing the material located downstream of the edge of both mirrors. The minimum thickness of the KB box downstream wall has to be optimally dimensioned. An asymmetric shape of the last KB mirror is also considered. The mirror could be shortened on the downstream side instead of removing the same length of material on both sides, so keeping the center, but now asymmetric, without sensible loss in the flux on the sample (see figure 37). Another issue will be that the resulting available working distance has to host a sample rotation stage used for tomography.

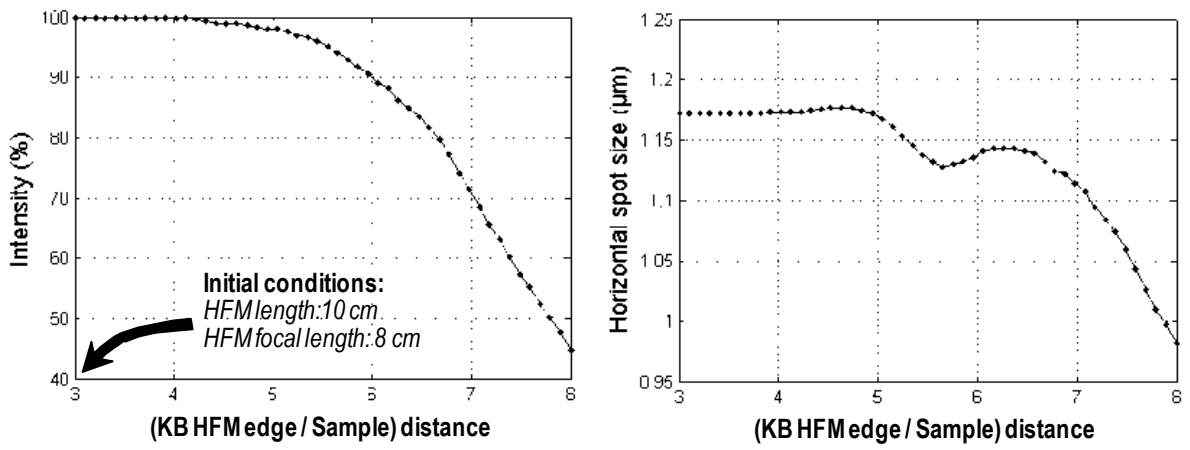

Figure 37: Assessment of the relative intensity and the horizontal spot size evolution as a function of the length of the horizontally focusing KB mirror, using ray tracing . The length is shortened by removing material on its downstream side. Its focal length being fixed, the demagnification doesn't change. 2 cm of shortening decreases the flux to 98 %, whereas 3 cm significantly drops the flux to 90 %. Calculations were made at 12.4 keV with an incident angle of 3 mrad.

Spatial stability of the sample

The spatial stability of the sample position, and so, the sample stage's spatial accuracy must be consistent with the size of the focal spot. This stability is affected as well by vibrations as by the materials thermal expansion.

- Thermal expansion minimization considerations

Table 6 shows the thermal expansion as a function of temperature differences for some materials and gives so an estimate for possible sample drifts in regard to the thermal

instabilities. The daily thermal stability of the standard NSLS-II hutches is guaranteed $\Delta T = 0.3^{o}C$. Considering that the main metallic parts of the stages are made from aluminum, the sample displacement due to the stage dilatations / contractions is not acceptable. A way to avoid this is to replace Al stage plates by INVAR stage plates. It is also foreseen to place sample stage and KB vessel on a single stiff INVAR plate. This is necessary as well to have a reference frame for the determination of positions. Finite element analysis will be made soon to model the thermal expansion of the sample stage for different daily thermal variations and different materials, taking into account the warming of the air by the sample stages motors. The results will help to clarify what thermal stability is needed within the end station hutch.

Table 7: examples of thermal expansion of different materials according to different temperature variations.

Thermal expansion					
	Therm. Exp. Coeff	dim. (cm)	expansion (nm)		
			$\Delta T = 1^{o}C$	$\Delta T = 0.1^{o}C$	$\Delta T = 0.01^{o}C$
Granite	8.50E-06	1000	*85000*	8500	850
Steel	1.20E-05	15	*1800*	180	18
Invar	1.20E-06	15	*180*	18	1.8
Aluminium	2.30E-05	15	*3450*	345	34.5

- Vibration minimization considerations

The NSLS II experimental floor has been designed so it can meet certain floor vibration criteria which will allow for vibration-sensitive experiments to be conducted on its beamlines. Based on both experience data from other vibration-sensitive facilities and special instrument needs both wide-band and narrow-band criteria have been established. For the narrow-band criteria where the tonal characteristics of the floor vibration are considered, the limit of 25 nm integrated rms displacement of the floor for the frequency range above 4 Hz which encompasses the incoherent vibration environment has been established as the experimental floor goal. Based on the spectral content of the experimental floor vibration and the dynamic properties of the probe system supported on the floor, the integrated rms displacement experienced by the sample stage will increase unless active and/or passive vibration isolation principles are implemented.
The second and experience-based criteria that is aimed at on the NSLS-II experimental floor is one based on floor rms velocity spectra expressed in 1/3rd octave band scale. This wide-band criteria (shown in fig. 38 below as VC-criteria curves) are widely used in vibration-sensitive facilities under the principle that floor vibration energy is shared by neighboring frequencies rather than concentrating on specific tones. The goal for the

NSLS-II experimental floor is meeting the spectral velocity threshold of the VC-E curve (3.12 μm.sec^{-1}).

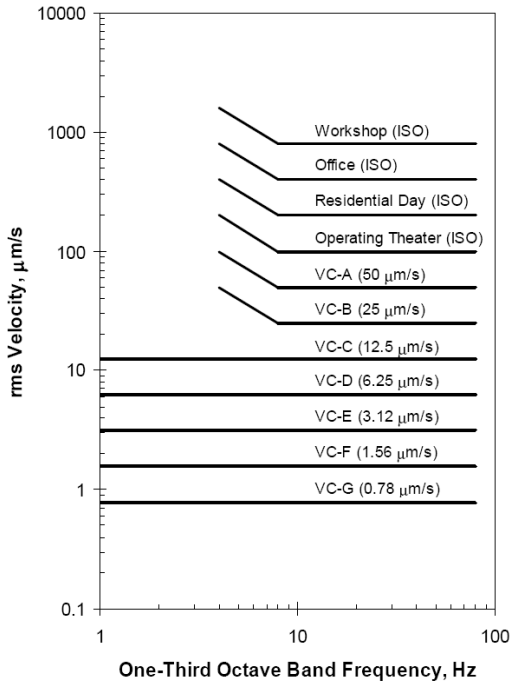

Figure 38: Vibration Criteria Curves used for NSLS-II Experimental Floor Wide-Band limits (*data courtesy, N. Simos, NSLS-II*).

To prevent the NSLS II experimental floor (or hutch floor) vibration from amplifying as it propagates through the experiment support structure, passive and active isolation principles are being explored. Figure 39 depicts recent measurements made on passive and active systems under consideration. As shown in fig. 39 (left), passive system inherently suffers from the inability to reduce vibrations in the lower frequency regime (around the natural frequency of the support system) and even inducing amplification of the floor vibration. Active isolation systems (Figure 39b) on the other hand appear to have eliminated the amplification concerns and are capable of de-amplifying the floor vibration in the lower frequency regime. While these two systems are being evaluated for implementation in the SRX beamline staging, it is assessed that achieving displacements of ~20-30 nm for the Zone Plate or KB branch is feasible provided that no amplification takes place at the final stage (above the experiment table).

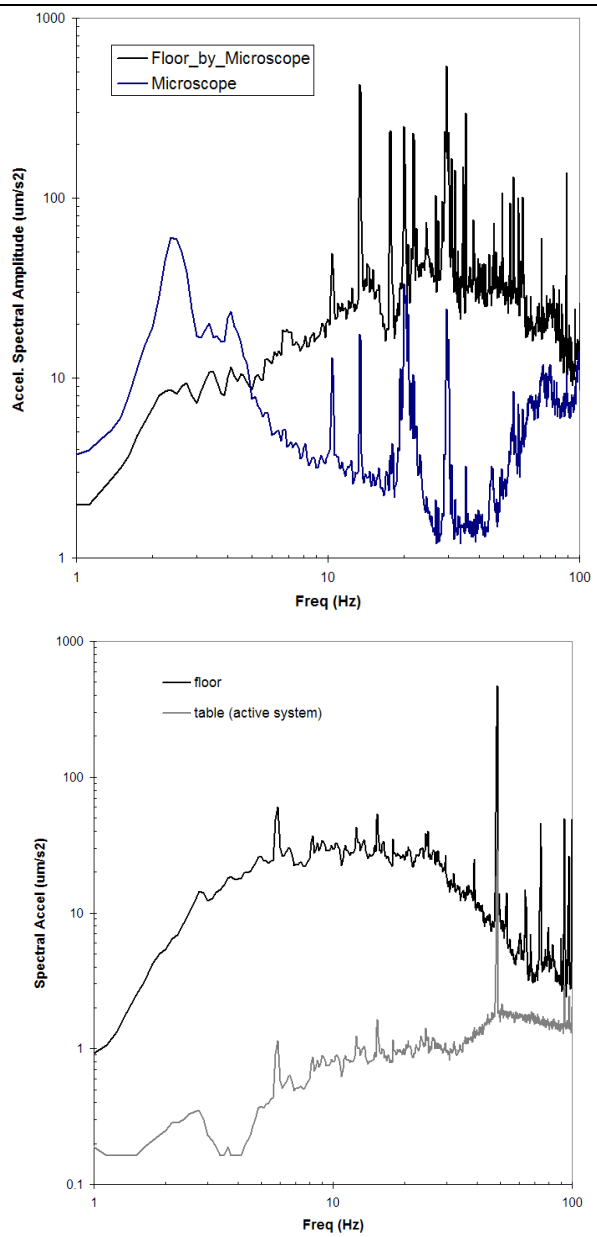

Figure 39: (left) passive system vibration isolation, (right) active system isolation (*data courtesy, N. Simos, NSLS-II*).

Sample considerations

The SRX beamline is designed to be very versatile and will therefore host experiments for a wide spectrum of research areas. Nevertheless, an attempt has been made in table 8 to describe the needs in sample preparation, sample environment and sample size, the needs for specific techniques in data acquisition, and the need for resolution and scan size for several scientific fields that could be seen as major shareholders of the beam time available at this beamline. It becomes clear, that both, moderate resolution as well as high resolution is needed in addition to short dwell times, enabling large images, as well as stable positioning for high spectral resolution.

Table 8: Sample definition and possible mapping and spectroscopy settings for a list of major scientific topics.

Methods \ Samples		Mineral Grains in Rock Thin Sections	Intact Geo Specimens	Micro Particles (< 10 µm)	Nano Particles (approx. 100 nm)	Microtome and FIB Sections	Dispersed Powders	Colloids in fluid cells	Biofilms and microbial suspensions	Large Bio Samples Thin Sections	Bio Samples	Possible Detectors for these experiments
	Details \ Mounts	25 mm round x 1.5 mm thick silica substrate	Fiber	TEM grids, SiN, Kapton, Fiber; 5x5x0.1mm; 10 mg	Si3N4; Kapton, TEM Grids, Capillary	TEM grids, Si_3N_4	Si_3N_4; Kapton	**Fluid cell**	Si_3N_4; Kapton, TEM Grids, Capillary	Polymer substrates	TEM Grids, Capillaries	
	Sample condition	dry, sections	dry	dry & aqueous	dry & aqueous	dry	dry & aqueous	aqueous	aqueous & cryo	dry & cryo	cryo	
Trace element content	**Technique**	XRF single spot	XRF single spot	XRF single spot	XRF single spot	XRF single spot	XRF single spot	XRF single spot	XRF single spot	XRF single spot	XRF single spot	**Vortex ME4** at 90 degs (130 eV resolution)
	Spotsize	1 µm	1 µm	1 µm	0.1 µm	0.1 µm	0.1 µm	0.1 µm	0.1 µm	1 µm	0.1 µm	
Trace element distribution (2D)	**Technique**	XRF imaging	XRF imaging	XRF imaging	XRF imaging	XRF imaging	XRF imaging	XRF imaging	XRF imaging	XRF imaging	XRF imaging	**Vortex ME4** at 90 degs (130 eV resolution); **MAIA**
	Spotsize	1 µm	1 µm	1 µm	0.1 µm	0.1 µm	0.1 µm	0.1 µm	0.1 µm	1 µm	1 µm	
Trace element distribution (3D)	**Technique**	-	FMCT	FMCT	FMCT	-	-	-	FMCT	-	FMCT	**Vortex ME4** at 90 degs (130 eV resolution); **MAIA**
	Spotsize	-	1 µm	1 µm	0.1 µm	0.1 µm	0.1 µm	-	0.1 µm	-	0.1 µm	
Element speciation	**Technique**	single spot	single spot	single spot	single spot & image stacks	single spot & image stacks	single spot & image stacks	single spot & image stacks	single spot & image stacks	single spot	single spot & image stacks	**Vortex ME4** at 90 degs (130 eV resolution)
	Spotsize	1 µm	1 µm	1 µm	0.1 µm	0.1 µm	0.1 µm	0.1 µm	0.1 µm	1 µm	0.1 µm	
Phase Identification		Yes	Yes	Yes	Yes	Yes	Yes	No	Yes	No	No	**Image plate** (e.g., MAR345); **CCD** (e.g., Rayonix 165)
	Course Motion (Range, Resolution)	20x20 mm^2, 0.5 µm	20x20 mm^2, 0.5 µm	5x5 mm^2, 0.5 µm	1x1 mm^2, 0.5 µm	5x5 mm^2, 0.5 µm	10x10 mm^2, 0.5 µm	10x10 mm^2, 0.5 µm	5x5 mm^2, 0.5 µm	20x20 mm^2, 0.5 µm	1x1 mm^2, 0.5 µm	
	Fine Motion (Range, Resolution)	-	-	500x500 $µm^2$, 100 nm	200x200 $µm^2$, 30 nm	200x200 $µm^2$, 30 nm	200x200 $µm^2$, 30 nm	500x500 $µm^2$, 100 nm	200x200 $µm^2$, 30 nm	-	200x200 $µm^2$, 30 nm	

Infrastructure

Surveying of Beamline Components at NSLS-II using a laser tracker.

The NSLS-II facility, including the storage ring tunnel and experimental floor, is fitted with a network of survey monuments referenced to a pair of monuments in the center of the ring. This network will be regularly surveyed with a laser tracker to create a robust and accurate network of arbitrarily positioned monuments. Monuments can be added as required, including inside hutches and on the storage ring wall etc. Positioning a laser tracker on a tripod such that it can view more than three monuments allows it to calculate its position, and the position of any new monuments.

Precision machined holes in components are surveyed prior to installation, relative to the component aperture, crystal, mirror or grating surface etc., fitting a reflector into the precision hole allows the laser tracker to survey the absolute reflector position so that the aperture or optic position can be accurately calculated. This system of surveying is extremely accurate, globally (within the NSLS-II complex) components may be positioned to within 100 microns, and where components are close to one another (within a few meters, without sighting restrictions) the accuracy improves to ~30 μm.

Utilities requirements

Generally speaking, the SRX beamline needs a so-called "standard package" of utilities, as implemented at a particular beamline, for both branches. This includes the following utilities that would be taken from the facility-provided drop-off (on the ratchet wall) and delivered to the required location. It includes the interface specifications for providers of the utilities (water, air, cryogens, telecom, etc.).

1. Electrical power distribution: all electrical outlets in the enclosures and along the beamline, plus wiring to light fixtures, electrical outlets, fans, hoists, (etc.) inside the enclosures. Also includes electrical power outlets in the cabin or user area.
2. Distribution of deionized (Process) water at ~20°C
3. LN2 distribution
4. Experimental gases distribution, which includes facility compressed gas (N2 or air) and any local gas distribution from gas cylinders into hutches, etc.
5. Fire detection equipment and connection to facility system
6. Temperature sensors (inside enclosures)
7. Oxygen depletion sensor
8. Communications, including fiber optic cable reticulation and CAT6 LAN with switches and racks (including outlets in the cabin or user area)
9. Cabling and piping support structures, including for EPS and PSS
10. Gas exhausts from enclosures to common exhaust manifold in building

As a specific non-standard utility, both SRX beamline branches need to perform experiments with nano-sized particles and materials. This is mandatory to fulfill the needs of the scientific communities listed as main users. A possible solution to comply with the safety standards set for handling these materials would be, to assemble an

enclosure on the optical tables carrying the sample stages. This enclosure will the be separately filtered.

Special beamline requirements

Research with nanomaterials and nanoparticles

In environmental sciences as well as in bio and life sciences, nanomaterials play an important role. The interaction of nanoparticles with other substances in the environment and with cells or whole organisms is still only poorly understood. Therefore, it will be necessary for the SRX beamline to be able to host experiments with nanomaterials. This asks for specific procedures when dealing with these samples. For instance, the sample environment within the end station has to be under lower than ambient pressure, to be able to filter escaping particles before they cause harm. As the hutches are designed to have higher than ambient air pressure, we want to implement an additional casing, probably made of some acrylic glass with sliding doors for access. This casing could then be kept at lower than ambient pressure, using an extra hose. It will enable HEPA filtering as well.

Research with actinides

Storage and transport processes of radioactive materials in the environment are scientific topics of great importance. To work with radioactive materials, not only the end station has to be prepared for it, but a special laboratory space for sample treatment has to allocated. As this has to happen in the larger frame of NSLS-II instead of only the SRX beamline, discussions have been started, attention will be paid to this topic, but no final decisions have been made yet.

Summary of Day 1 performance

At day 1 of operation the KB branch will be able to host experiments. In the fully developed state, the end station will contain two sets of KB mirrors, for very high spatial resolution and for moderate resolution at high flux. The latter, a set of large KB mirrors as described in previous chapters, will be implemented at day 1, will be operational and should provide sub-micron spatial resolution. X-ray fluorescence imaging of samples under ambient conditions will then be possible using either a commercially available vortex silicon drift detector or the MAIA detector, if the latter is available. Furthermore, XANES spectroscopy of samples, again under ambient condition, shall be possible, provided, that the required synchronization between IVU 21 undulator and the monochromator is fully functional. The end station should be able to host a variety of different samples from earth and environmental sciences as well as from material sciences, as for instance described to some extend in Table 8.

Future upgrade options

Zone plate branch

The zone plate branch is still part of the mature scope connected to the SRX beamline. It would be of great benefit to promptly not only continue with design efforts related to the KB branch but to intensify them to a full design and construction of this branch. The ZP branch is aiming for lower X-ray energies, allowing studies at important absorption edges as phosphorus, sulfur, chlorine or calcium. Especially as there are only very little possibilities worldwide for studying these elements, the ZP branch would immediately broaden the scientific community showing interest in experiments.

Experiments with cryo-cooled samples

To work successful with samples from biology, microbiology and life science, it is important to be able to work with cryo-cooled samples. Radiation damage is a serious issue especially when studying soft matter and tissue. Cryo-cooling ensures stability of these delicate samples throughout the experiments.

Coherent diffraction imaging

Although studies with a very high spatial resolution will be possible at the SRX beamline, this is not enough for studying single nano-sized particles and their impact on cells or on other substances in the environment. To investigate single nanotubes, nanocrystals or other nanoparticles, coherent diffraction imaging might be the technique of choice. A CCD detector will be necessary to record the diffraction pattern, additional manpower might be necessary for the experiments and the data analysis. The former is in the mature scope, the latter has to be applied for.

Appendix A: Schedule

September 30	2010	Preliminary Design Report
October 19-20	2010	PDR Technical Review
November 15-17	2010	DOE review
November	2010	Technical Design – Approval of Long Lead Term Procurement
January	2011	Start Long Lead Time Procurements
September 30	2011	Complete Final Design Report
February 07	2012	Complete Final Design Report
February	2012	Start Installation
May	2012	Start Sub-System Testing
April	2012	Start Other Procurement
November	2012	Complete Long Lead Time Procurements
August	2013	End Procurement
August	2013	Start Integrated Testing
January	2014	Complete Installation
February	2014	Complete Sub-System Testing
February	2014	Beam-ready
May	2014	Complete Integrated Testing – Beamline available for Commissioning
June	2015	CD-4, Approve Start of Operations

Appendix B: Reference Drawings

Personal Protection System

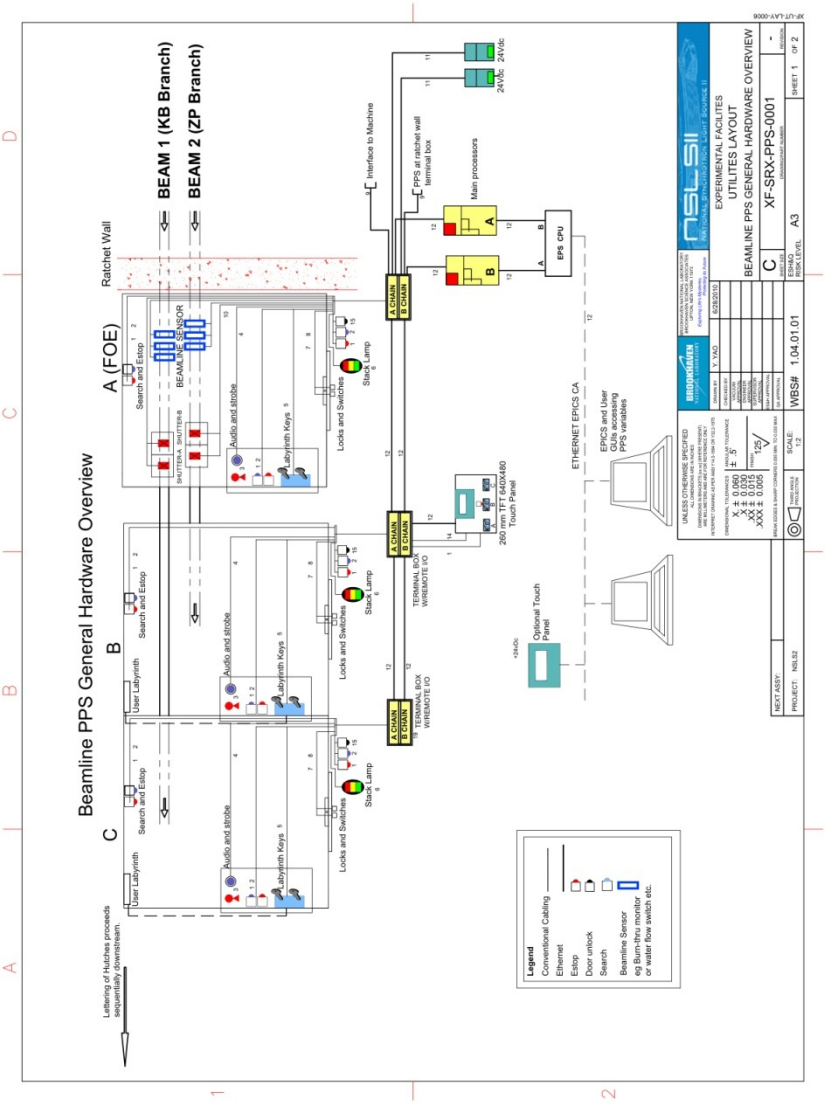

Figure B1.1: Schematic layout for Personnel Protection System (PPS) for the SRX Beamline

Controls diagrams

The control diagram of the SRX beamline is displayed in five consecutive drawings on the next five pages. The diagram starts at the ratchet wall and follows the path of the X-rays through the FOE, the secondary source into the end station.

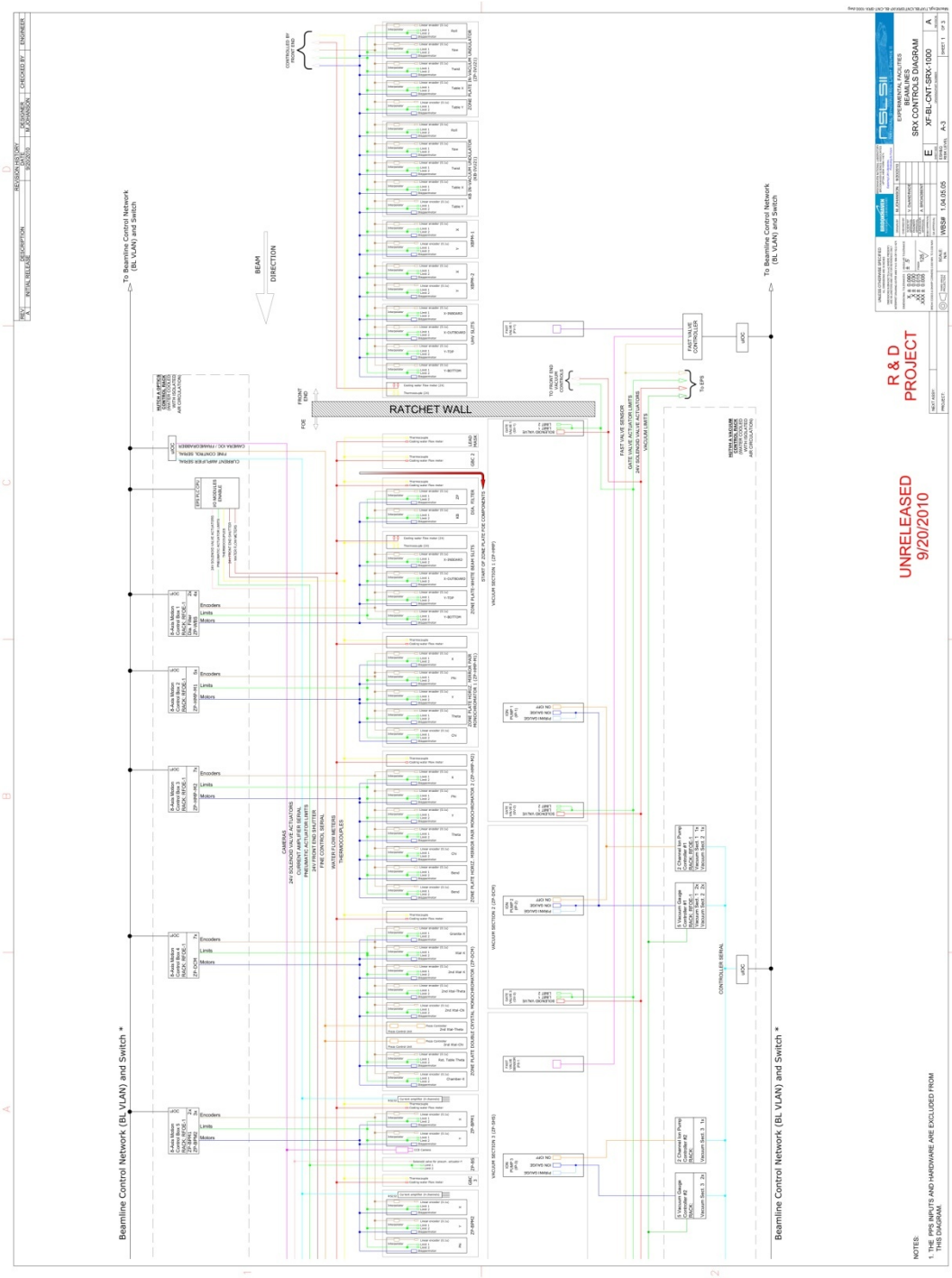

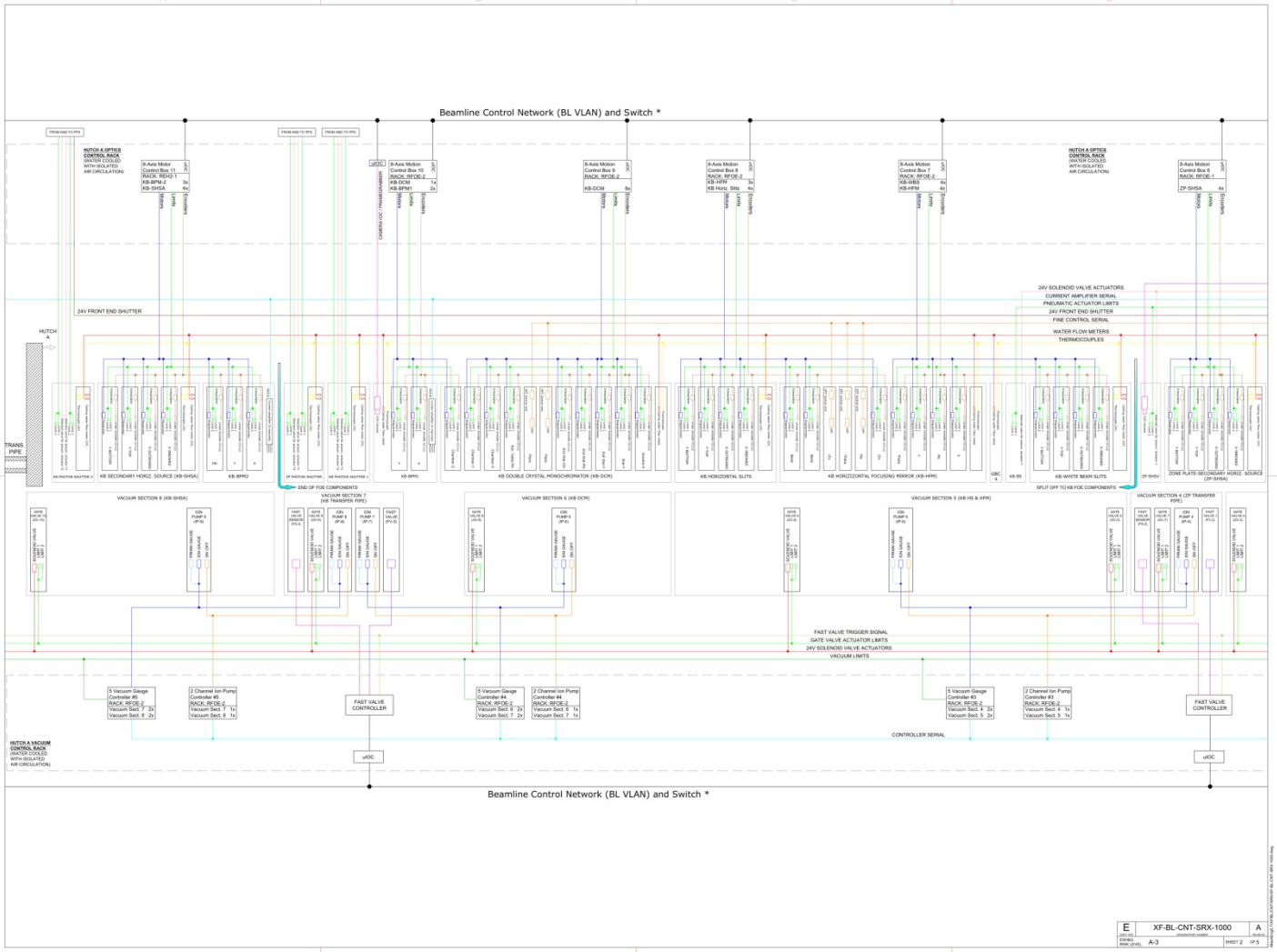
Beamline Control Network (BL VLAN) and Switch *
HUTCH A OPTICS CONTROL RACK (WATER COOLED WITH ISOLATED AIR CIRCULATION)
8-Axis Motor Control Box 11 RACK: RE9Q-1
KB-BPM-2 2x
KB-SHSA 4x
8-Axis Motion Control Box 10 RACK: RF0E-2
KB-DCM 1x
KB-BPM1 2x
8-Axis Motion Control Box 9 RACK: RF0E-2
KB-DCM 8x
8-Axis Motion Control Box 8 RACK: RF0E-2
KB-HFM 3x
KB Horiz. Slits 4x
8-Axis Motion Control Box 7 RACK: RF0E-2
KB-HBS 4x
KB-HFM 4x
8-Axis Motion Control Box 6 RACK: RF0E-1
ZP-SHSA 4x
24V FRONT END SHUTTER
24V SOLENOID VALVE ACTUATORS
CURRENT AMPLIFIER SERIAL
PNEUMATIC ACTUATOR LIMITS
FINE CONTROL SERIAL
WATER FLOW METERS
THERMOCOUPLES
HUTCH A
TRANS. PIPE
KB SECONDARY HORIZ. SOURCE (KB-SHSA)
KB-BPM2
KB-BPM1
KB DOUBLE CRYSTAL MONOCHROMATOR (KB-DCM)
KB HORIZIZONTAL SLITS
KB HORIZIZONTAL FOCUSING MIRROR (KB-HFM)
KB-WHITE BEAM SLITS
ZONE PLATE-SECONDARY HORIZ. SOURCE (ZP-SHSA)
END OF FOE COMPONENTS
SPLIT OFF TO KB FOE COMPONENTS
VACUUM SECTION 8 (KB-SHSA)
VACUUM SECTION 7 (KB TRANSFER PIPE)
VACUUM SECTION 6 (KB DCM)
VACUUM SECTION 5 (KB HS & HFM)
VACUUM SECTION 4 (ZP TRANSFER PIPE)
FAST VALVE TRIGGER SIGNAL
GATE VALVE ACTUATOR LIMITS
24V SOLENOID VALVE ACTUATORS
VACUUM LIMITS
5 Vacuum Gauge Controller #5 RACK: RF0E-2 Vacuum Sect. 7 2x Vacuum Sect. 8 2x
2 Channel Ion Pump Controller #5 RACK: RF0E-2 Vacuum Sect. 7 1x Vacuum Sect. 8 1x
FAST VALVE CONTROLLER
5 Vacuum Gauge Controller #4 RACK: RF0E-2 Vacuum Sect. 6 2x Vacuum Sect. 7 2x
2 Channel Ion Pump Controller #4 RACK: RF0E-2 Vacuum Sect. 6 1x Vacuum Sect. 7 1x
5 Vacuum Gauge Controller #3 RACK: RF0E-2 Vacuum Sect. 4 2x Vacuum Sect. 5 2x
2 Channel Ion Pump Controller #3 RACK: RF0E-2 Vacuum Sect. 4 1x Vacuum Sect. 5 1x
CONTROLLER SERIAL
HUTCH A VACUUM CONTROL RACK (WATER COOLED WITH ISOLATED AIR CIRCULATION)
Beamline Control Network (BL VLAN) and Switch *
E
XF-BL-CNT-SRX-1000
A
A-3
SHEET 2 OF 5

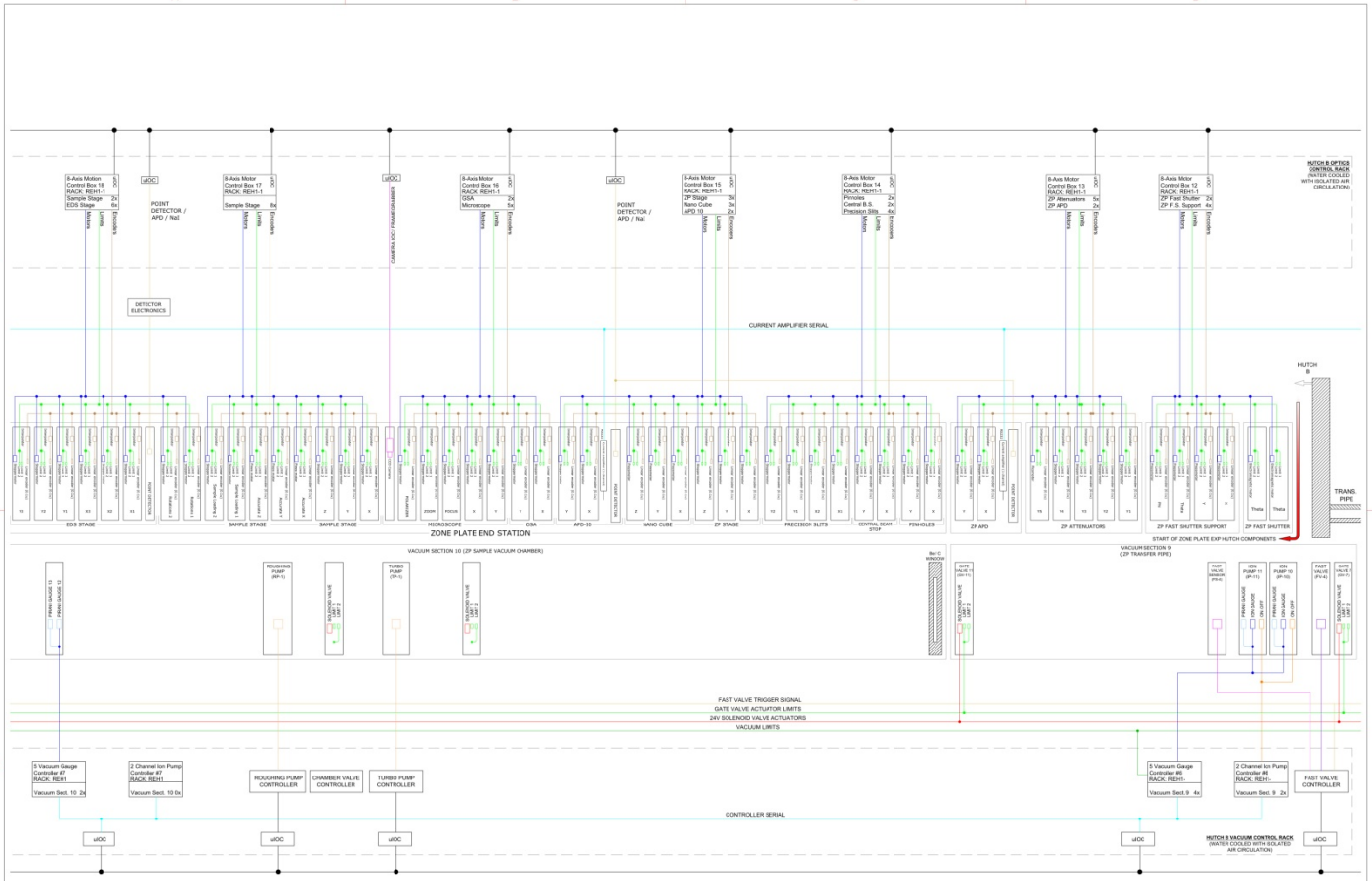

E	XF-BL-CNT-SRX-1000	A
A-3	SHEET 3 OF 5	

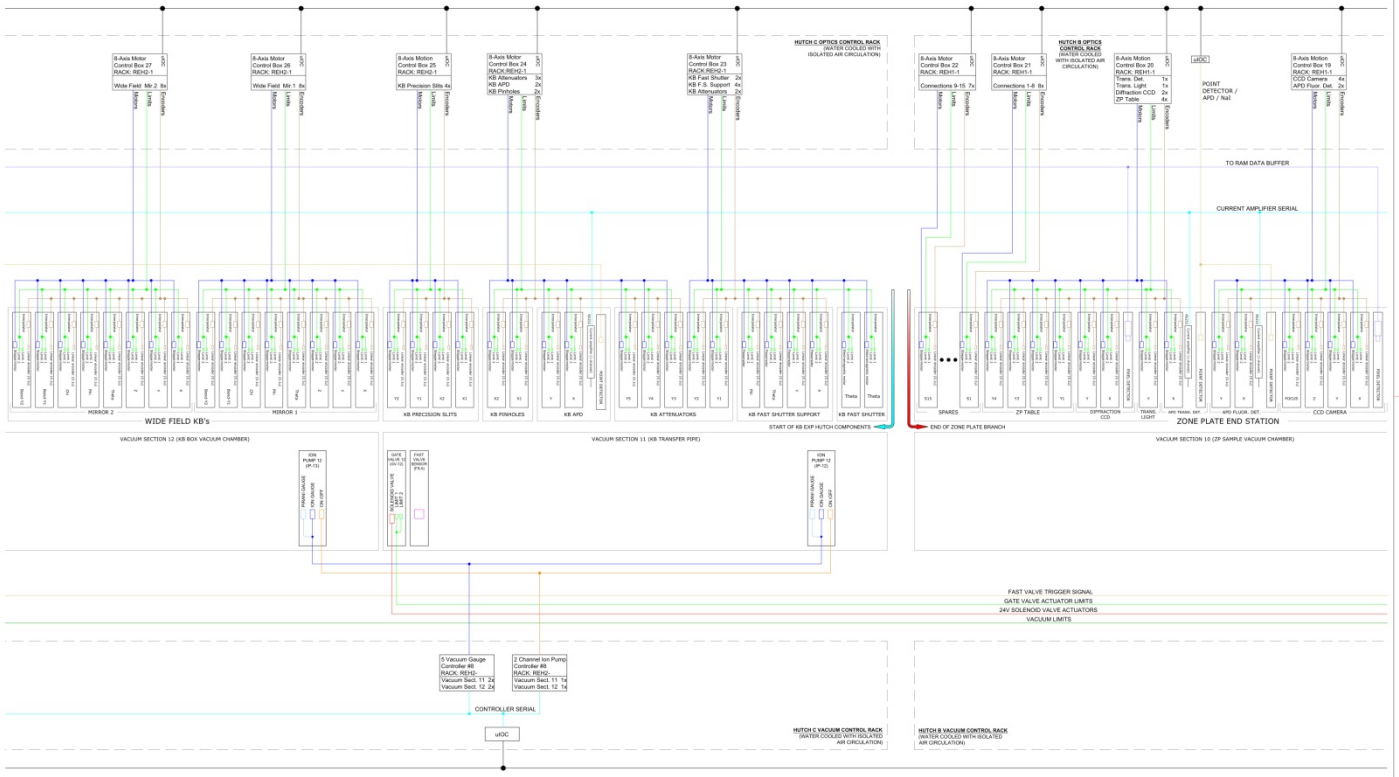

E	XF-BL-CNT-SRX-1000	A
LRC DIS. ENG&D RISK LEVEL A-3		SHEET 4 OF 5

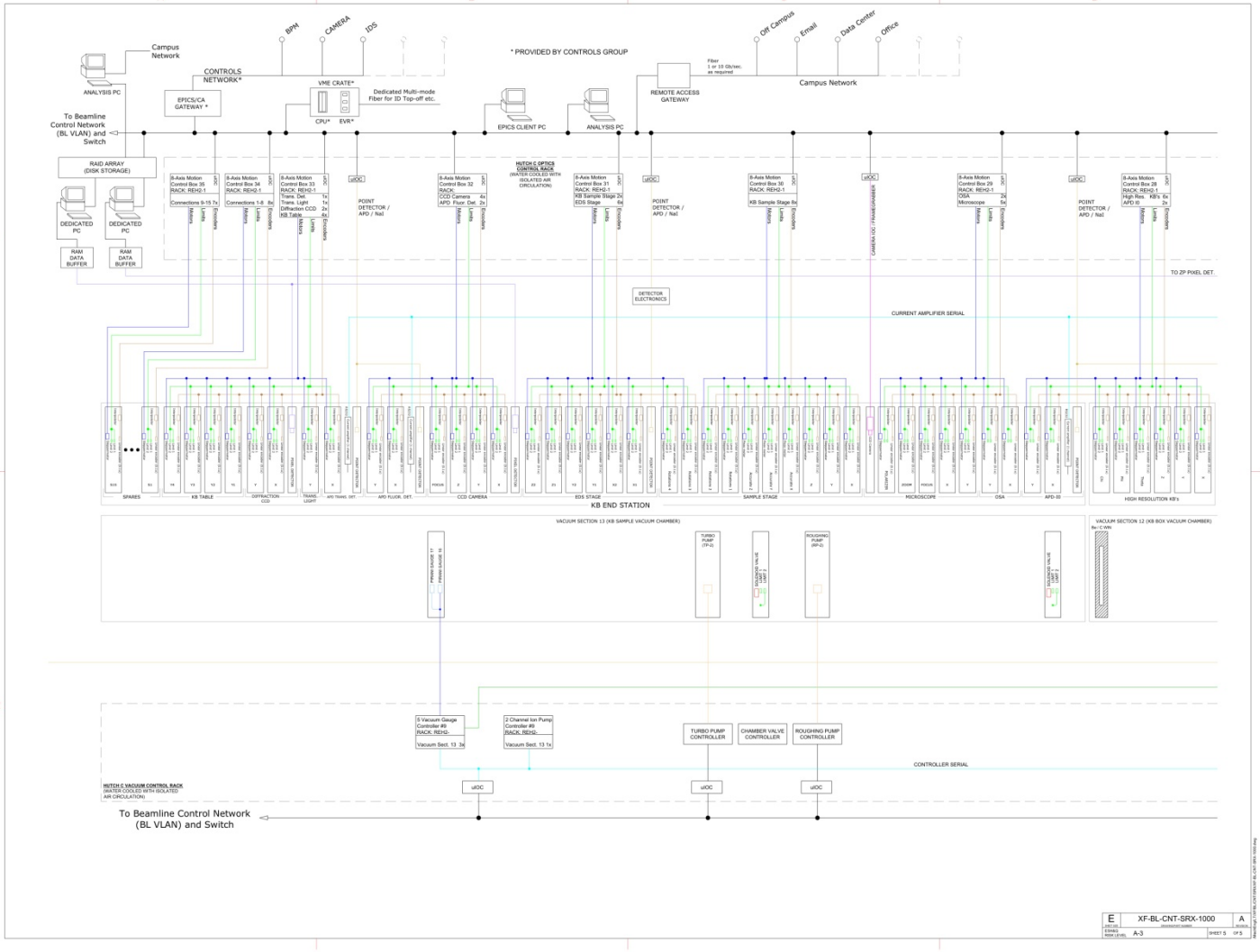

E	XF-BL-CNT-SRX-1000	A
ESHQ A-3	SHEET 5 OF 5	

Front end ray tracing (preliminary)

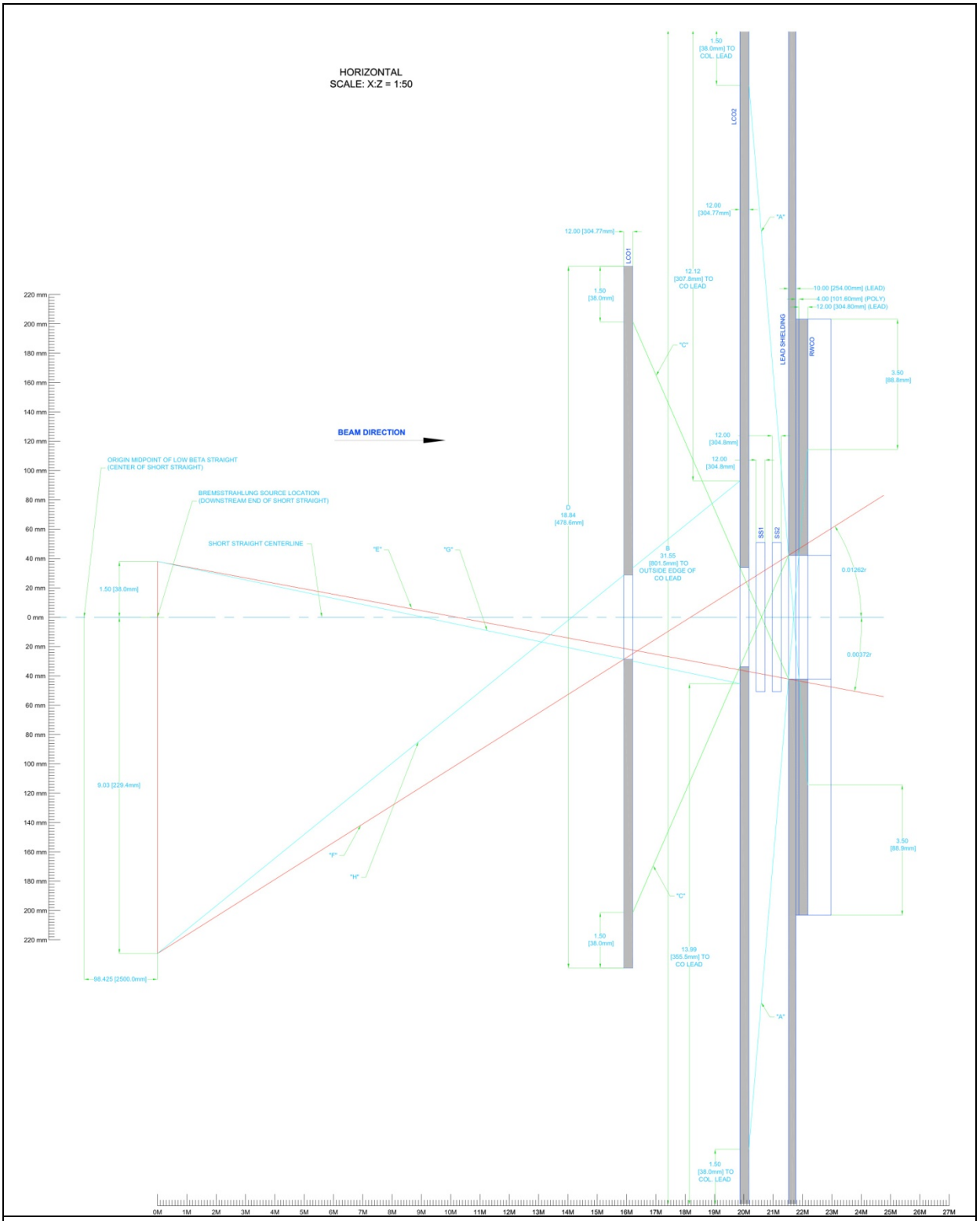

Figure B3.1: Bremsstrahlung ray-tracing through interim setup of front end components (horizontal).

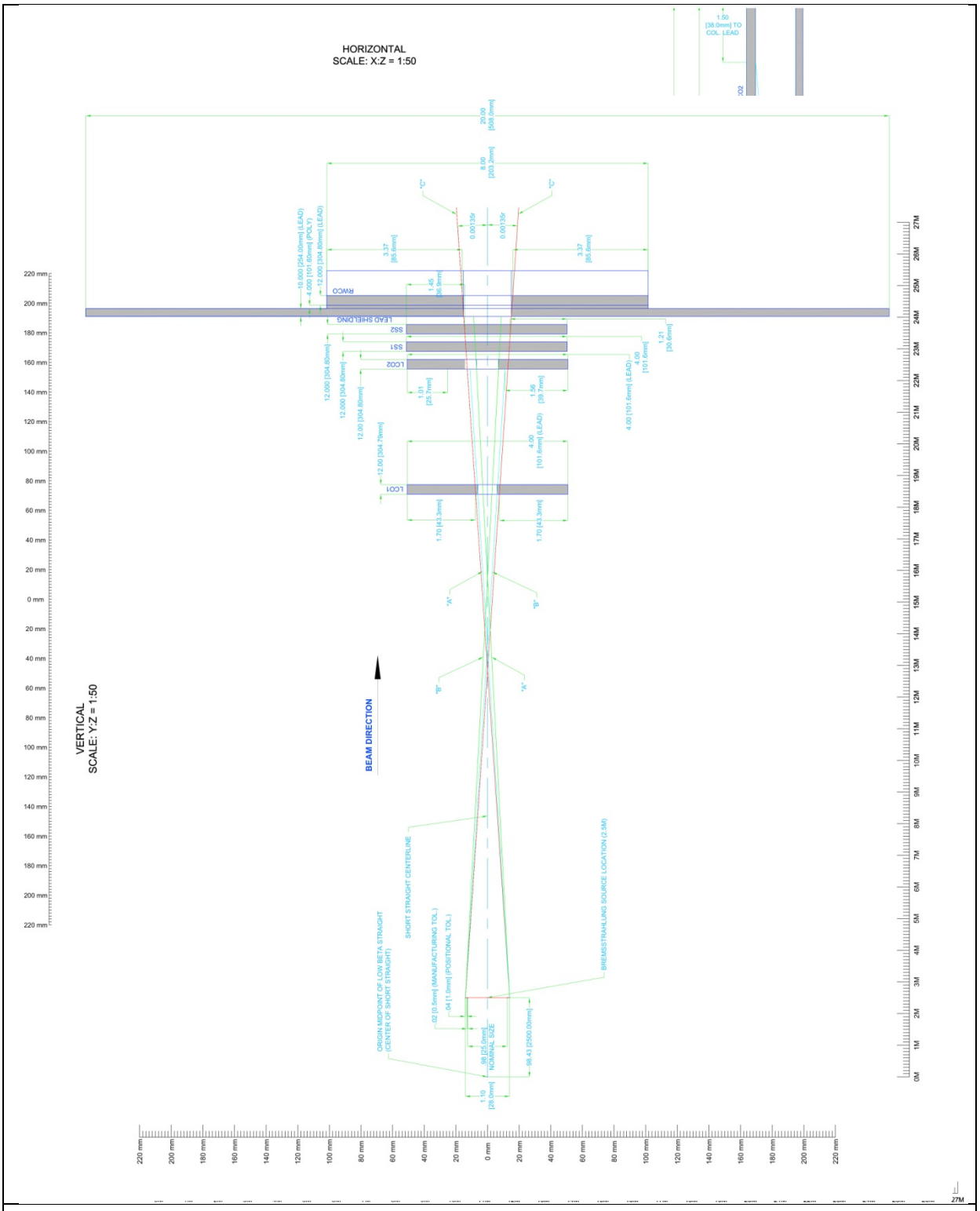

Figure B3.2: Bremsstrahlung ray-tracing through interim setup of front end components (vertical).

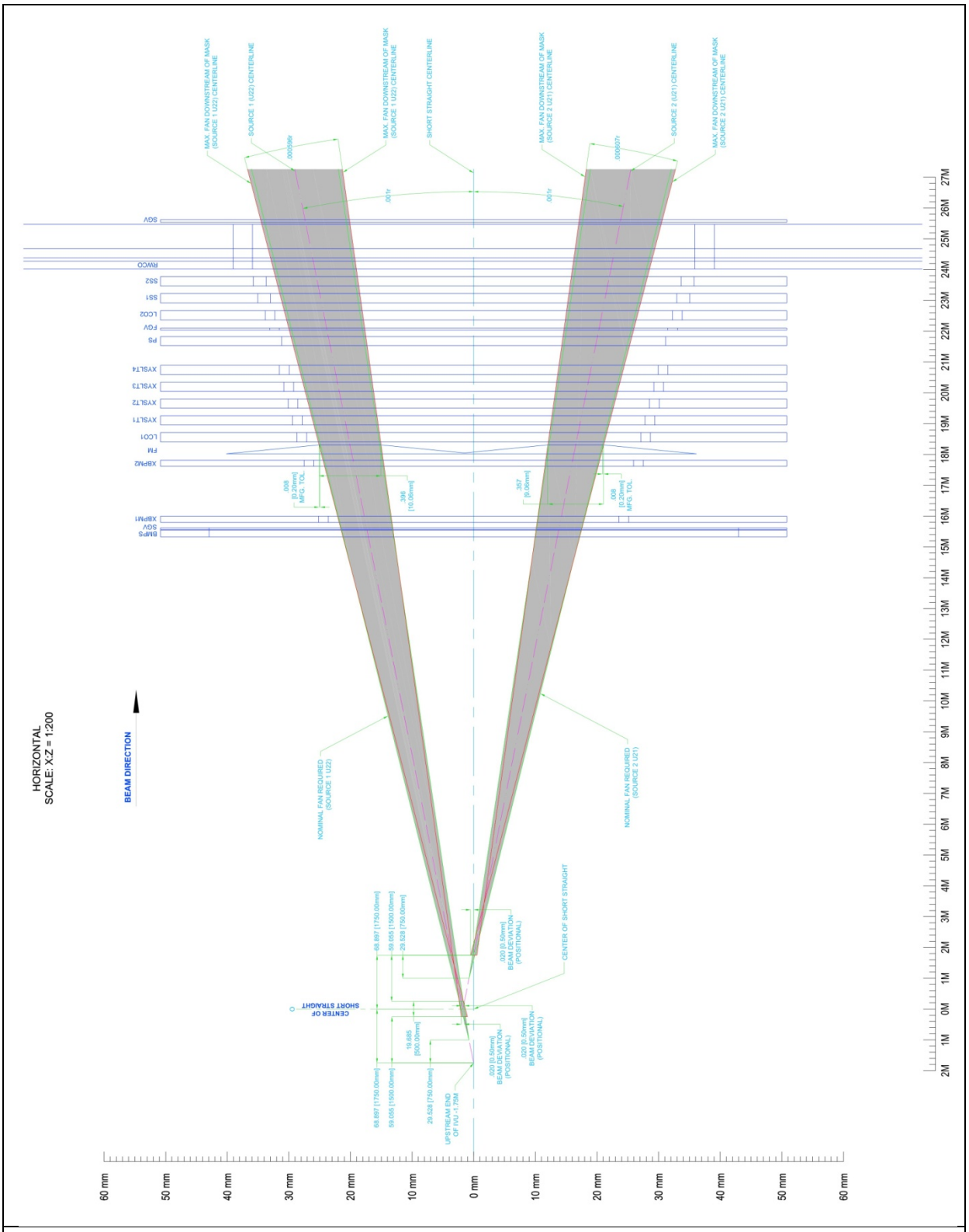

Figure B3.3: Bremsstrahlung ray-tracing through interim setup of front end components (vertical).

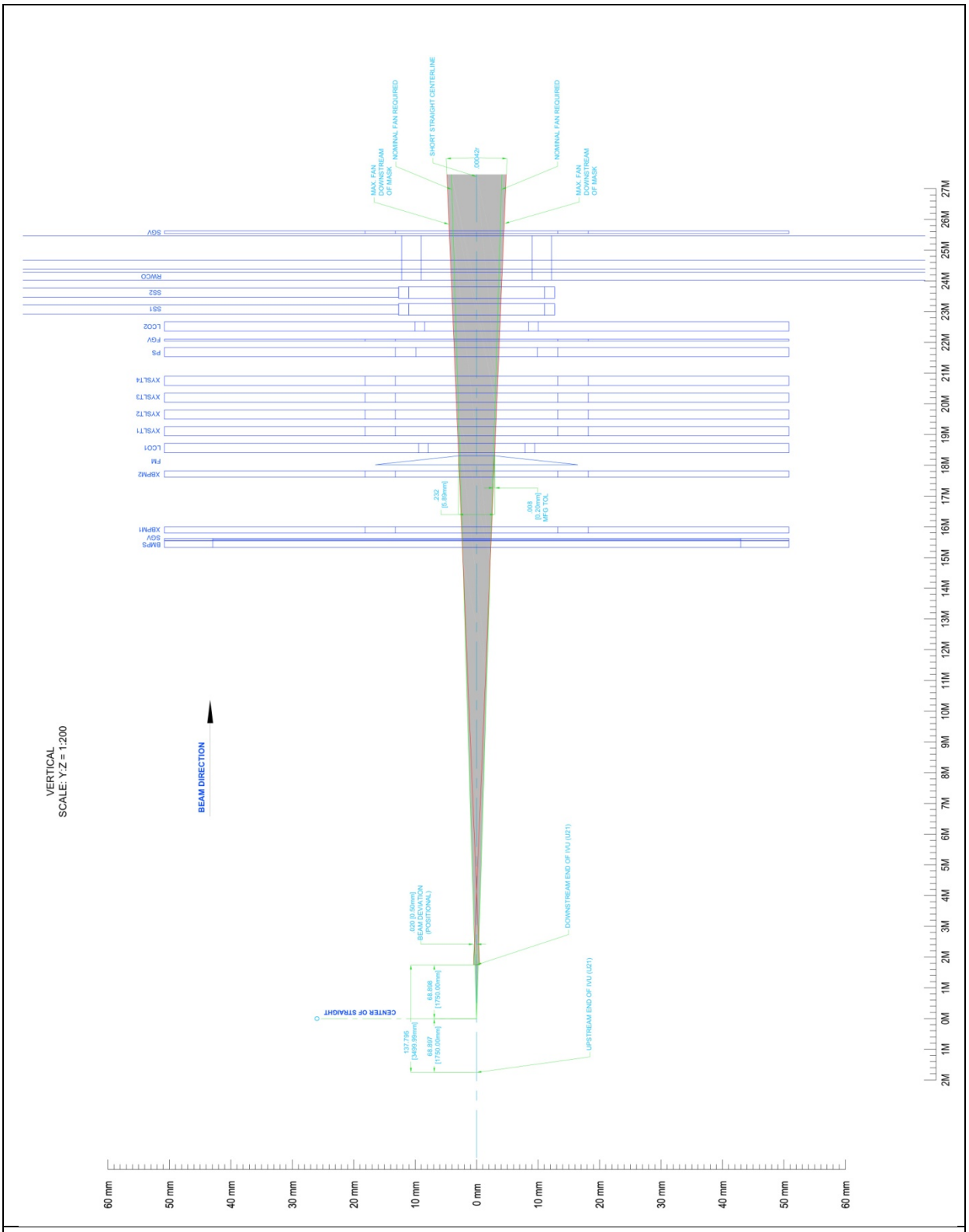

Figure B3.4: Bremsstrahlung ray-tracing through interim setup of front end components (vertical).

Raytracing KB branch

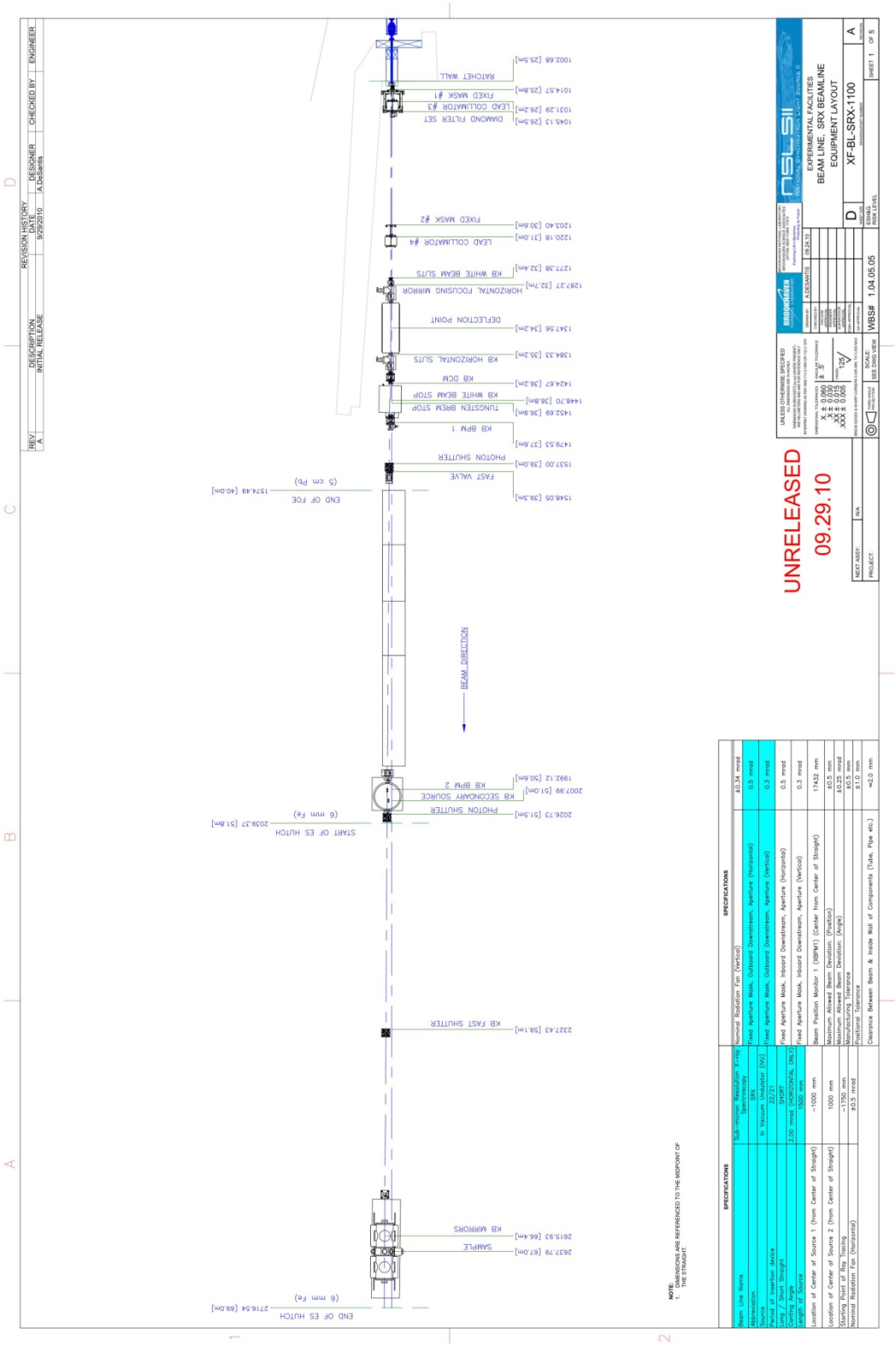

Figure B4.1: Ray tracing diagram displaying the relevant optical components.

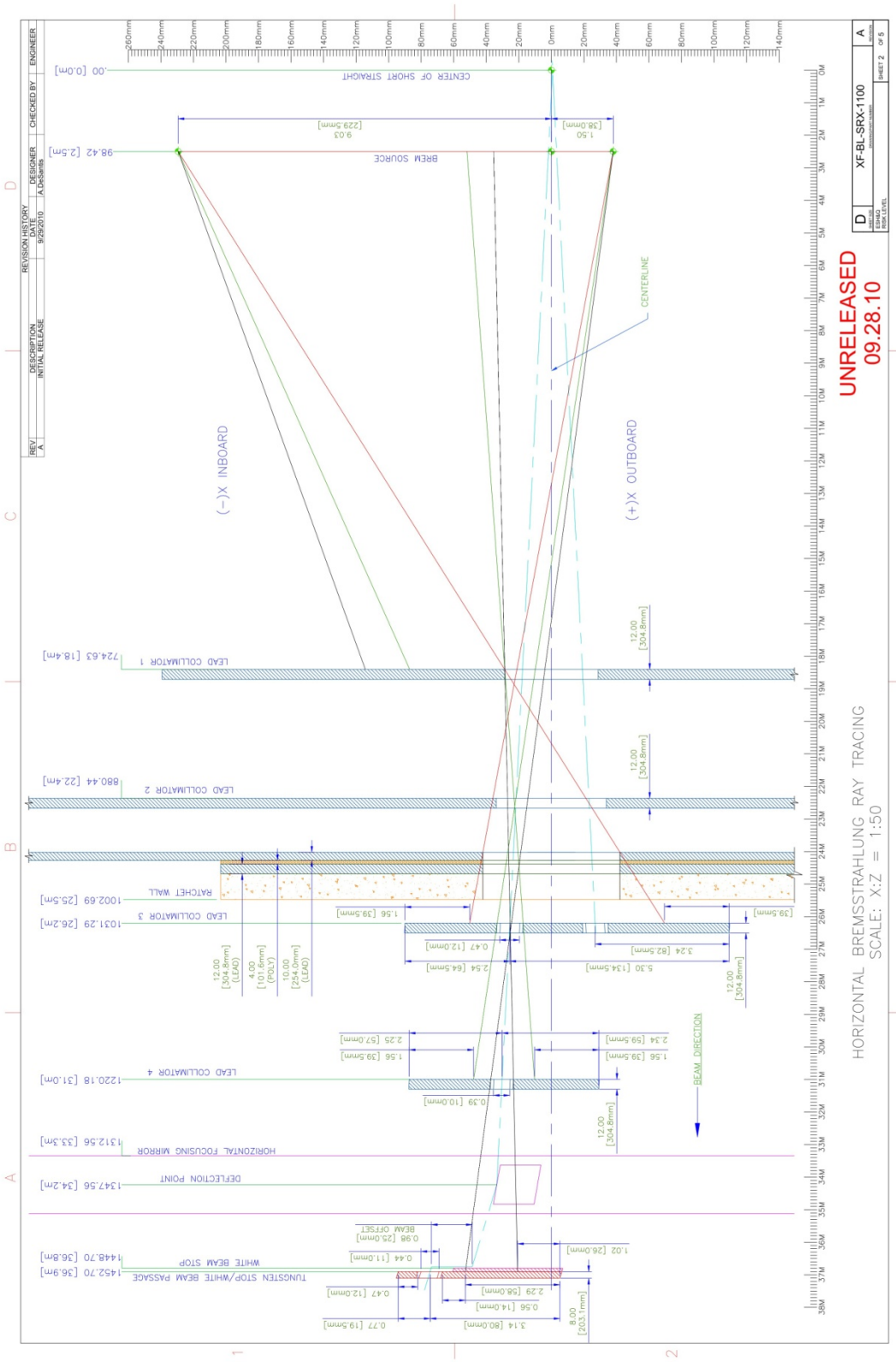

Figure B4.2: Horizontal Bremsstrahlung ray tracing for the KB branch of the SRX beamline.

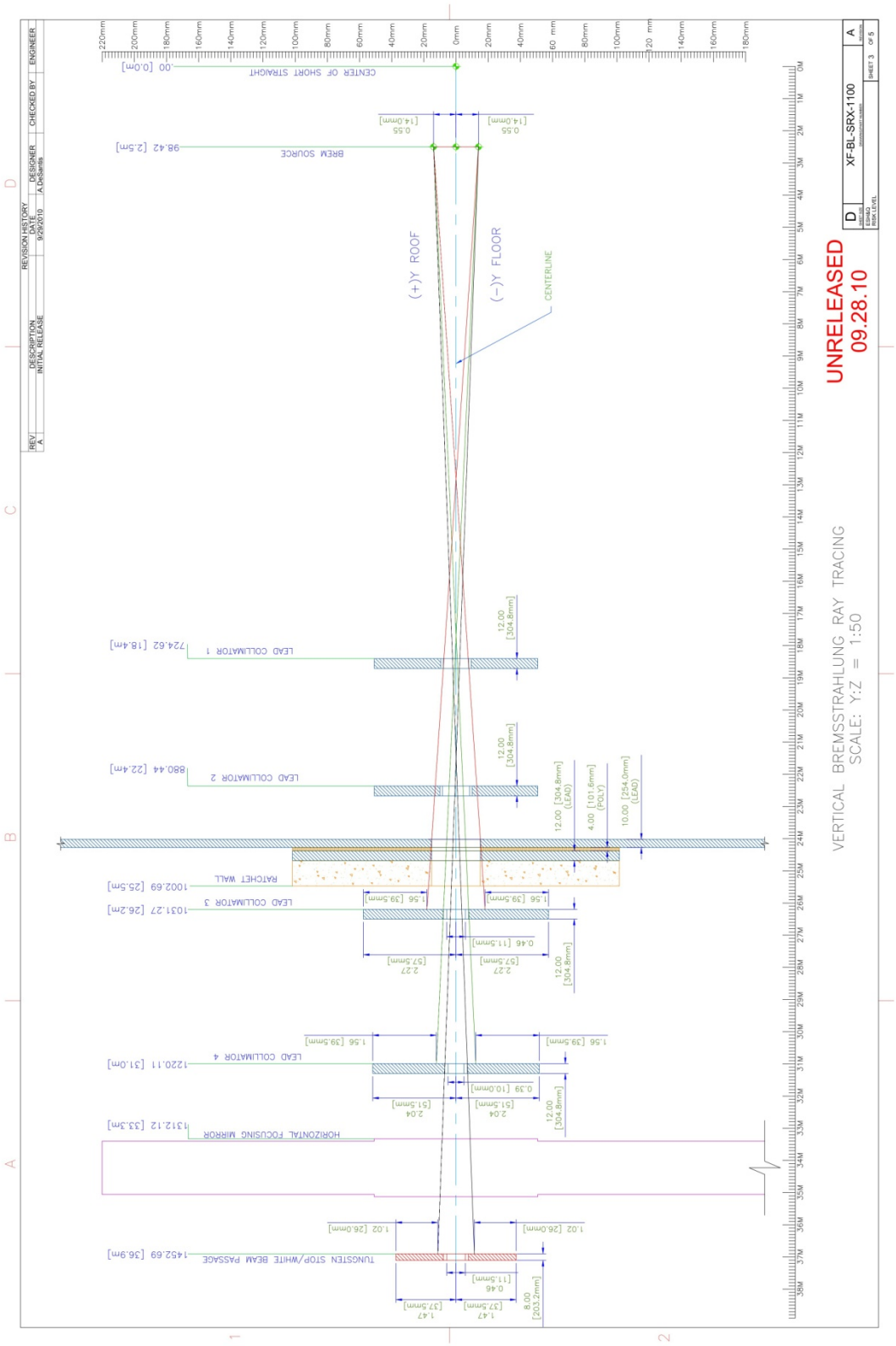

Figure B4.3: Vertical Bremsstrahlung ray tracing for the KB branch of the SRX beamline.

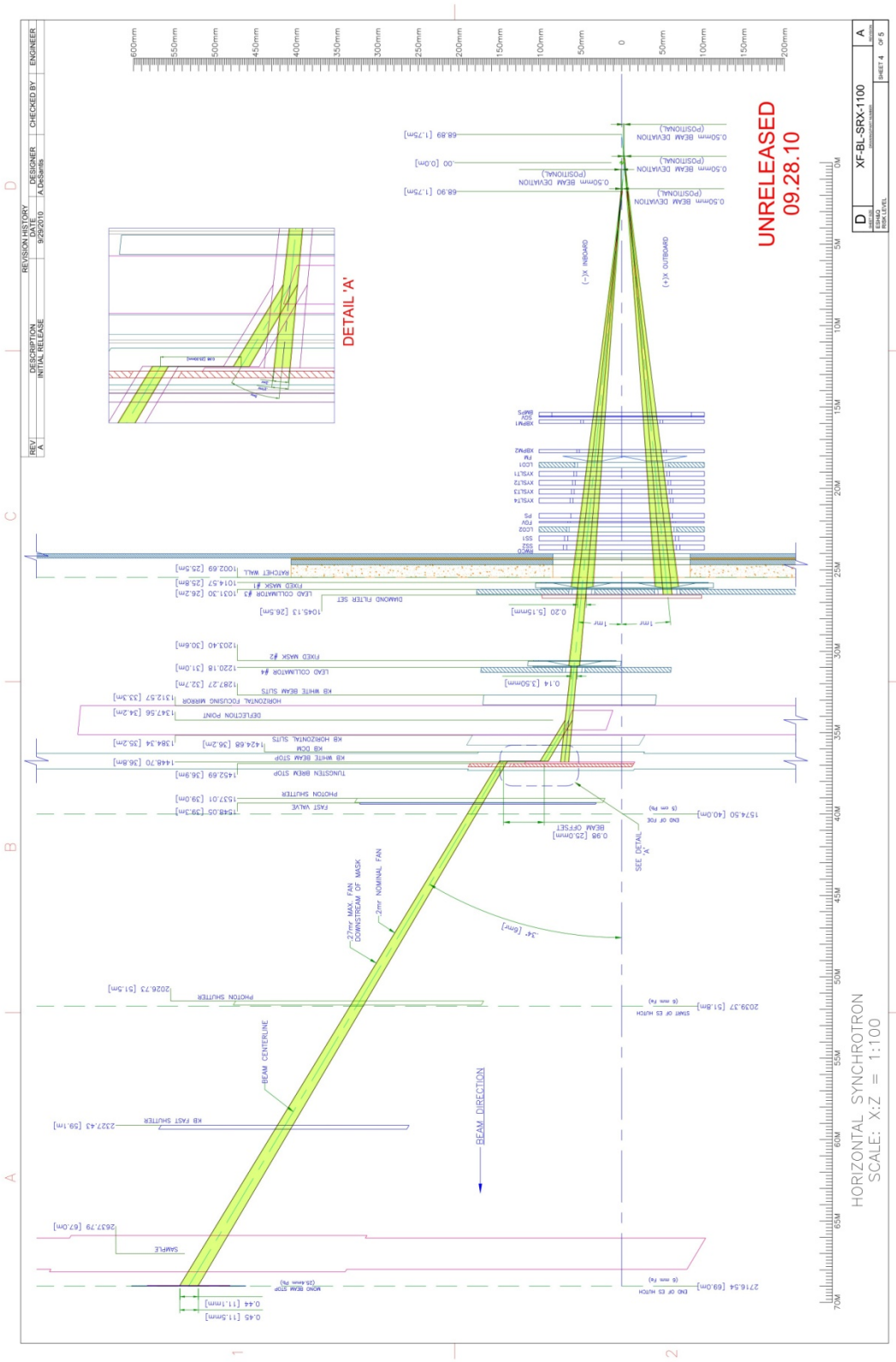

Figure B4.4: Horizontal synchrotron radiation ray tracing for the KB branch of the SRX beamline.

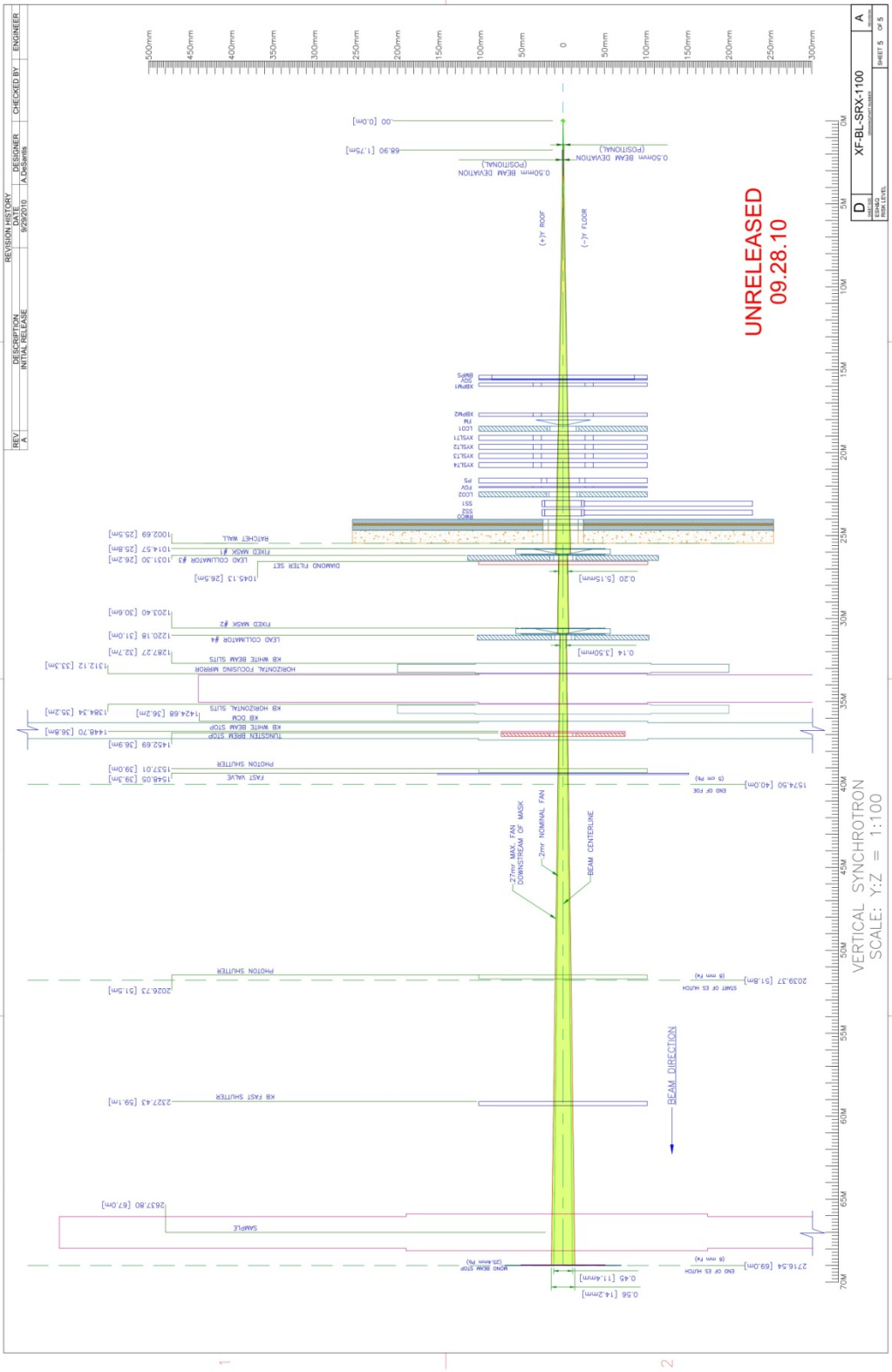

Figure B4.5: Vertical synchrotron radiation ray tracing for the KB branch of the SRX beamline.

Appendix C: Feasibility of Design and Procurement Plan

First optical enclosure

The first optical enclosure (FOE) shows a dense sequence of optical components. The beam defining optics of both branches are lined up without big distances along the path of the beam. Due to the small canting angle, there is as well laterally only very little space between the beams. It is however mandatory, that manipulations of one beam do not influence any settings of the other beam. The task will be to build mirror chambers and monochromators allowing for a second beam to pass without blockage, deviation or scattering.

Due to this complexity in the FOE, we strongly opt for a procurement of these parts as one optical package. We envision a two-step procedure, where in a first step the components for the KB-branch will be procured and installed, and in a second step, delayed in time until funding is available, the components for the second branch will be assembled. For the first step, the supplier has to make adequate beam transport bridging the gaps, open by the now missing ZP components, but assuring at the same time, that these components will fit it. The vendor would be asked to implement into his design all parts of both beamlines, but would get a purchase order only for the KB branch. In a second step, the beam transport will be removed and the actual parts will be fit in and aligned, when funding is secured.

Discussions about the FOE, the spatial constraints and the complexity of two beams in a canted geometry took place several times with possible suppliers of beam defining slits, monochromators, and mirror assemblies. We introduced during several meetings with a list of vendors not only the specifications of single optical components but we asked as well how feasible the complete design of the FOE is. We were reassured, that this design is not on the easy side of fabrication, however, is absolutely possible to manufacture.

The company IDT has participated in the design of the SRX beamline on the conceptual level and is therefore named here as an example. IDT designs, manufactures and installs beamline components as well as complete beamlines. Again as an example for the feasibility of our design, parallels can be drawn to already installed beamlines. IDT has built the complete XFM beamline at the Australian Synchrotron, which is a design with many similarities. The XFM beamline has a horizontal monochromator, as needed for the KB branch, that performs very well. Figure xx shows a picture of that monochromator as installed and a design model, taken from an IDT information leaflet. As well in this figure, a stability measurement can be seen, made at the XFM beamline. A series of over 100 repetitions of taking the same spectrum yields a reproducibility of $\Delta E = 0.05$ eV. This shows the extreme stability of this horizontal monochromator.

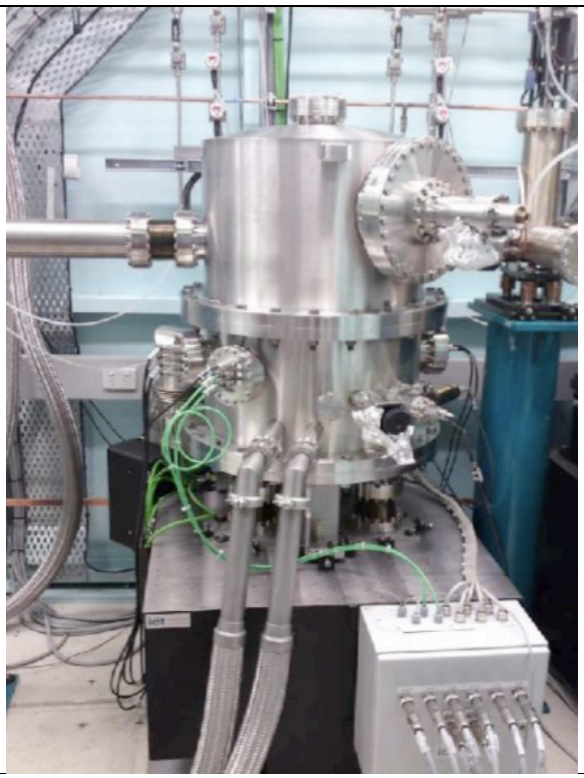

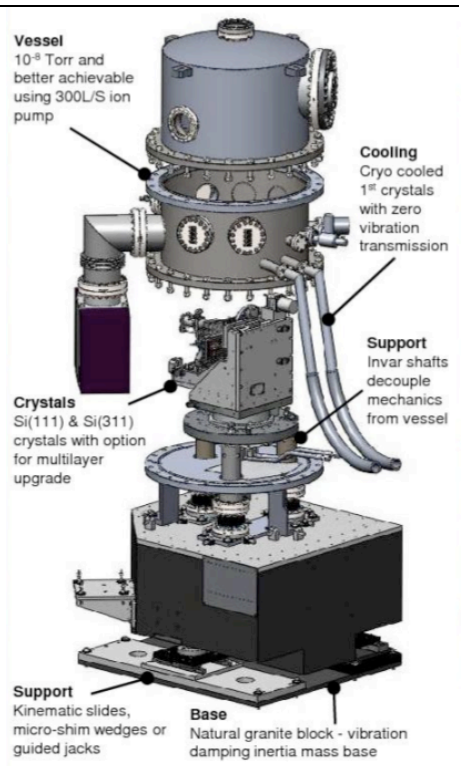

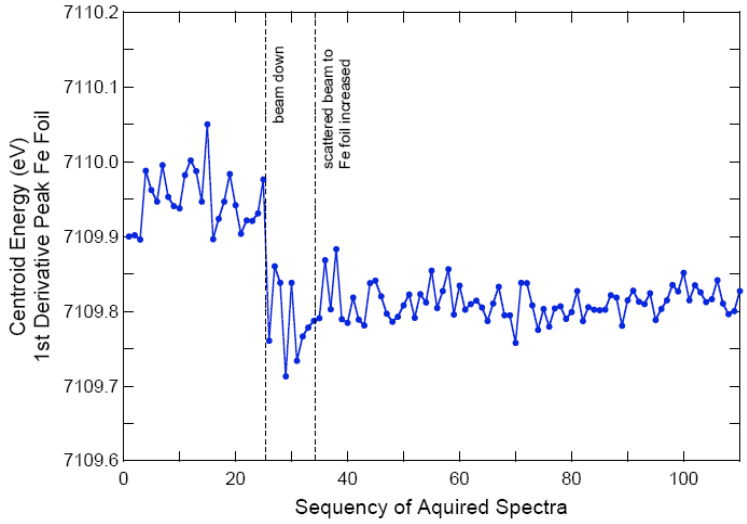

Figure C.1: Top left: Picture of the horizontally deflecting DCM. **Top right:** Design model of that DCM. **Bottom left:** Stability measurement, showing the reproducibility of the centroid energy in more than 100 repetitions.

End station

There are three components of the end station that need attention, the KB mirrors, the mechanical mount and scanning stage for the sample and the detectors.

The KB mirrors are described above. We think that we will be able to best match the excellent beam characteristics given by NSLS-II when working double-tracked. A set of large KB mirrors shall deliver a sub-µm sized spot ensuring maximum flux at the same time. In addition, we want to make use of the world-wide best emittance by trying to focus the beam into a sub-100 nm spot. The former should not cause problems, as several suppliers fabricate KB mirrors that are capable of producing a sub-micron spot. The latter is of course much more demanding. The recent results of the company JTec show, that this is challenging but not impossible.